

EUROPEAN ORGANISATION FOR NUCLEAR RESEARCH (CERN)



Submitted to: JHEP



CERN-EP-2025-094
18th June 2025

Measurements of differential cross-sections of $WbWb$ production in the dilepton channel in $p p$ collisions at $\sqrt{s} = 13$ TeV using the ATLAS detector

The ATLAS Collaboration

At the Large Hadron Collider, the $WbWb$ final state is expected to be dominated by $t\bar{t}$ production with a contribution from single-top processes. Differential cross-sections for $WbWb$ production in the dilepton decay channel are measured at the particle level as a function of various kinematic variables. The analysis is based on data from proton–proton collisions at a centre-of-mass energy of $\sqrt{s} = 13$ TeV, recorded by the ATLAS detector at the Large Hadron Collider over the period from 2015 to 2018, corresponding to an integrated luminosity of 140 fb^{-1} . Measurements are performed within the fiducial phase-space defined by the presence of two b -jets and one electron and one muon of opposite charges. The differential cross-sections are corrected for detector effects and unfolded to the particle level. Results are compared with predictions from Monte Carlo event generators at next-to-leading order in perturbative quantum chromodynamics. These measurements provide valuable constraints on the modelling of $WbWb$ production and the interference between doubly resonant and singly resonant $WbWb$ production.

Contents

1	Introduction	3
2	The ATLAS detector	4
3	Data and Monte Carlo samples	5
3.1	MC simulated samples	5
4	Object reconstruction and event selection	9
4.1	Detector-level object reconstruction	10
4.2	Detector-level event selection	11
4.3	Sensitivity to $t\bar{t}$ and tW interference	13
4.4	Particle-level object definition	16
4.5	Particle-level selection	16
5	Cross-section extraction	17
5.1	Measured distributions at the particle level	18
5.2	Unfolding corrections	19
5.3	Systematic uncertainties	22
5.4	Uncertainty summary	25
6	Results	26
6.1	χ^2 calculation	26
6.2	Differential cross-sections in the $2b$ -exclusive region	27
6.3	Differential cross-sections in the $2b$ -inclusive region	28
6.4	Integrated fiducial cross-section	35
7	Conclusions	36

1 Introduction

Top-quark pair ($t\bar{t}$) production is one of the most extensively studied processes at the Large Hadron Collider (LHC) [1] and constitutes a critical background for many searches for physics beyond the Standard Model (BSM). The differential cross-sections for $t\bar{t}$ production have been both measured [2–6] and calculated [7–14] with high precision across a broad kinematic range. However, these typically rely on the narrow-width approximation for top-quark decays, effectively separating $t\bar{t}$ production from the production of a single top quark in association with a W boson and a b -quark (tWb). Due to their identical $WbWb$ final states, processes with one or two time-like top-quark propagators (referred to as singly and doubly resonant, respectively) interfere. This interference becomes evident when comparing leading-order (LO) $t\bar{t}$ production with next-to-leading-order (NLO) tW production, as illustrated in Figure 1.

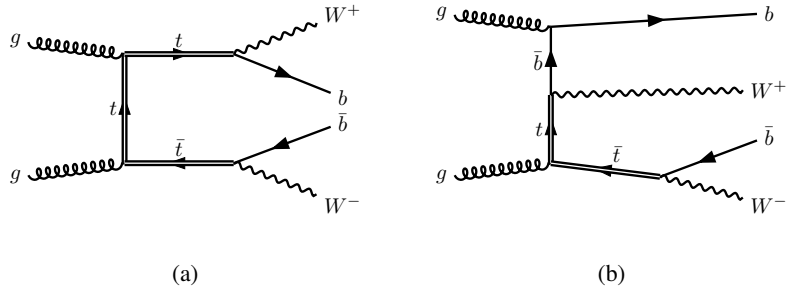


Figure 1: Representative Feynman diagrams corresponding to gluon-initiated (a) $t\bar{t}$ and (b) tWb single-top-quark processes. The top quarks are indicated by double fermion lines.

This quantum interference feature has been extensively studied from a theoretical perspective [15–19] and provides a significant source of uncertainty for measurements of many Standard Model (SM) processes and BSM searches. Fixed-order calculations of the full next-to-leading-order $pp \rightarrow l^+l^- \bar{v}b\bar{b}$ process, where l denotes a lepton of any flavour, include the correct treatment of the interference between $t\bar{t}$ and tW and have set the stage for corresponding predictions matched to a parton shower [20–25]. While ATLAS previously measured this interference-sensitive region using 36.1 fb^{-1} of data collected at $\sqrt{s} = 13 \text{ TeV}$ [26], the present work significantly enhances the sensitivity by leveraging the full Run 2 data sample of 140 fb^{-1} collected by the ATLAS detector between 2015 and 2018. This larger data sample, coupled with optimised event selection, improved calibrations, and refined modelling of uncertainties, achieves a substantial reduction in the total measurement uncertainty. The analysis focuses on events with one electron and one muon, which provide a clean signature for studying these processes.

Additionally, several observables are measured for the first time for the combined $t\bar{t}$ and tW signal process. These measurements are crucial for validating the modelling of fundamental kinematic distributions in Monte Carlo (MC) generators that account for interference effects in $WbWb$ final states.

2 The ATLAS detector

The ATLAS detector [27] at the LHC covers nearly the entire solid angle around the collision point.¹ It consists of an inner tracking detector surrounded by a thin superconducting solenoid, electromagnetic and hadronic calorimeters, and a muon spectrometer incorporating three large superconducting air-core toroidal magnets.

The inner-detector system (ID) is immersed in a 2 T axial magnetic field and provides charged-particle tracking in the range $|\eta| < 2.5$. The high-granularity silicon pixel detector covers the vertex region and typically provides four measurements per track, the first hit generally being in the insertable B-layer (IBL) installed before Run 2 [28, 29]. It is followed by the SemiConductor Tracker (SCT), which usually provides eight measurements per track. These silicon detectors are complemented by the transition radiation tracker (TRT), which enables radially extended track reconstruction up to $|\eta| = 2.0$. The TRT also provides electron identification information based on the fraction of hits (typically 30 in total) above a higher energy-deposit threshold corresponding to transition radiation.

The calorimeter system covers the pseudorapidity range $|\eta| < 4.9$. Within the region $|\eta| < 3.2$, electromagnetic calorimetry is provided by barrel and endcap high-granularity lead/liquid-argon (LAr) calorimeters, with an additional thin LAr presampler covering $|\eta| < 1.8$ to correct for energy loss in material upstream of the calorimeters. Hadronic calorimetry is provided by the steel/scintillator-tile calorimeter, segmented into three barrel structures within $|\eta| < 1.7$, and two copper/LAr hadronic endcap calorimeters. The solid angle coverage is completed with forward copper/LAr and tungsten/LAr calorimeter modules optimised for electromagnetic and hadronic energy measurements, respectively.

The muon spectrometer (MS) comprises separate trigger and high-precision tracking chambers measuring the deflection of muons in a magnetic field generated by the superconducting air-core toroidal magnets. The field integral of the toroids ranges between 2.0 and 6.0 T m across most of the detector. Three layers of precision chambers, each consisting of layers of monitored drift tubes, cover the region $|\eta| < 2.7$, complemented by cathode-strip chambers in the forward region, where the background is highest. The muon trigger system covers the range $|\eta| < 2.4$ with resistive-plate chambers in the barrel, and thin-gap chambers in the endcap regions.

The luminosity is measured mainly by the LUCID–2 [30] detector that records Cherenkov light produced in the quartz windows of photomultipliers located close to the beampipe.

Events were selected by the first-level trigger system implemented in custom hardware, followed by selections made by algorithms implemented in software in the high-level trigger [31]. The first-level trigger accepted events from the 40 MHz bunch crossings at a rate close to 100 kHz, which the high-level trigger further reduced in order to record complete events to disk at about 1.25 kHz.

A software suite [32] is used in data simulation, in the reconstruction and analysis of real and simulated data, in detector operations, and in the trigger and data acquisition systems of the experiment.

¹ ATLAS uses a right-handed coordinate system with its origin at the nominal interaction point (IP) in the centre of the detector and the z -axis along the beam pipe. The x -axis points from the IP to the centre of the LHC ring, and the y -axis points upwards. Polar coordinates (r, ϕ) are used in the transverse plane, ϕ being the azimuthal angle around the z -axis. The pseudorapidity is defined in terms of the polar angle θ as $\eta = -\ln \tan(\theta/2)$ and is equal to the rapidity $y = \frac{1}{2} \ln \left(\frac{E+p_z}{E-p_z} \right)$ in the relativistic limit. Angular distance is measured in units of $\Delta R \equiv \sqrt{(\Delta y)^2 + (\Delta \phi)^2}$.

3 Data and Monte Carlo samples

This analysis uses the proton–proton collision data at a centre-of-mass energy of 13 TeV collected by the ATLAS detector during Run 2 operations (2015–2018). This data was recorded during stable beam LHC operations with the ATLAS detector fully functioning. After all quality criteria are applied [33], the recorded data corresponds to an integrated luminosity of 140 fb^{-1} [34].

3.1 MC simulated samples

Various MC generators were employed to produce simulated events, which are used to estimate contributions from signal and background processes, determine detector resolution and acceptance correction factors, and evaluate systematic uncertainties. Additionally, MC generators facilitate comparisons between unfolded data and theoretical predictions. All samples were normalised according to the best available theoretical cross-section predictions, as detailed in the following sections.

The responses of the ATLAS detector and trigger were simulated [35] based on the detailed model implemented in the GEANT4 framework [36]. The ATLAS fast-simulation package ATLFAST-II, which parametrised hadronic showers in the electromagnetic and hadronic calorimeters [37], was employed to estimate some of the signal modelling uncertainties.

The effect of multiple interactions in the same and neighbouring bunch crossings (pile-up) was modelled by overlaying the simulated hard-scattering event with inelastic proton–proton (pp) events generated with PYTHIA 8.186 [38] using the NNPDF2.3LO set of parton distribution functions (PDF) [39] and the A3 set of tuned parameters [40] (tune). The MC events were weighted to reproduce the distribution of the average number of interactions per bunch crossing ($\langle\mu\rangle$) observed in the data. The $\langle\mu\rangle$ value in data was rescaled by a factor of 1.03 ± 0.04 to improve agreement between data and simulation in both charged-particle track distributions and the visible inelastic pp cross-section [41].

All simulated events were processed using the same reconstruction algorithms and analysis chain as the data, and corrections were applied so that the object reconstruction and identification efficiencies, energy scales and energy resolutions in simulation matched those determined from data.

If not stated otherwise, some common settings were defined for the different MC simulations and theoretical calculations. The top-quark mass m_{top} was set to 172.5 GeV. The PYTHIA 8 parton shower (PS) used the A14 set of tuned parameters [42] and the NNPDF2.3LO PDF set. EvtGEN [43] was used for the decays of the bottom and charm hadrons for the samples showered with PYTHIA 8 and HERWIG 7 [44, 45].

3.1.1 Nominal signal sample

MC samples produced with specific settings and parameters are used as the nominal signal sample for the analysis. The signal samples are defined as a combination of the $t\bar{t}$ and tW samples from the same generators and parton showers. Contributions from non-resonant $WWbb$ production are negligible [18] and, if not explicitly stated, are not included in the simulated samples. This is cross-checked with the PowHEG+PYTHIA 8 $bb4l$ sample described below.

At NLO, it is crucial to avoid double-counting tWb events with $m_{bW} \sim m_{\text{top}}$, whose diagrams are already included, at NLO, in the definition of the $t\bar{t}$ sample. The default scheme employed in this analysis is

diagram removal (DR) [16], where all doubly resonant amplitudes are excluded from the tW sample. Alternative methods [16, 17, 46] include diagram subtraction (DS), which subtracts gauge-invariant terms corresponding to doubly resonant contributions rather than removing them. This approach preserves a more accurate representation of interference effects between the $t\bar{t}$ and tW processes. In the rest of the paper, unless explicitly stated, the tW samples were generated using the DR scheme.

In this analysis, the nominal $t\bar{t}$ and tW were both generated with PowHEG Box v2 [47–50] and interfaced to PYTHIA 8 [51], with the settings and parameters described below, and are referred to as ‘PWG+PY8’.

$t\bar{t}$ production The production of $t\bar{t}$ events was simulated using the PowHEG Box v2 generator, which provides matrix elements at next-to-leading order in the strong coupling constant α_s with the NNPDF3.0NLO [52] PDF set. The h_{damp} parameter, which controls the matching in PowHEG and effectively regulates the high transverse momentum (p_T) radiation against which the $t\bar{t}$ system recoils, was set to $1.5 m_{\text{top}}$ [19]. The functional form of the renormalisation and factorisation scale was set to the default scale $\sqrt{m_{\text{top}}^2 + p_T^2}$, where p_T^2 is evaluated with the kinematics of the underlying $2 \rightarrow 2$ PowHEG process. The events were interfaced to PYTHIA 8.230 for the parton shower and hadronisation. The $p_{T,\text{hard}}$ parameter, which regulates how the PYTHIA 8 radiation phase space is determined to avoid overlaps with the regions of the phase space already covered by PowHEG [53], was set to $p_{T,\text{hard}} = 0$. The modelling of second and subsequent gluon emission in the $t \rightarrow Wb$ process was performed by recoiling the gluon against b -quarks, which is the default strategy in PowHEG [54].

The nominal $t\bar{t}$ sample was normalised to the cross-section prediction at next-to-next-to-leading order (NNLO) in perturbative quantum chromodynamics (QCD) including the resummation of next-to-next-to-leading logarithmic (NNLL) soft-gluon terms calculated using Top++2.0 [7–13] with the PDF4LHC21 PDF set [55] in the five-flavour scheme. For pp collisions at a centre-of-mass energy of $\sqrt{s} = 13$ TeV, this cross-section is $\sigma(t\bar{t})_{\text{NNLO+NNLL}} = 834^{+21}_{-30}(\text{scale}) \pm 21(\text{PDF}+\alpha_s) \pm 23(m_{\text{top}})$ pb. The uncertainties in the cross-section due to the PDF and α_s are calculated using the PDF4LHC prescription with the MSHT2020 [56], CT18 [57] and NNPDF3.1 [58] PDF sets. The uncertainties in the cross-section due to the choice of renormalisation scale μ_r and factorisation scale μ_f are determined by varying the scales independently up and down by a factor of two, while ensuring that they do not differ from each other by more than a factor of two. This procedure is used consistently throughout the analysis whenever scale uncertainties are evaluated. The scale uncertainty is defined as the envelope of the resulting cross-section values. The uncertainties due to the top-quark mass m_{top} are evaluated by varying m_{top} by ± 1.0 GeV.

tW production The nominal single-top-quark tW associated production was simulated using the PowHEG Box v2 [59] generator that provides matrix elements at NLO in QCD in the five-flavour scheme, with the NNPDF3.0NLO PDF set. The functional form of the renormalisation and factorisation scales was set to $H_T/2$, where H_T is defined as the scalar sum of the p_T of all outgoing partons. The DR scheme was employed to treat the interference with $t\bar{t}$ production. The events were interfaced to PYTHIA 8.230. As in the nominal $t\bar{t}$ sample, the $p_{T,\text{hard}}$ parameter was set to $p_{T,\text{hard}} = 0$.

The predicted cross-section of tW production in pp collisions at a centre-of-mass energy of 13 TeV is $\sigma(tW) = 79.3 \pm 2.8$ pb and was computed at NLO in QCD with the addition of third-order corrections to soft-gluon emissions by resumming NNLL terms [60]. The PDF4LHC21 PDF set was used. The quoted uncertainty includes the uncertainty due to the choice of μ_r and μ_f and the uncertainty in the PDFs. The

uncertainty from the scale choice is determined by varying the scales simultaneously up and down by a factor of two. The PDF uncertainties are based on the Hessian method and include the uncertainty in α_s .

The perturbative orders at which the total cross-sections are calculated differ between the $t\bar{t}$ and tW processes. The $t\bar{t}$ cross-section is calculated at NNLO+NNLL, while the tW cross-section is calculated at NLO+NNLL. The impact of this difference on the measurement is included as a source of systematic uncertainty. The impact on the predictions of the normalised differential cross-sections is found to be negligible by comparing the predictions obtained with the nominal settings (with the $t\bar{t}$ and tW processes normalised to NNLO+NNLL and NLO+NNLL, respectively) to the predictions obtained without the higher-order corrections (with the $t\bar{t}$ and tW processes normalised to NLO).

3.1.2 Alternative signal samples

Several additional $t\bar{t}$ and tW samples are considered for evaluating modelling systematic uncertainties and for comparison with data.

Samples for systematic uncertainties and comparison with data

tW PWG+PY8 (DS) This sample is similar to the nominal PWG+PY8 sample but used the DS scheme. Combined with the nominal $t\bar{t}$ sample, it is referred to as ‘PWG+PY8 (DS)’.

$t\bar{t}$ and tW PWG+PY8 ($h_{\text{damp}} = 3m_{\text{top}}$) This sample was generated with the same settings as the nominal PWG+PY8 sample but with the h_{damp} parameter set to $3m_{\text{top}}$. This sample is referred to as ‘PWG+PY8 (h_{damp})’.

$t\bar{t}$ and tW PWG+H7 This sample consists of $t\bar{t}$ events simulated using the same PowHEG Box v2 set-up with the same settings as the nominal sample but interfaced to HERWIG 7.1.3, which uses an angular-ordered parton-shower model, with the MMHT2014LO PDF set [61]. This sample used the HERWIG 7.1 default set of tuned parameters. For the tW process, events simulated with the PowHEG Box v2 generator using the same settings as the nominal sample were interfaced to HERWIG with the same configuration set-up as the $t\bar{t}$ sample. The DR scheme was employed to treat the interference with $t\bar{t}$ production. This sample is referred to as ‘PWG+H7’.

$t\bar{t}$ and tW PWG+PY8 ($p_{T,\text{hard}} = 1$) This sample is similar to the nominal PWG+PY8 sample but used $p_{T,\text{hard}} = 1$ instead of $p_{T,\text{hard}} = 0$ [62, 63]. It is referred to as ‘PWG+PY8 ($p_{T,\text{hard}}$)’.

$t\bar{t}$ and tW PWG+PY8 (mass variations) These samples are based on the nominal PWG+PY8 set-up but incorporate variations in the top-quark mass by ± 3.5 GeV around the nominal mass of 172.5 GeV. These variations are used to assess the impact on the measured differential cross-sections of the assumed top-quark mass in the simulated $t\bar{t}$ and tW processes. These samples are utilised solely for evaluating systematic uncertainties, as described in Section 5.3.3, and are not used for direct comparisons with data.

Samples only for comparison with data

$t\bar{t}$ PWG+PY8 (recoil) This sample is similar to the nominal $t\bar{t}$ PWG+PY8 sample but uses a different recoil strategy. In this variation, the gluon recoils against the top-quark itself during the second and subsequent gluon emissions in the $t \rightarrow Wb$ process [64]. The tW samples were kept at their nominal settings. This sample is referred to as ‘PWG+PY8 (recoil)’.

PWG+PY8 $bb4l$ This sample was produced using a generalisation of PowHEG that generates $l^+\nu l^-\bar{\nu} b\bar{b}$ final states. This approach accounts for quantum interference effects between the $t\bar{t}$ and tW production modes, and off-shell and non-resonant effects [25]. Events were simulated using the POWHEG BOX RES framework [65], with matrix elements at NLO in QCD with the NNPDF3.0NLO PDF set in the four-flavour scheme. A general NLO+PS matching technique that allows a consistent treatment of resonances, referred to as ‘resonance-aware matching’ [66, 67], was employed. The renormalisation and factorisation scales were set using the functional form:

$$\left[\left(m_{\text{top}}^2 + p_{T,t}^2 \right) \left(m_{\text{top}}^2 + p_{T,\bar{t}}^2 \right) \right]^{\frac{1}{4}},$$

where the masses and transverse momenta of the (anti)top-quarks are defined in the underlying Born phase space, based on the final state (off-shell) decay products. For diagrams involving an intermediate Z boson, the scales were set to $\frac{\sqrt{p_Z^2}}{2}$, where $\mathbf{p}_Z = \mathbf{p}_{l^+} + \mathbf{p}_{l^-} + \mathbf{p}_\nu + \mathbf{p}_{\bar{\nu}}$. The h_{damp} parameter was set to $1.5 m_{\text{top}}$. For the POWHEG–PYTHIA matching, a special UserHook (PowhegBB4l tms) was employed [46]. This generator is still under review within the ATLAS experiment, and a complete set of systematic uncertainties is not yet available; therefore, it cannot be used as a nominal sample.

$t\bar{t}$ NNLO reweighting To assess the impact of NNLO corrections on the agreement between data and simulation, the nominal PWG+PY8 $t\bar{t}$ sample was reweighted at parton level to match the NNLO QCD + NLO electroweak (EW) parton-level predictions presented in Ref. [68]. The reweighting was applied as a function of three variables: $p_T(t)$, $m(t\bar{t})$, and $p_T(t\bar{t})$, using the kinematic distributions of the top quarks in the MC samples after initial- and final-state radiation. The predictions for $p_T(t)$ and $m(t\bar{t})$ were calculated at NNLO in QCD with NLO EW corrections using the NNPDF3.0QED PDF set and dynamic renormalisation and factorisation scales of $m_T(t)/2$ for $p_T(t)$ and $H_T/4$ for $m(t\bar{t})$, as proposed in Ref. [68]. The prediction for $p_T(t\bar{t})$ was calculated at NNLO in QCD [14, 69] with the NNPDF3.0 PDF set and μ_r and μ_f set to $H_T/4$. All predictions assume $m_{\text{top}} = 173.3$ GeV. The reweighting was performed iteratively, ensuring that the reweighted MC sample agrees well with the higher-order predictions for each variable. The reweighted predictions are not equivalent to full NNLO+PS calculations but are used to estimate the effect of NNLO contributions on the measured observables. Since this reweighting is currently unavailable for tW production, the nominal tW DR POWHEG+PYTHIA 8 MC is used for this sample. While this sample, along with the MiNNLO_{PS} sample described below, improves the modelling accuracy of the $t\bar{t}$ component of the $WbWb$ process, it does not enhance the tW component. This sample is referred to as ‘PWG+PY8 (NNLO rew.)’.

$t\bar{t}$ NNLO+PS The first matched computation of top-quark pair production at NNLO in QCD, incorporating all-order radiative corrections through parton-shower simulations, is detailed in Ref. [70] and referred to as the MiNNLO_{PS} procedure. For generating this sample, the NNPDF3.0 NNLO PDF set was utilised, with PYTHIA 8.230 used for the fragmentation and underlying-event simulation. This sample was normalised to the same cross-section calculated with the Top++ 2.0 program at NNLO+NNLL in QCD, as previously mentioned. For the tW process, the nominal sample is used. This sample is referred to as ‘PWG+PY8 MiNNLO_{PS}’.

All the alternative samples were normalised to the same total cross-section as the nominal sample, with two exceptions: the PWG+PY8 mass variation samples, which were normalised to their respective higher-order cross-section calculations, and the PWG+PY8 $bb4l$ sample, which was normalised to the cross-section obtained directly from the MC simulation without corrections for higher-order calculations.

3.1.3 Background samples

Several processes share the same final state (two b -quarks, two charged leptons) as the $WbWb$ process. The events produced by these backgrounds need to be estimated and subsequently subtracted from the data to determine the $WbWb$ cross-sections. They are all estimated by using MC simulation. The processes considered are Z +jets production, diboson final states ($WW/ZZ/WZ$), $t\bar{t}$ produced in association with weak bosons ($t\bar{t} + W/Z/H$, collectively referred to as $t\bar{t}X$) and, for the background due to fake and non-prompt leptons, single-lepton $t\bar{t}$, tW and W +jets processes.

The production of Z +jets and W +jets events was simulated with the SHERPA 2.2.1 [71] generator using NLO matrix elements for up to two partons, and LO matrix elements for up to four partons calculated with the COMIX [72] and OPENLOOPS [73–75] libraries. They were matched with the SHERPA parton shower [76] based on Catani–Seymour dipole factorisation using the MEPS@NLO prescription [77–80] using the set of tuned parameters developed by the SHERPA authors. The NNPDF3.0NNLO set of PDFs was used and the samples were normalised to an NNLO prediction [81]. The Z +jets events lead to the same final state as the signal process when the Z boson decays into two τ -leptons, which in turn decay into an electron and a muon; on the other hand, W +jets events can mimic the signal signature only via the presence of fake or non-prompt leptons. The contribution from both processes is negligible in the signal regions considered.

The diboson processes were simulated with the SHERPA 2.2.2 and 2.2.1 generators including off-shell effects and Higgs boson contributions, where appropriate. The samples were generated by using matrix elements at NLO accuracy in QCD for up to one additional parton and at LO accuracy for up to three additional parton emissions. Samples for the loop-induced processes $gg \rightarrow VV$ were generated by using LO-accurate matrix elements for up to one additional parton emission for both fully leptonic and semileptonic final states. In this set-up, multiple matrix elements (NLO for up to one additional parton and LO for up to three additional partons) were matched and merged with the SHERPA parton shower. The virtual QCD corrections for matrix elements at NLO accuracy were provided by the OPENLOOPS library. The NNPDF3.0NNLO set of PDFs was used, along with a dedicated set of tuned parton-shower parameters developed by the SHERPA authors.

The production of $t\bar{t} + W/Z$ events was simulated using the MADGRAPH5_AMC@NLO 2.3.3 [82] generator at NLO with the NNPDF3.0NLO PDF set and interfaced to PYTHIA 8.210.

The production of $t\bar{t}H$ events was simulated using the PowHEG Box v2 [83] generator at NLO with the NNPDF3.0NLO PDF set interfaced to PYTHIA 8.230.

The background arising from events containing fake or non-prompt leptons, referred to as ‘Fakes’, is estimated by using MC simulations. Specifically, these are events where at least one reconstructed lepton does not match a generated lepton from the hard-scattering process. The samples used for this estimation include single-lepton $t\bar{t}$, tW , and W +jets processes, generated by using the same set-ups described earlier.

4 Object reconstruction and event selection

The following sections describe the detector- and particle-level objects used to characterise the final-state event topology and to define the fiducial phase-space regions for the measurements.

4.1 Detector-level object reconstruction

Events are required to have a primary vertex with at least two associated tracks. The primary vertex is selected as the one with the largest $\sum p_T^2$, where the sum is over all tracks with transverse momentum $p_T > 0.5 \text{ GeV}$ that are associated with the vertex. Events are considered only if they were accepted by at least one of the single-muon or single-electron triggers [31, 84, 85], which are highly efficient for leptons with $p_T^l > 27 \text{ GeV}$.

Electrons are identified using both the tracking information from the inner detector and energy deposits in the electromagnetic calorimeter [86]. The electrons are required to satisfy the reconstruction and identification quality requirements corresponding to the tight working point (WP) [87] and to have $|\eta| < 1.37$ or $1.52 < |\eta| < 2.47$ and $p_T > 28 \text{ GeV}$. To ensure that each reconstructed electron comes from a primary interaction vertex, tracks matched to electrons are required to satisfy $|z_0 \sin \theta| < 0.5 \text{ mm}$ and $|d_0|/\sigma(d_0) < 5$, where z_0 and d_0 are the longitudinal and transverse impact parameters of the electron track, respectively. Finally, each reconstructed event must satisfy the tight working point (*PLVTight*) of the isolation requirements based on boosted decision trees trained to separate prompt and non-prompt electrons and muons [88].

Muons are identified using the tracking information from the muon detector and the inner detector. The muons are required to satisfy the reconstruction and identification *Medium* quality requirement and to have $|\eta| < 2.5$ and $p_T > 28 \text{ GeV}$ [89, 90]. Muons are required to come from a primary vertex, by requiring the ID tracks to pass $|z_0 \sin \theta| < 0.5 \text{ mm}$ and $|d_0|/\sigma(d_0) < 3$, and to fulfil the *PLVTight* isolation requirement.

Jets are reconstructed using the anti- k_t algorithm [91] with radius parameter $R = 0.4$ implemented in FastJet [92] using particle flow objects (PFlow) [93]. To reduce the number of jets originating from pile-up, an additional selection criterion based on a jet-vertex tagging (JVT) technique is applied. The JVT is a likelihood discriminant that combines information from several track-based variables [94], and is only applied to jets with $p_T < 60 \text{ GeV}$ and $|\eta| < 2.4$. The jet energy and direction are calibrated using an energy- and η -dependent simulation-based calibration scheme with in situ corrections based on data [95]. Jets are required to have $p_T > 25 \text{ GeV}$ and $|\eta| < 2.5$.

The DL1r flavour tagging algorithm [96] is employed to identify jets containing b -hadrons. This tagger uses a deep neural network to exploit the distinctive features of b -hadrons, such as the impact parameters of tracks and the displaced vertices reconstructed in the inner detector. It also incorporates discriminating variables from a recurrent neural network, which capture spatial and kinematic correlations among tracks originating from the same b -hadron. For each jet, the algorithm computes a multivariate b -tagging discriminant, classifying the jet as b -tagged if this discriminant exceeds a predefined threshold. Operating points corresponding to b -tag efficiencies of 70% and 85% in $t\bar{t}$ MC events are used [97].

To avoid the reconstruction of the same energy deposits in the detector as multiple objects, overlap removal is applied first between electrons and muons that share a track, with the electron being removed in such cases. Next, if an electron is within $\Delta R = 0.2$ of one or more jets, the closest jet to the electron is removed. If there are still jets within $\Delta R = 0.4$ of the electron, the electron is removed. Jets with fewer than three tracks within $\Delta R = 0.4$ of muons are removed, whereas if the jet has at least three tracks, the muon is removed and the jet is retained.

The missing transverse energy E_T^{miss} in the event is the magnitude of the missing transverse momentum vector $\mathbf{p}_T^{\text{miss}}$, defined as the negative vector sum of the p_T of all selected and calibrated physics objects in

the event, with an extra track-based term added to account for soft energy in the event that is not associated with any of the selected objects [98].

4.2 Detector-level event selection

The event selection comprises a set of requirements based on the general event quality and on the reconstructed objects, defined in Section 4.1, that characterise the final-state event topology.

The analysis focuses on the $e\mu$ final state of the dileptonic decay channel, excluding the ee and $\mu\mu$ channels. The large number of events collected in the $e\mu$ channel allow for precise measurements while significantly reducing the impact of the Z +jets background, which is more prominent in the ee and $\mu\mu$ channels due to the presence of same-flavour leptons and contributes to the $e\mu$ channel through the Z boson decay into a pair of τ -leptons.

Each event is required to contain exactly one electron and one muon, of opposite electric charges, both with $p_T > 28 \text{ GeV}$, with at least one of the two leptons matched to an electron or muon trigger object.

Finally, at least two jets with $p_T > 25 \text{ GeV}$, b -tagged using the 70% WP, are required. This requirement is referred to as $N_{b\text{-tags}} \geq 2$, while the region defined by these requirements is referred to as the $2b$ -inclusive signal region.

A selection of detector-level event distributions after the full event selection is shown in Figure 2. The data and simulated distributions (obtained using both the DR and DS schemes for the simulation of the tW process) generally show good agreement. One exception is the lepton transverse momentum distribution, which appears softer in data compared to the nominal signal and background simulation. Similar discrepancies were observed in previous measurements at $\sqrt{s} = 13 \text{ TeV}$ [3, 99, 100]. Another exception is the b -tagged jet multiplicity distribution, which shows an excess in data compared to the simulation at higher multiplicity values. The impact of this mismodelling has been tested for all measured observables in this phase space and found to be negligible. For most distributions, no significant differences are observed between the DR and DS schemes. To enhance sensitivity to the interference between the $t\bar{t}$ and tW processes, the variable m_{\minimax}^{bl} is defined in a region with a veto on additional b -tagged jets, as described in the next section.

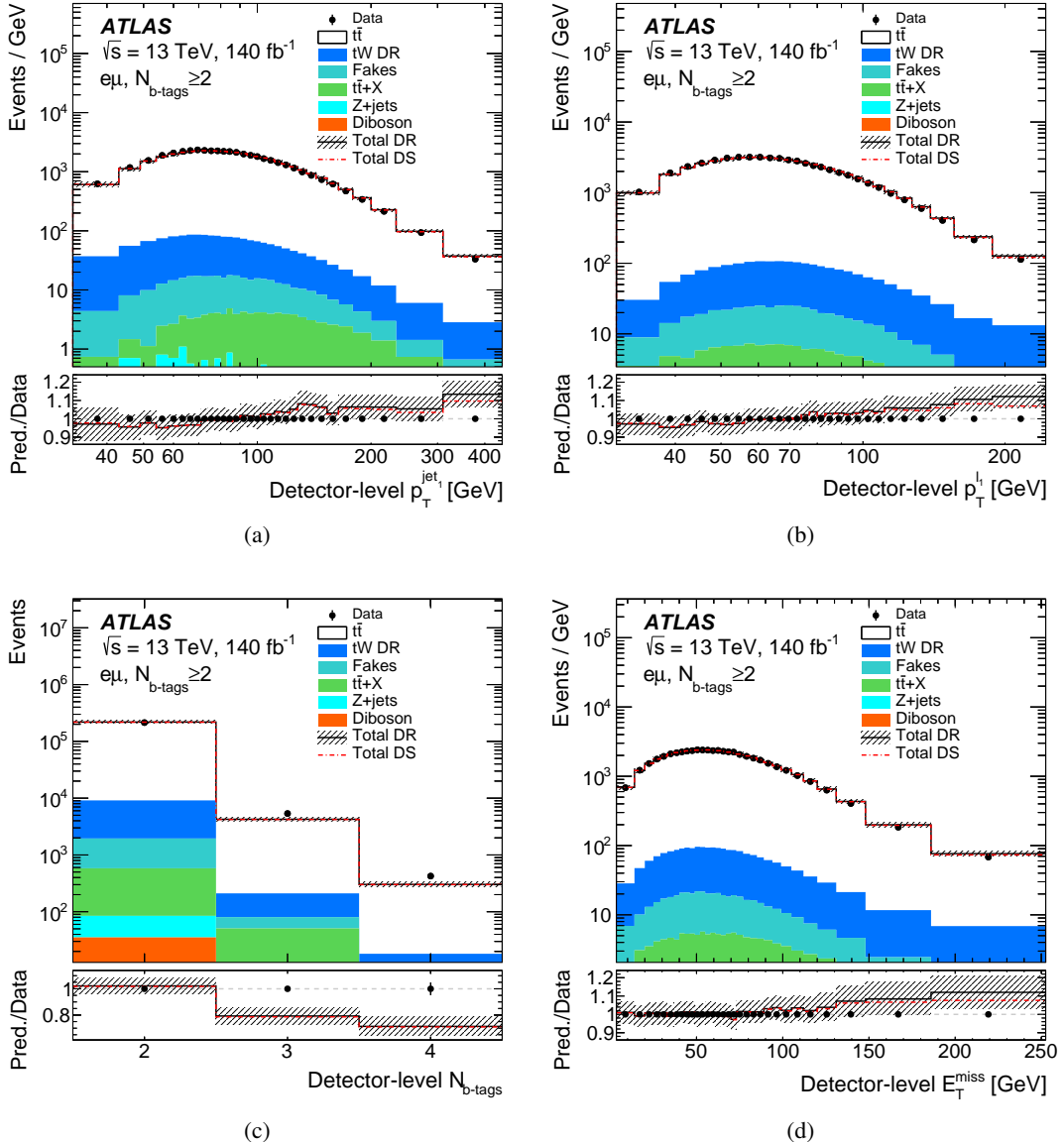


Figure 2: Comparison of data and MC predictions for the p_T of (a) the leading jet and (b) the leading lepton, (c) the number of b -tagged jets and (d) the E_T^{miss} in the 2 b -inclusive signal region. The total MC predictions are obtained by employing either the DR or DS schemes for the generation of the tW sample. The hatched area indicates the combined statistical and systematic uncertainties in the total prediction, excluding systematic uncertainties related to the signal modelling and normalisation. Events beyond the range of the horizontal axis are included in the last bin and their yield normalised to the bin width, for presentation purposes. The lower panels show the ratios of the predictions to the data.

4.3 Sensitivity to $t\bar{t}$ and tW interference

The observable that is most sensitive to the interference between double and single top production is m_{minimax}^{bl} and is defined as:

$$m_{\text{minimax}}^{bl} \equiv \min \left\{ \max \left(m^{b_1 l_1}, m^{b_2 l_2} \right), \max \left(m^{b_1 l_2}, m^{b_2 l_1} \right) \right\},$$

where b_i and l_i represent the two b -jets and two leptons, respectively. This definition ensures that, for doubly resonant events, the value of m_{minimax}^{bl} is constrained to be smaller than the mass of the top quark. For this reason, this variable is sensitive to the interference for high mass values (above about 180 GeV) due to the suppression of doubly resonant contributions. The sensitivity of m_{minimax}^{bl} to interference effects was first explored in Ref. [26]. However, the presence of additional b -jets in doubly resonant events can spoil the constraint, resulting in a high value of m_{minimax}^{bl} due to the combinatorics between b -jets and leptons. Moreover, given the sensitivity of m_{minimax}^{bl} to the number of b -tagged jets, limiting the signal region to events with exactly two b -tagged jets reduces the impact of the mismodelling of the b -tagged jet multiplicity at higher values, as shown in Figure 2(c). Therefore, a veto on additional b -jets is used to suppress the contributions of the combinatorics and enhance sensitivity to interference effects. Following a dedicated optimisation of the phase space, the best results are achieved by discarding events with additional b -tagged jets using the 85% WP. This additional requirement is referred to as $N_{b\text{-tags}} = 2$, while the region defined by these requirements is referred to as the $2b$ -exclusive signal region. This region is only used to measure the differential cross-section as a function of m_{minimax}^{bl} , while the differential cross-sections as a function of all other variables are measured in the $2b$ -inclusive region.

The detector-level distribution for the m_{minimax}^{bl} variable is shown in Figure 3 for events satisfying the $2b$ -exclusive selection. The comparison between predictions obtained with the DR and DS schemes shows the region of the distribution that is sensitive to the different schemes used to model the interference, while a selection of detector-level event distributions in the $2b$ -exclusive signal region are shown in Figure 4 for some object kinematic variables. In this case, no major difference is observed between the predictions obtained with the DR and DS schemes and the same level of agreement between data and MC predictions is observed as in the $2b$ -inclusive signal region.

The observed and expected numbers of events after the two event selections are shown in Table 1.

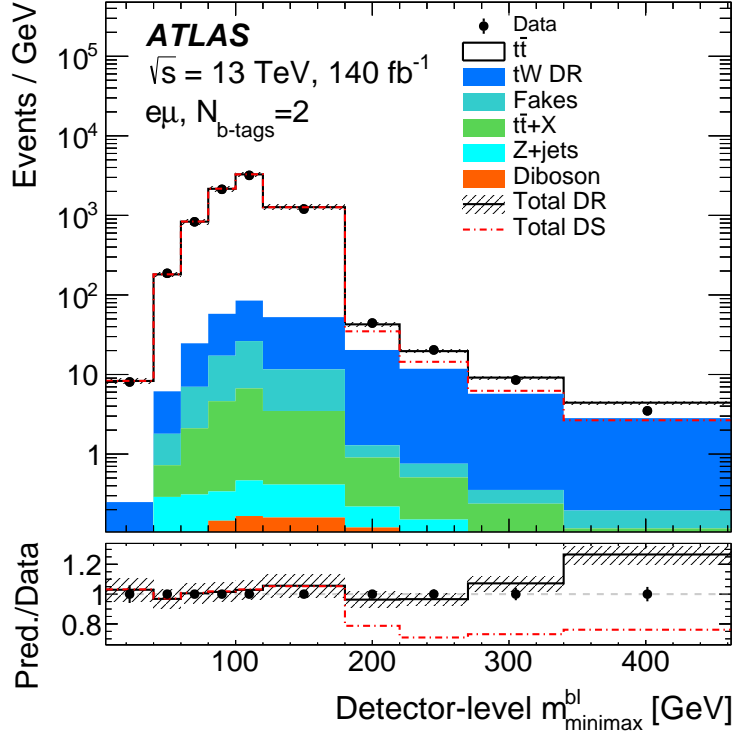


Figure 3: Comparison of data and MC predictions for the $m_{\text{minimax}}^{\text{bl}}$ variable in the 2 b -exclusive signal region. The total MC predictions are obtained by employing either the DR or DS schemes for the generation of the tW sample. The hatched area indicates the combined statistical and systematic uncertainties in the total prediction, excluding systematic uncertainties related to the signal modelling and normalisation. Events beyond the range of the horizontal axis are included in the last bin and their yield normalised to the bin width, for presentation purposes. The lower panel shows the ratio of the predictions to the data.

Table 1: Observed and expected number of events after both the event selections. The uncertainties include the MC statistical uncertainties and all systematic uncertainties except for the signal modelling and normalisation. The purity is defined as the ratio of the expected number of signal ($t\bar{t} + tW$) events to the expected number of total events.

Sample	$e\mu, N_{b\text{-tags}} = 2$		$e\mu, N_{b\text{-tags}} \geq 2$	
$t\bar{t}$	200000 ± 12000	($\pm 6\%$)	214000 ± 13000	($\pm 6\%$)
tW (DR)	6900 ± 400	($\pm 6\%$)	7300 ± 400	($\pm 6\%$)
$t\bar{t}X$	500 ± 70	($\pm 13\%$)	800 ± 110	($\pm 13\%$)
Diboson	32 ± 13	($\pm 40\%$)	36 ± 15	($\pm 40\%$)
Z+jets	47 ± 18	($\pm 40\%$)	51^{+20}_{-19}	($\pm 40\%$)
Fakes	1300 ± 700	($\pm 50\%$)	1400 ± 700	($\pm 50\%$)
Total expected	209000 ± 12000	($\pm 6\%$)	224000 ± 13000	($\pm 6\%$)
Purity	0.9910 ± 0.0031	($\pm 0.32\%$)	0.9898 ± 0.0032	($\pm 0.32\%$)
Data	202738		219882	
MC/Data	1.03 ± 0.06	($\pm 6\%$)	1.02 ± 0.06	($\pm 6\%$)

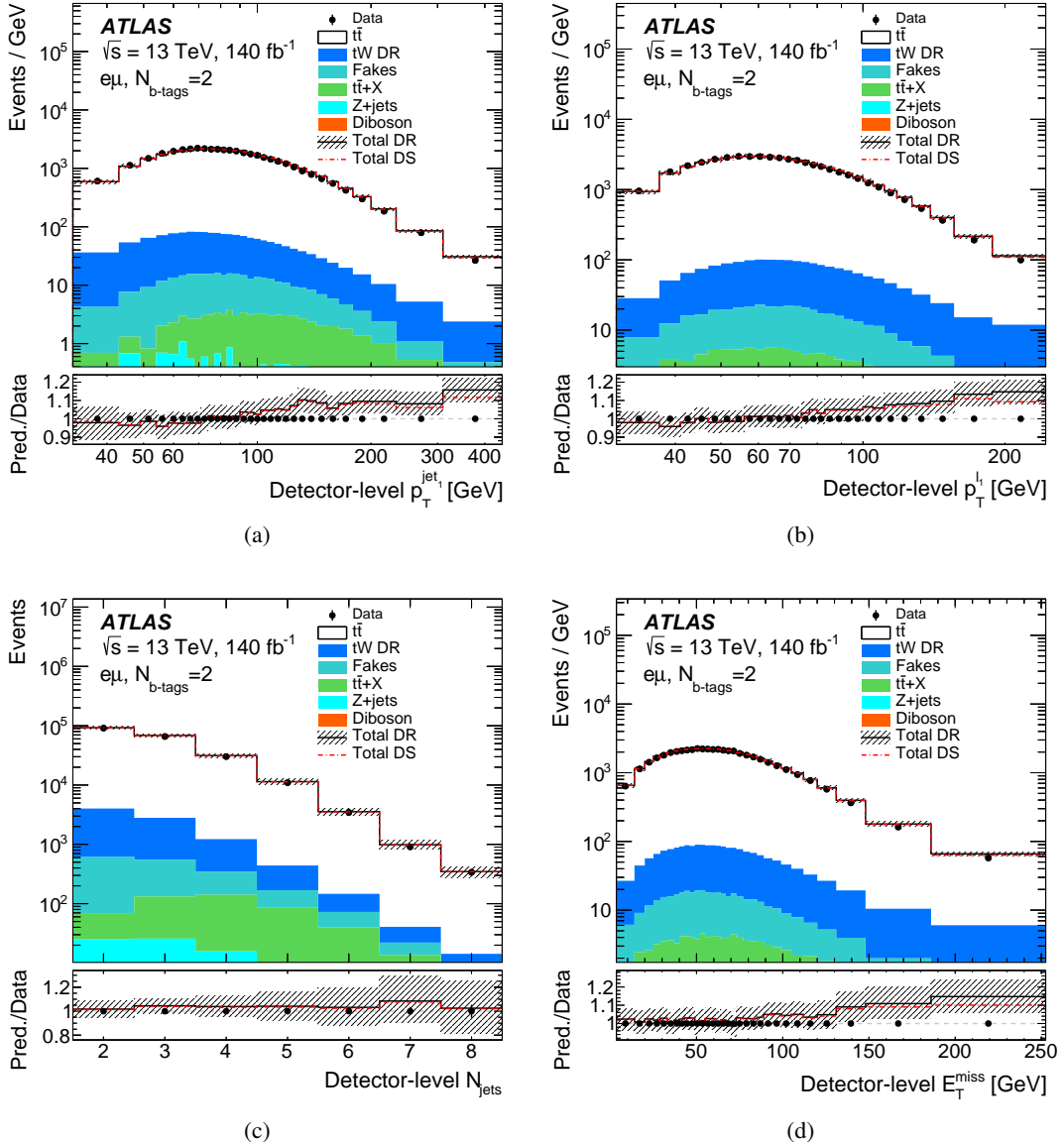


Figure 4: Comparison of data and MC predictions for the p_T of (a) the leading jet and (b) the leading lepton, (c) the number of jets and (d) the E_T^{miss} in the $2b$ -exclusive signal region. The total MC predictions are obtained by employing either the DR or DS schemes for the generation of the tW sample. The hatched area indicates the combined statistical and systematic uncertainties in the total prediction, excluding systematic uncertainties related to the signal modelling and normalisation. Events beyond the range of the horizontal axis are included in the last bin and their yield normalised to the bin width, for presentation purposes. The lower panels show the ratios of the predictions to the data.

4.4 Particle-level object definition

In addition to the detector-level objects, ‘particle-level’ objects are also defined. These objects are identified using generator-level information from stable particles in the generator record, defined as those that satisfy $c\tau > 10$ nm, with τ being the particle lifetime, without any simulation of their interaction with the detector components. The particle-level objects are used to define the fiducial phase-space regions and variables of interest for the measurements.

Particle-level electrons and muons are required to not originate from a hadron, either directly or via an intermediate τ -lepton decay. With this requirement, a τ -lepton is accepted as a parent of the electron or a muon only if the τ -lepton itself comes directly from a W . Leptons that come from a quark or hadron, including hadronically decaying τ -lepton, are rejected. With this definition, all particle-level leptons originate from the decays of EW bosons without requiring a direct match to a W boson. Their momentum is calculated to include the radiation loss due to final-state radiation (FSR) photons (‘dressing’), classified as photons within $\Delta R = 0.1$ that do not originate from hadron decays. The transverse momentum and η requirements are the same as the detector-level signal objects.

Particle-level jets are reconstructed by clustering generated particles (excluding those identified as leptons or neutrinos from EW boson decays), with the anti- k_t algorithm with a radius parameter of $R = 0.4$. The ghost-association procedure [101] is used to match b -hadrons with $p_T > 5$ GeV to jets where generator-level jet clustering is run as usual, except that the energy of all b -hadrons is set to a negligible value. All the particle jets containing a constituent b -hadron are considered b -tagged after this procedure.

The particle-level missing transverse momentum is calculated from the four-vector sum of all neutrinos, except those coming from hadron decays, either directly or via τ -lepton decays.

Particle-level objects are subject to different overlap removal criteria relative to detector-level objects, after dressing and jet reconstruction. Muons and electrons within $\Delta R = 0.4$ of a jet are excluded. No electron–muon overlap removal is applied at the particle level.

4.5 Particle-level selection

Using particle-level objects, two fiducial regions are defined by applying selections that replicate the detector-level ones as closely as possible:

- one electron and one muon with $p_T > 28$ GeV and $|\eta| < 2.5$;
- at least two jets with $p_T > 25$ GeV and $|\eta| < 2.5$;
- at least two jets tagged as b -jets with the b -hadron ghost-association matching;
- *only for $m_{\min\max}^{bl}$* : exactly two b -jets, tagged with the b -hadron ghost-association matching.

These requirements define the particle-level $2b$ -inclusive and $2b$ -exclusive fiducial regions, labelled as $e\mu, N_{b\text{-jets}} \geq 2$ and $e\mu, N_{b\text{-jets}} = 2$ respectively. The measured observables are unfolded to these phase spaces.

5 Cross-section extraction

The differential cross-sections are derived from detector-level events, which are corrected for detector and reconstruction effects—a process commonly referred to as ‘unfolding’. This correction accounts for efficiency, acceptance, and resolution effects, with the latter handled using an iterative Bayesian unfolding procedure [102], implemented via the `RooUnfold` package [103].

For each observable, the unfolding procedure starts from the number of events observed in data at detector level in bin j of the distribution (N_{data}^j), from which the background event yield (N_{bkg}^j), estimated as described in Section 3.1.3, is subtracted. Then the unfolding corrections, described below, are applied. All corrections are evaluated using the nominal Powheg+Pythia 8 MC simulation of the $t\bar{t} + tW$ signal sample.

As the first step, an acceptance correction (f_{acc}^j) is applied. The acceptance correction in bin j is defined as the fraction of signal events reconstructed in this bin that also satisfy the particle-level selection:

$$f_{\text{acc}}^j \equiv \frac{N_{\text{reco}\wedge\text{part}}^j}{N_{\text{reco}}^j}, \quad (1)$$

where $N_{\text{reco}\wedge\text{part}}^j$ is the number of events that satisfy both the detector-level selection and the particle-level selections in a given detector-level bin j , and N_{reco}^j is the number of events that satisfy the detector-level selection in the same bin. This correction is a bin-by-bin factor that accounts for events that are generated outside the fiducial phase-space region but satisfy the detector-level selection.

The resulting detector-level distribution is then corrected for the effects of the detector resolution to produce the particle-level distribution. The procedure uses as input a migration matrix \mathcal{M} derived from the simulated signal sample that maps the particle-level bin i in which an event is generated to the bin j in which it is reconstructed. The probability for particle-level events to be reconstructed in the same bin is represented by the diagonal elements, and the off-diagonal elements describe the fraction of particle-level events that migrate into other bins. Therefore, the elements of each row sum to unity. The procedure is performed via the iterative Bayesian unfolding, using four iterations to balance the stability relative to the previous iteration and the growth of the statistical uncertainty. The effect of varying the number of iterations by one is found to be negligible.

Finally, an efficiency correction ε is applied to the unfolded spectrum, correcting the result by a bin-by-bin factor to the fiducial phase space. The efficiency correction in bin i is defined as the fraction of the events generated in a particle-level bin i that satisfy the detector-level selection:

$$\varepsilon^i \equiv \frac{N_{\text{part}\wedge\text{reco}}^i}{N_{\text{part}}^i},$$

where $N_{\text{part}\wedge\text{reco}}^i$ is the number of events that satisfy both the particle-level selection and the detector-level selection in a given particle-level bin i , and N_{part}^i is the number of events that satisfy the particle-level selection in the same bin. This factor corrects for the inefficiency of the event selection and reconstruction.

The absolute differential cross-section is then obtained by dividing the unfolded distribution by the integrated luminosity and the bin width. The extraction of the absolute differential cross-section for an

observable X at particle-level is then given by the following expression:

$$\frac{d\sigma_{\text{fid}}^i}{dX^i} \equiv \frac{1}{\mathcal{L} \cdot \Delta X^i} \cdot \frac{1}{\varepsilon^i} \cdot \sum_j \mathcal{M}^{-1} \cdot f_{\text{acc}}^j \cdot \left(N_{\text{obs}}^j - N_{\text{bkg}}^j \right), \quad (2)$$

where the index j iterates over bins of observable X at detector level while the index i labels bins at particle-level, ΔX^i is the bin width, \mathcal{L} is the integrated luminosity and \mathcal{M}^{-1} is the inverted migration matrix obtained from the iterative unfolding procedure. The integrated fiducial cross-section is obtained by integrating the unfolded cross-section over the bins, and its value is used to compute the normalised differential cross-sections:

$$\frac{1}{\sigma_{\text{fid}}^i} \cdot \frac{d\sigma_{\text{fid}}^i}{dX^i}.$$

This definition is applied for all uncertainties affecting the measurement, ensuring that the correlation between the uncertainties in the integrated fiducial cross-section (σ_{fid}) and the differential cross-section in each bin ($d\sigma_{\text{fid}}^i$) is accounted for. This correlation can lead to a partial cancellation of uncertainties when computing the normalised differential cross-sections, thereby reducing their overall impact compared to the absolute differential cross-sections.

5.1 Measured distributions at the particle level

A total of 11 observables are chosen for the differential cross-section measurement.

The differential cross-section as a function of the m_{minimax}^{bl} variable is measured in the $2b$ -exclusive fiducial phase space, while differential cross-sections as a function of variables related to the number of jets and the kinematics of jets, leptons and $E_{\text{T}}^{\text{miss}}$, are measured in the $2b$ -inclusive fiducial phase space. Specifically, these are:

- $p_{\text{T}}^{\text{jet}_1}$: transverse momentum of the leading jet;
- $p_{\text{T}}^{\text{jet}_2}$: transverse momentum of the subleading jet;
- $p_{\text{T}}^{l_1}$: transverse momentum of the leading lepton;
- $p_{\text{T}}^{l_2}$: transverse momentum of the subleading lepton;
- m_{T}^{bb4l} : transverse mass m_{T} of the $bb4l$ system, with $m_{\text{T}} = \sqrt{E^2 - p_z^2} = \sqrt{p_{\text{T}}^2 + m^2}$. The $bb4l$ system is built as the vector sum of the four-momenta of the leading and subleading b -jets, the two charged leptons, and the $E_{\text{T}}^{\text{miss}}$ as a proxy for the neutrinos;
- p_{T}^{bb4l} : transverse momentum of the $bb4l$ system;
- p_{T}^{bb} : transverse momentum of the b -jet pair, built using the leading and subleading b -jets;
- p_{T}^{bbll} : transverse momentum of the $bbll$ system, built using the leading and subleading b -jets and the two charged leptons;
- m_{T}^{bbll} : invariant mass of the $bbll$ system;
- N_{jets} : number of jets.

These observables are selected to cover several aspects of the modelling of the $t\bar{t}$ and tW processes, including their interference effects. Some of the observables are chosen based on their sensitivity to specific theoretical uncertainties or discrepancies observed in previous measurements, while others are selected because they show significant differences among the predictions from various MC models.

For each observable, the binning is chosen to guarantee good diagonality of the migration matrix and to ensure a sufficient number of events in each bin. The binning is optimised to balance statistical precision and resolution effects, and it is validated using the same procedures described in Ref. [2]. For all the observables, the first and last bins do not contain under- and overflow events, except for the number of jets, where the last bin includes overflow events.

5.2 Unfolding corrections

Examples of acceptance, efficiency, and migration matrices for the m_{minimax}^{bl} variable (in the $2b$ -exclusive region) are shown in Figure 5, and for the number of jets (in the $2b$ -inclusive region) in Figure 6. The low values for the efficiency, in Figures 5(b) and 6(b), averaging at around 23%, are mostly related to the requirements of having two isolated leptons and two b -tagged jets. The acceptance and efficiency corrections are compared with those obtained with various MC generators used to evaluate the signal modelling uncertainties. This comparison illustrates the impact of signal modelling variations on the final measurement.

In Figure 5, a sharp drop in the acceptance and efficiency corrections at high values of m_{minimax}^{bl} is observed. This drop is primarily due to the $t\bar{t}$ component of the sample, which populates the high- m_{minimax}^{bl} region when at least one of the two b -tagged jets in the event does not originate from the decay of a top quark. For such events to enter the $2b$ -exclusive region, a third b -jet from radiation must be present, and one of the b -jets from the top-quark decay must not be selected. The latter requirement significantly reduces the probability of these events satisfying the selection criteria at both particle- and detector-level, leading to the observed low acceptance and efficiency. For the rest of the variables, where the separation between $t\bar{t}$ and tWb is less pronounced, the acceptance and efficiency corrections are more stable across the phase space, as shown in Figure 6 for the number of jets.

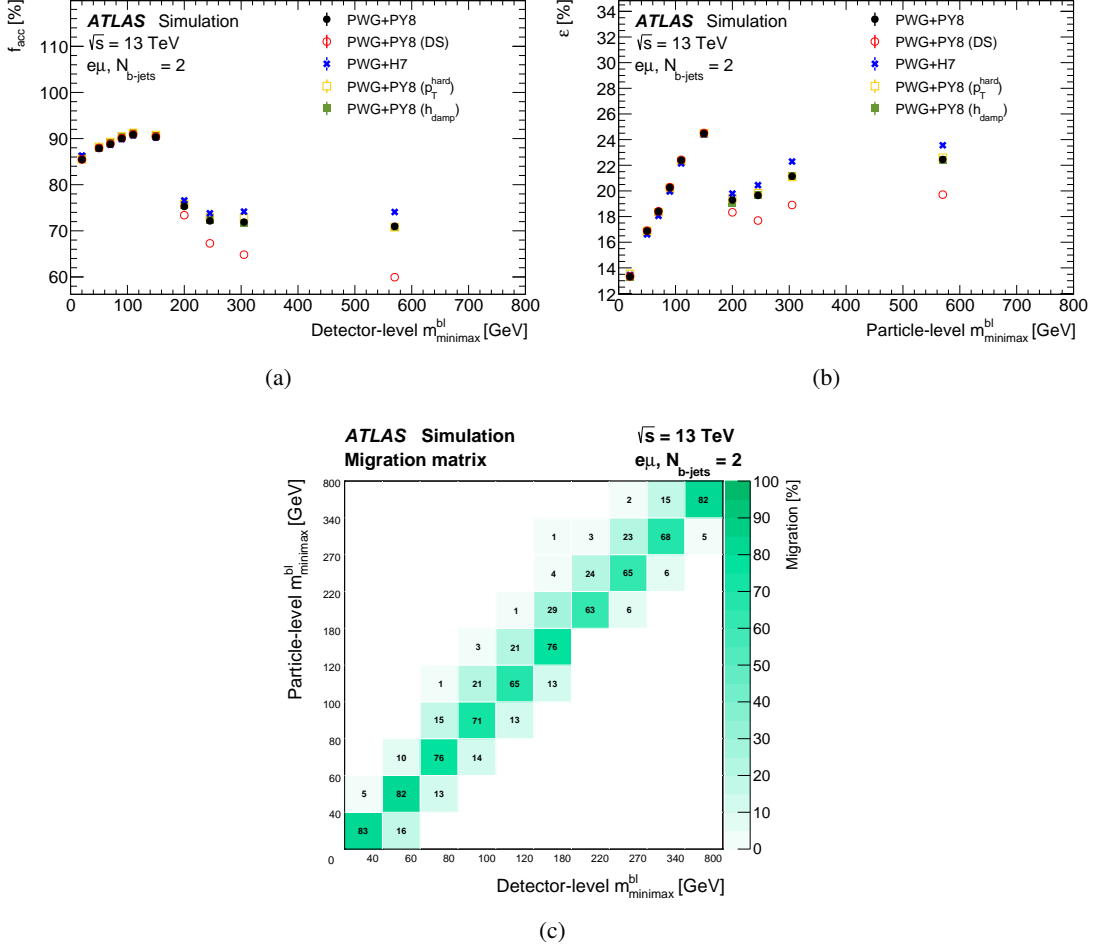


Figure 5: The (a) acceptance (f_{acc}) and (b) efficiency (ε) corrections and (c) the migration matrix for the $m_{minimax}^{bl}$ variable in the $2b$ -exclusive region. The nominal acceptance and efficiency corrections, provided by Powheg+Pythia 8 with the DR scheme, are compared with the corrections obtained with some MC generators used to evaluate the signal modelling uncertainties. In the migration matrix, only bins where the migration is greater than 1% are shown.

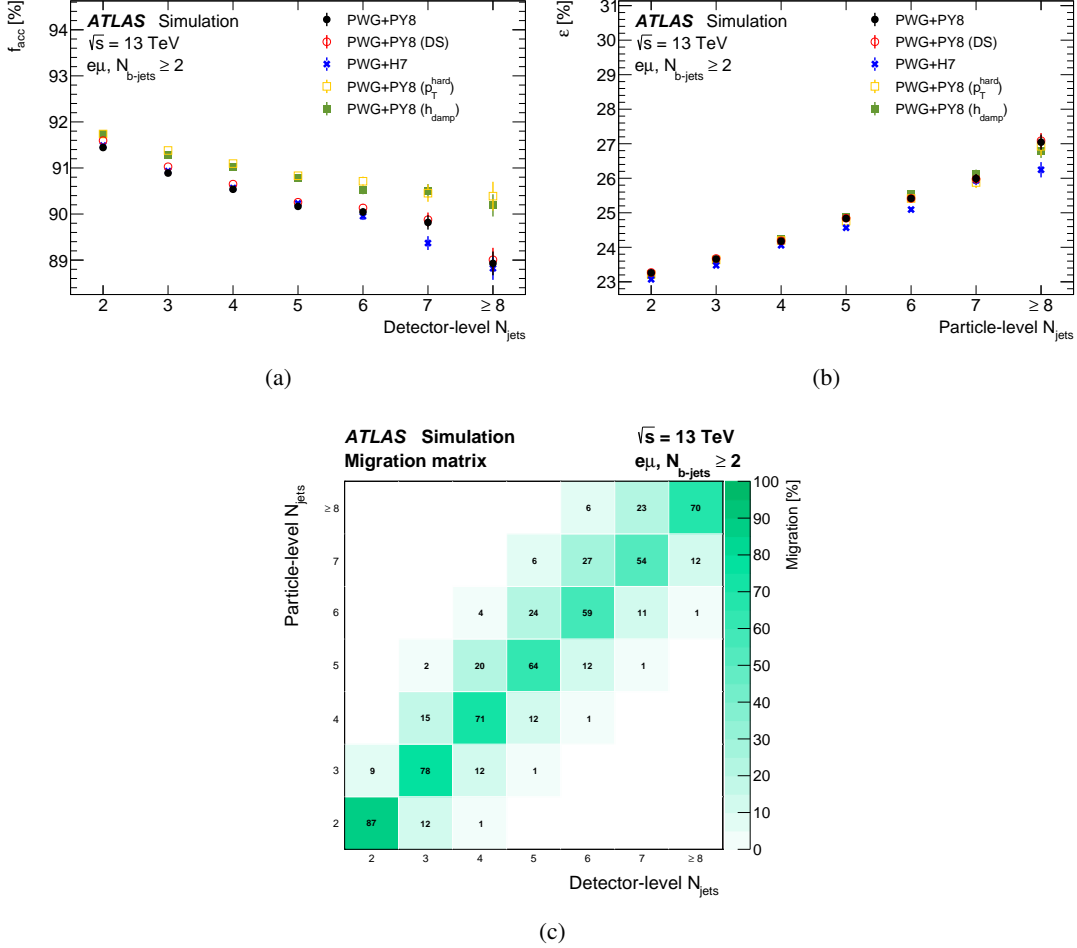


Figure 6: The (a) acceptance (f_{acc}) and (b) efficiency (ε) corrections and (c) the migration matrix for the N_{jets} variable in the $2b$ -inclusive region. The nominal acceptance and efficiency corrections, provided by Powheg+Pythia 8 with the DR scheme, are compared with the corrections obtained with some MC generators used to evaluate the signal modelling uncertainties. In the migration matrix, only bins where the migration is greater than 1% are shown.

5.3 Systematic uncertainties

This section describes the estimation of systematic uncertainties related to object reconstruction and calibration, signal modelling, and background estimation.

5.3.1 Uncertainty propagation

To evaluate the impact of each uncertainty after the unfolding, the reconstructed signal and background distributions in simulation are varied and unfolded using corrections from the nominal PowHEG+PYTHIA 8 signal sample. The unfolded distribution is compared with the corresponding particle-level spectrum, and the relative difference is assigned as the uncertainty in the measured distribution. For single-sided systematic uncertainties, such as most of the signal modelling ones, the relative difference is symmetrised to obtain a two-sided uncertainty. All detector- and background-related systematic uncertainties are evaluated using the same generator, while alternative generators and generator set-ups are employed to assess modelling systematic uncertainties. In these cases, the corrections derived from the nominal generator are used to unfold the detector-level spectra of the alternative generator, and the comparison between the unfolded distribution and the alternative particle-level spectrum is used to assess the corresponding uncertainty.

5.3.2 Object reconstruction and calibration

Leptons and E_T^{miss} Electrons and muons both have uncertainties associated with the understanding of the energy/momentum scale and resolution [86, 90]. These uncertainties are calculated by modifying the momentum of the reconstructed leptons and propagating these changes through the analysis chain. The lepton reconstruction efficiency in simulated events is corrected by scale factors derived from measurements of these efficiencies in data using a control region enriched in $Z \rightarrow ee$ and $Z \rightarrow \mu\mu$ events [87, 89]. The calibration of the efficiency of the lepton reconstruction and identification comes with associated uncertainties, and these are propagated via changes to the scale factors for the leptons. Similarly, the scale factors for the trigger efficiencies are varied to account for uncertainties in the measurements of the efficiencies of the lepton triggers [84, 85].

The uncertainty associated with E_T^{miss} is calculated by propagating the energy scale and resolution systematic uncertainties to all jets and leptons in the E_T^{miss} calculation. Additional E_T^{miss} uncertainties arising from tracks not associated with any reconstructed objects are also included [98].

Jets The impact of the uncertainty in the jet energy scale (JES) and resolution (JER) is estimated by varying the jet energies according to the uncertainties derived from simulation and in situ calibration measurements [95], parameterised by 30 independent variations for the JES and 13 for the JER. The JER uncertainty is evaluated by smearing both the (pseudo-)data and MC events. The uncertainty originating from the JVT requirement on jets is assessed by varying its associated scale factor [94].

Flavour tagging Differences in the b -tagging efficiencies between the data and simulation are corrected using scale factors [97, 104, 105]. The corrections are applied for the tagging efficiency of b -jets and the mis-tag rates of c - and light-jets, with corresponding uncertainties derived for each jet flavour. A principal component analysis is performed to diagonalise the covariance matrix given the input systematic uncertainties considered in the calibration of the tagging efficiencies. This results in a number of orthogonal eigen-variations for each jet flavour, which are then used as separate two-sided uncertainties. Three additional components are considered, corresponding to the uncertainties associated with the efficiency extrapolation to high jet p_T (> 400 GeV), derived separately for b -jets, c - and light-jets.

Pile-up Variations of the scale factors used to match the pile-up to the data are used to evaluate the uncertainty in the pile-up modelling.

5.3.3 Signal modelling uncertainties

A limited understanding of the modelling of signal processes is a significant source of uncertainty. The impact of these uncertainties is evaluated using alternative predictions, as described in Section 3.1, following the procedure outlined above. Signal modelling uncertainties affecting both the $t\bar{t}$ and tW processes are classified as ‘hard scattering’ when they affect the matching of the matrix element and parton shower, ‘parton shower’ when they affect the parton showering and hadronisation, and ‘generator parameters’, when they affect other settings of the PowHEG+PYTHIA 8 generator. All these uncertainties are considered correlated between the $t\bar{t}$ and tW processes. Uncertainties affecting only the modelling of the $t\bar{t}$ and tW processes are classified as ‘ $t\bar{t}$ modelling’ and ‘ tW modelling’, respectively.

Hard scattering The uncertainty related to the matrix-element calculation and the parton-shower matching procedure is evaluated by comparing the nominal sample with an alternative sample obtained by setting the $p_{T,\text{hard}}$ parameter in PYTHIA 8 to 1. This parameter regulates the definition of the vetoed region of the showering, and its variation is based on the studies described in Ref. [63].

Parton shower The uncertainty due to the choice of the hadronisation model and other non-perturbative aspects of the parton shower is evaluated using the PowHEG+HERWIG 7.1.3 samples for the $t\bar{t}$ and tW processes.

Generator parameters The uncertainty due to the choice of the μ_r and μ_f scales in the hard scatter is evaluated using predictions obtained with PowHEG+PYTHIA 8, where μ_r and μ_f in the hard scatter are varied independently by a factor 0.5 and 2. The uncertainties in the initial-state radiation are obtained by varying the scales in the showering model according to the Var3c eigentune of the A14 tune [106].

The uncertainties in the tuning of final-state radiation in the parton shower are obtained by changing the momentum scale settings of μ_r^{FSR} in PYTHIA 8 by a factor of 0.5 or 2 relative to the nominal scale. Another parameter affecting the modelling of the additional radiation in PowHEG+PYTHIA 8 is h_{damp} . The uncertainty due to the choice of this parameter is estimated by using a dedicated PowHEG+PYTHIA 8 sample where h_{damp} is multiplied by a factor of two relative to the nominal value.

The uncertainty due to the choice of the top-quark mass in the MC simulations is estimated by using two additional simulation samples, for both the $t\bar{t}$ and tW processes, with varied top-quark mass values of 169 GeV and 176 GeV which, besides the mass of the top quark, have the same set-up as the nominal sample. The final uncertainty is then scaled by 1/7 to match the effect of a ± 0.5 GeV shift in the top-quark mass, reflecting the precision of the top-quark mass measurements performed by ATLAS and CMS [107, 108]. The impact of the choice of different PDF sets is assessed by applying an event-by-event reweighting procedure to the nominal Powheg+Pythia 8 $t\bar{t}$ and tW samples following the PDF4LHC15 prescription [109] and using the PDF4LHC15_30 sets.

tW modelling A significant component of the uncertainty is represented by the difference between the DR and DS approaches, used to remove the overlap between the $t\bar{t}$ and tW samples. The tW (DS) sample is used instead of the tW (DR) to form the alternative signal, with $t\bar{t}$ remaining the nominal for the alternative sample.

Signal normalisation Differential cross-section measurements, performed by unfolding background-subtracted distributions in data, are typically insensitive to the overall normalisation of the signal sample. This is because the signal sample contributes to the unfolding only through efficiency, acceptance, and migration corrections. These corrections, being ratios of yields, do not depend on the total cross-section. This principle holds when the signal sample consists of a single process, as in the case of $t\bar{t}$ differential cross-sections. However, in this analysis, the signal comprises the sum of two processes: the tW and $t\bar{t}$ production. This composition makes the unfolding corrections sensitive to the relative normalisation between the two processes. Consequently, two sources of systematic uncertainty are considered: ‘ $t\bar{t}$ normalisation’ and ‘ tW normalisation’, and assigned to the ‘ $t\bar{t}$ modelling’ and ‘ tW modelling’ categories, respectively. These uncertainties are estimated by independently varying the normalisation of the $t\bar{t}$ and tW samples, while keeping the normalisation of the other sample fixed to its nominal value. The variations are defined by rescaling the samples by $1 \pm \delta_{xs}$, where δ_{xs} is the relative error on the $t\bar{t}$ (NNLO+NNLL) and tW (NLO+NNLL) cross-sections, amounting to 5.2% and 3.5% respectively, as described in Section 3.1.1.

5.3.4 Uncertainties in the background processes

A global uncertainty, accounting for variations in PDFs, α_s , μ_f and μ_r , is applied to the MC prediction of the Z+jets background components. This uncertainty is parameterised as a function of the number of jets in the event, as calculated in Ref. [110].

A conservative normalisation uncertainty of 50% is applied to the diboson background, including the uncertainty in the cross-section and a contribution due to the presence of additional jets, as discussed in Ref. [111].

The uncertainties in the cross-section calculation for the processes $t\bar{t}Z$, $t\bar{t}W$ and $t\bar{t}H$ composing the $t\bar{t}X$ sample are respectively 13.3%, 12.5%, and 9.9% [112]. A conservative uncertainty of 13.3% is assigned to all the processes contributing to the $t\bar{t}X$ background.

Finally, a 50% normalisation uncertainty is assigned to the background due to fake and non-prompt leptons to reflect the uncertainty in evaluating it from MC. This is validated in regions with similar kinematic requirements as the signal regions but with the two leptons of the same charge, where the contribution of

events with fake/non-prompt leptons is expected to dominate, contributing around 60% of the total event yield.

5.3.5 Other uncertainties

The uncertainty due to the number of data events is propagated through the unfolding by creating Poisson-smeared pseudo-experiments that are passed through the unfolding procedure. For normalised differential cross-sections, the normalisation procedure is applied for each pseudo-experiment. The procedure is replicated 10k times, then the final statistical uncertainty is evaluated from the standard deviation in each bin over the 10k pseudo-experiments.

To account for the limited number of events in the MC samples, pseudo-experiments are used to evaluate the impact of finite number of events. The number of events in each bin is smeared by a Gaussian distribution with mean equal to the yield of the bin, and standard deviation equal to the uncertainty of the bin. The resulting systematic uncertainty is found to be negligible in most cases.

The uncertainty in the combined 2015–2018 integrated luminosity is 0.83% [34], obtained using the LUCID-2 detector [30] for the primary luminosity measurements, complemented by measurements using the inner detector and calorimeters. This uncertainty is propagated to the unfolded results by varying the luminosity by $\pm 0.83\%$ in the reconstructed simulated spectra and unfolding them using the nominal corrections.

5.4 Uncertainty summary

The breakdown of the impact of the different categories of uncertainties is shown in Figure 7 for the measured normalised differential cross-section as a function of $m_{\min\max}^{bl}$ and the leading lepton p_T . For clarity, only the most relevant contributions are shown.

As shown in Figure 7(a), in the last four bins of the $m_{\min\max}^{bl}$ distribution that are most sensitive to the interference, the uncertainty is dominated by the modelling uncertainties, in particular those related to the choice of the scheme used to treat the $t\bar{t}/tW$ interference, the parton shower, and those related to the matrix element matching, and by the statistical uncertainty. The total uncertainty is around 10% or lower in all bins except the first one, which is a significant reduction compared to the same region of phase space measured in Ref. [26] where the uncertainty was above 20%. This significant improvement is achieved due to the new modelling uncertainties and improved object calibrations and to an optimisation of the selection and binning of the distribution. In the lower mass region, the total uncertainty is dominated by the jet and parton shower uncertainties.

For the other distributions, the uncertainties are dominated by jet uncertainties, especially for jet observables, and modelling uncertainties, especially in the tails of the distributions. The statistical component can also be significant in the extreme regions of phase space, as visible in the subleading jet p_T breakdown plot shown in Figure 7(b). For these distributions, the total uncertainties are also below 10% in almost all the bins.

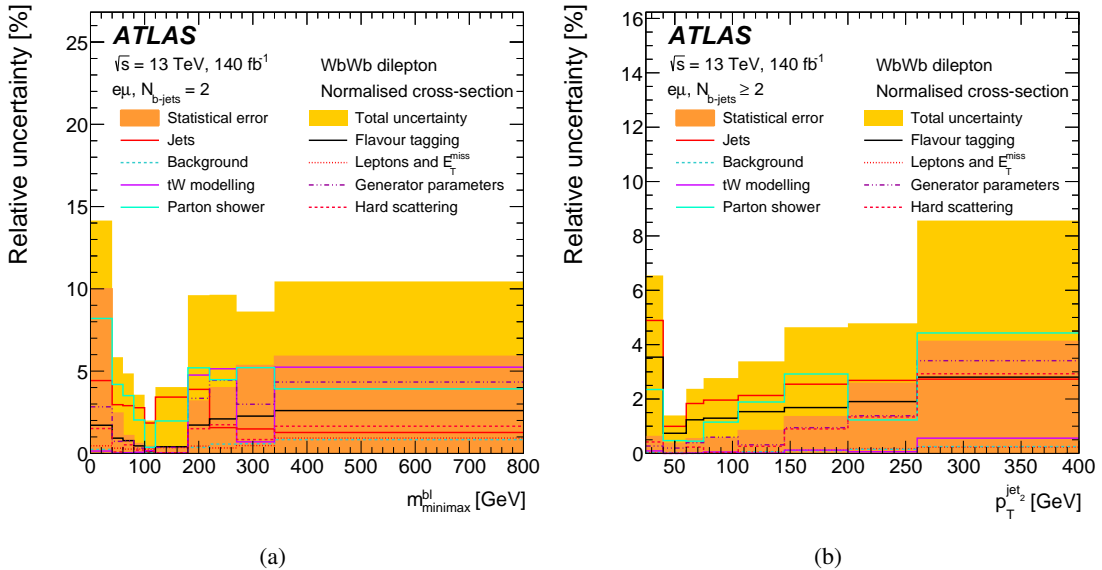


Figure 7: Uncertainties in the particle-level normalised differential cross-sections as a function of (a) m_{\minim}^{bl} and (b) the subleading jet p_T . The bands represent the statistical and total uncertainty in the data.

6 Results

The measured normalised differential cross-sections are presented in Sections 6.2 and 6.3. The agreement of the different models with the measured differential cross-sections is assessed by computing the χ^2 , and corresponding p -values, of the measured differential cross-sections relative to theoretical predictions employing the full experimental covariance matrix. The χ^2 values are computed for the specific sample configurations described, without including theoretical uncertainties. This approach avoids assumptions about the correlation schemes for each comparison and ensures clarity in the interpretation of the results.

To facilitate comparisons with any future MC generator predictions, all differential cross-section measurements, both normalised and absolute, together with the experimental covariance matrices and full uncertainty breakdown, will be published in HEPData [113].

6.1 χ^2 calculation

The level of agreement between the measured cross-sections and the NLO+PS predictions is evaluated using a χ^2 test statistic. The p -value is extracted from the χ^2 and number of degrees of freedom (NDF), with the NDF equal to the number of bins (N_b) in the case of the absolute differential cross-sections. The χ^2 is computed using the formula:

$$\chi^2 = \mathbf{V}^T \times \mathbf{C}^{-1} \times \mathbf{V}$$

where \mathbf{V} represents the vector of residuals, defined as the difference between the measured differential cross-section and the prediction, and \mathbf{C} is the covariance matrix, which is built from the uncertainties described in the previous section.

Table 2: χ^2 and p -values quantifying the level of agreement between the measured normalised differential cross-sections and predictions for the m_{minimax}^{bl} variable.

Models	χ^2/NDF	p -value
PWG+PY8	12.8/9	0.17
PWG+PY8 (DS)	39.1/9	<0.01
PWG+PY8 ($bb4l$)	28.6/9	<0.01
PWG+PY8 (NNLO rew.)	12.8/9	0.17
PWG+PY8 MiNNLO _{PS}	17.6/9	0.04

For normalised differential cross-sections, the vector of differences between data and predictions \mathbf{V}_{N_b} is replaced with \mathbf{V}_{N_b-1} , which is the same quantity but obtained by discarding the last one of the N_b elements. Consequently, \mathbf{C}_{N_b-1} is the $(N_b - 1) \times (N_b - 1)$ sub-matrix derived from the full covariance matrix of the normalised measurements by discarding the corresponding row and column. The sub-matrix obtained in this way is invertible and allows the χ^2 to be computed. The χ^2 value does not depend on the choice of the element discarded for the vector \mathbf{V}_{N_b-1} and the corresponding sub-matrix \mathbf{C}_{N_b-1} . In this case, the NDF becomes $N_b - 1$.

6.2 Differential cross-sections in the $2b$ -exclusive region

The measured normalised differential cross-section as a function of m_{minimax}^{bl} , in the $2b$ -exclusive fiducial phase space, is shown in Figure 8. The measurement is compared with PowHEG+PYTHIA 8 predictions obtained by employing different interference schemes (namely $t\bar{t} + tW$ DR and DS and the full $bb4l$ final state) and by including higher-order corrections for the $t\bar{t}$ component, either by using the MiNNLO_{PS} method or the NNLO reweighting.

The χ^2 and p -values for the normalised differential cross-sections are summarised in Table 2. Among the available predictions, the sample where the tW process is simulated using the DR scheme exhibits the best agreement with the data. However, it still fails to accurately describe the shape of the tail of the m_{minimax}^{bl} distribution. It is worth highlighting the PWG+PY8 ($bb4l$) sample, which, while expected to be the most accurate model for describing the interference, does not fulfil this expectation. The PWG+PY8 ($bb4l$) prediction underestimates the cross-section in the tail of the distribution where the impact of the interference is larger. This measurement will be crucial for improving future versions of this generator.

No major difference relative to the nominal PowHEG+PYTHIA 8 sample is observed when comparing the predictions obtained with the samples where the $t\bar{t}$ process is modelled at NNLO either via the PWG+PY8 MiNNLO_{PS} MC or NNLO reweighting.

The PWG+PY8 (DS) prediction is the least compatible with the data and shows the worst agreement with the data above 180 GeV.

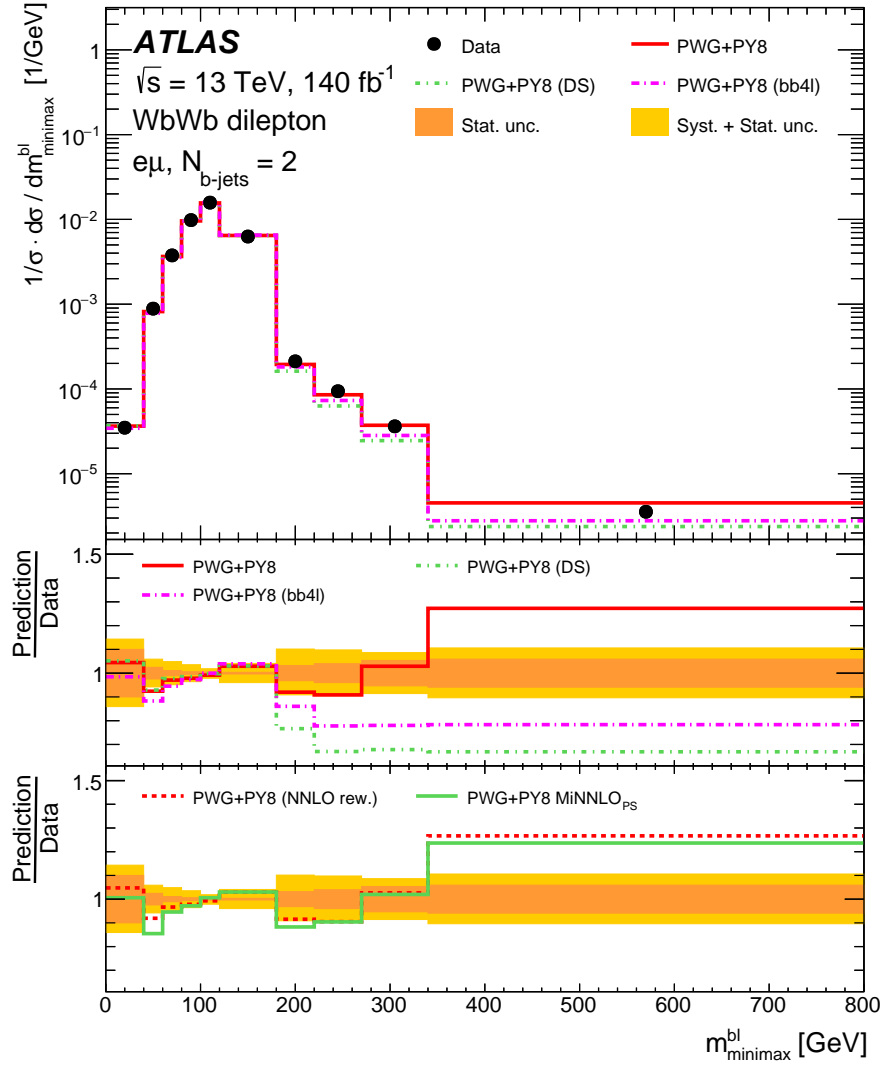


Figure 8: Relative differential cross-section measurement as a function of the m_{\minimax}^{bl} variable. The cross-section is unfolded to particle-level in the fiducial phase space. The measurement is compared with predictions provided by Powheg+Pythia 8 with different schemes for computing the $t\bar{t}/tW$ interference and with predictions where the $t\bar{t}$ component is simulated with an NNLO+PS MC generator or corrected to NNLO. The lower panels show the ratios of the predictions to the data with the bands showing the statistical and total uncertainties in the data.

6.3 Differential cross-sections in the 2b-inclusive region

The measured normalised differential cross-sections as a function of the kinematic variables of the $WbWb$ final-state objects, measured in the 2b-inclusive phase space, are presented in Figure 9 for the leading lepton and sub-leading lepton p_T and in Figure 10 for the leading jet and sub-leading jet p_T . Differential cross-sections as a function of the jet multiplicity are shown in Figure 11(a). Differential cross-sections as a function of additional variables, typically used for MC optimisation, are also measured. Specifically:

- the cross-sections as a function of the p_T of the bb system are shown in Figure 11(b)

Table 3: χ^2 and p -values quantifying the level of agreement between the measured normalised differential cross-sections and predictions provided by Powheg+Pythia 8 with different schemes for computing the $t\bar{t}/tW$ interference.

Observable	PWG+PY8		PWG+PY8 (DS)		PWG+PY8 ($bb4l$)	
	χ^2/NDF	p -value	χ^2/NDF	p -value	χ^2/NDF	p -value
N_{jets}	8.7/6	0.19	7.5/6	0.28	20.8/6	<0.01
m_{bbll}^{bl}	28.1/15	0.02	26.2/15	0.04	23.8/15	0.07
m_T^{bb4l}	18.9/12	0.09	13.1/12	0.36	12.2/12	0.43
p_T^{bb}	12.1/8	0.15	2.5/8	0.96	6.2/8	0.62
$p_T^{\text{jet}_1}$	16.4/7	0.02	16.8/7	0.02	15.1/7	0.03
$p_T^{\text{jet}_2}$	4.3/7	0.75	4.5/7	0.72	5.0/7	0.66
p_T^{bb4l}	50.6/8	<0.01	50.8/8	<0.01	122.9/8	<0.01
p_T^{bbll}	36.2/10	<0.01	30.5/10	<0.01	93.6/10	<0.01
$p_T^{l_2}$	23.5/11	0.02	19.1/11	0.06	15.5/11	0.16
$p_T^{l_1}$	39.4/15	<0.01	28.8/15	0.02	21.1/15	0.13

- the cross-sections as a function of the p_T and m_T of the $bb4l$ system are shown in Figure 12;
- the cross-sections as a function of the p_T and mass of the $bbll$ system are shown in Figure 13.

The compatibility with the data is evaluated by calculating the χ^2 and p -values, which are summarised in Tables 3 to 5. In general, most of the predictions are not able to describe simultaneously all observables. This was the case in other measurements both in dilepton and semileptonic final states [2, 3]. Among the NLO+PS models, one of the best predictions is provided by Powheg+Herwig 7, which is the only one providing a good modelling of both the leading jet and lepton p_T . The PWG+PY8 ($bb4l$) sample also shows a good description of the leading and subleading jets and leptons.

The inclusion of NNLO corrections for the $t\bar{t}$ component of the signal, either by applying the NNLO reweighting to the $t\bar{t}$ simulation or performing a full NNLO+PS simulation via PWG+PY8 MiNNLO_{PS}, described in Section 3.1.2, improves the predictions significantly, which is reflected by the p -values increasing systematically for almost all variables. In particular, PWG+PY8 (NNLO rew.) is the only prediction that can describe all the variables simultaneously. This effect is minor for m_{minimax}^{bl} in the $2b$ -exclusive phase space, since the NNLO corrections do not significantly change the shape of the $t\bar{t}$ component, which mostly populates the already well-modelled low m_{minimax}^{bl} region.

The models showing the worst compatibility with the data are those with alternative h_{damp} and $p_{T,\text{hard}}$ variations, which are compatible with only one observable. The other models have intermediate results. No NLO+PS MC can describe the p_T of the $bbll$ and $bb4l$ systems, which are more sensitive to higher-order effects and additional radiation.

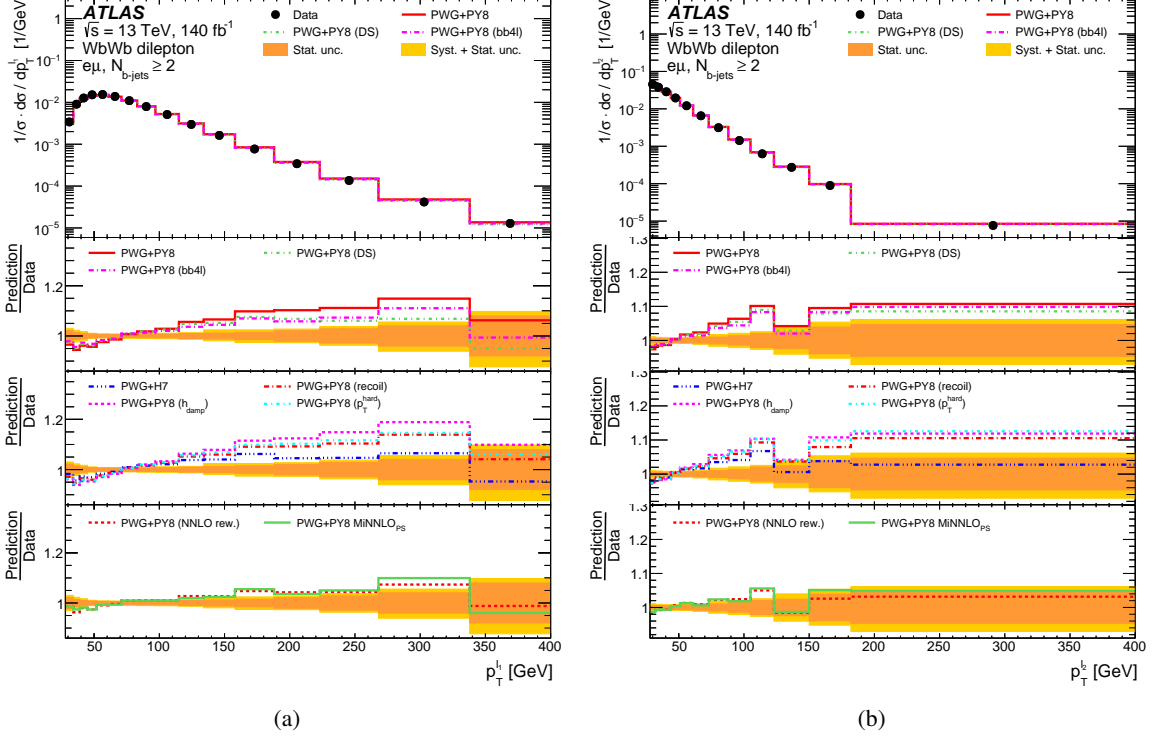


Figure 9: Relative differential cross-section measurement as a function of the (a) $p_T^{l_1}$ and (b) $p_T^{l_2}$ variables. The cross-section is unfolded to particle-level in the fiducial phase space. The measurement is compared with predictions provided by Powheg+Pythia 8 with different schemes for computing the $t\bar{t}/tW$ interference, with predictions obtained with different NLO+PS MC generators and predictions where the $t\bar{t}$ component is simulated with an NNLO+PS MC generator or corrected to NNLO. The lower panels show the ratios of the predictions to the data with the bands showing the statistical and total uncertainties in the data.

Table 4: χ^2 and p -values quantifying the level of agreement between the measured normalised differential cross-sections and predictions provided by different MC generators.

Observable	PWG+PY8 (h_{damp})		PWG+PY8 ($p_{T,\text{hard}}$)		PWG+PY8 (recoil)		PWG+H7	
	χ^2/NDF	p -value	χ^2/NDF	p -value	χ^2/NDF	p -value	χ^2/NDF	p -value
N_{jets}	7.8/6	0.25	23.0/6	<0.01	9.1/6	0.17	22.3/6	<0.01
m^{bbll}	30.8/15	<0.01	29.6/15	0.01	25.5/15	0.04	26.6/15	0.03
m^{bb4l}	23.3/12	0.03	18.1/12	0.11	16.2/12	0.18	15.3/12	0.22
p_T^{bb}	31.2/8	<0.01	10.3/8	0.24	10.4/8	0.24	8.0/8	0.44
$p_T^{jet_1}$	34.5/7	<0.01	17.5/7	0.01	11.7/7	0.11	10.1/7	0.18
$p_T^{jet_2}$	13.6/7	0.06	7.1/7	0.42	2.5/7	0.93	1.7/7	0.98
p_T^{bb4l}	69.5/8	<0.01	40.7/8	<0.01	46.2/8	<0.01	42.7/8	<0.01
p_T^{bbll}	76.4/10	<0.01	26.5/10	<0.01	31.8/10	<0.01	24.0/10	<0.01
$p_T^{l_2}$	27.2/11	<0.01	25.2/11	<0.01	20.6/11	0.04	14.0/11	0.23
$p_T^{l_1}$	53.1/15	<0.01	39.6/15	<0.01	34.8/15	<0.01	19.0/15	0.21

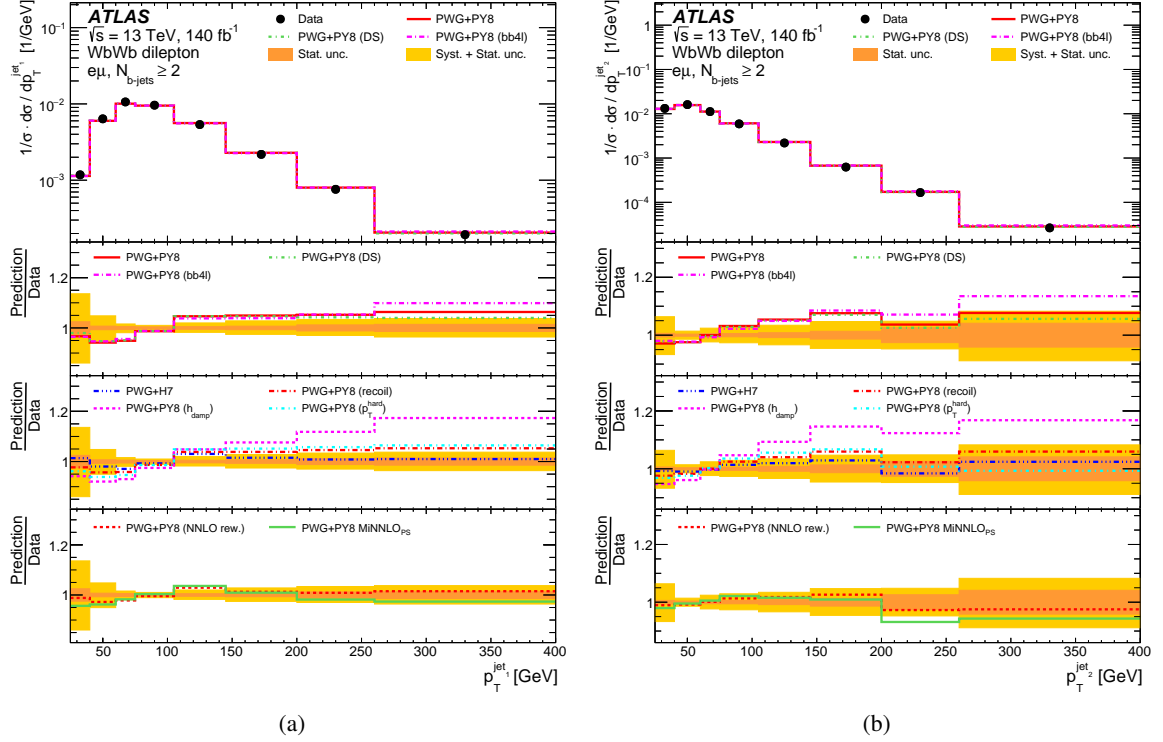


Figure 10: Relative differential cross-section measurement as a function of the (a) $p_T^{jet_1}$ and (b) $p_T^{jet_2}$ variables. The cross-section is unfolded to particle-level in the fiducial phase space. The measurement is compared with predictions provided by Powheg+Pythia 8 with different schemes for computing the $t\bar{t}/tW$ interference, with predictions obtained with different NLO+PS MC generators and predictions where the $t\bar{t}$ component is simulated with an NNLO+PS MC generator or corrected to NNLO. The lower panels show the ratios of the predictions to the data with the bands showing the statistical and total uncertainties in the data.

Table 5: χ^2 and p -values quantifying the level of agreement between the measured normalised differential cross-sections and predictions provided by Powheg+Pythia 8 with the NNLO reweight and MiNNLO_{PS}.

Observable	PWG+PY8 (NNLO REW.) χ^2/NDF	PWG+PY8 MiNNLO _{PS} χ^2/NDF	p -value	p -value
N_{jets}	5.5/6	15.2/6	0.48	0.02
m_{bbll}	25.8/15	23.8/15	0.04	0.07
m_{bb4l}	17.3/12	13.0/12	0.14	0.37
p_T^{bb}	4.2/8	2.9/8	0.84	0.94
$p_T^{jet_1}$	7.1/7	13.2/7	0.42	0.07
$p_T^{jet_2}$	2.6/7	6.4/7	0.92	0.49
p_T^{bb4l}	11.9/8	32.4/8	0.16	<0.01
p_T^{bbll}	12.9/10	16.0/10	0.23	0.10
$p_T^{l_2}$	9.2/11	9.4/11	0.60	0.58
$p_T^{l_1}$	11.8/15	13.4/15	0.70	0.57

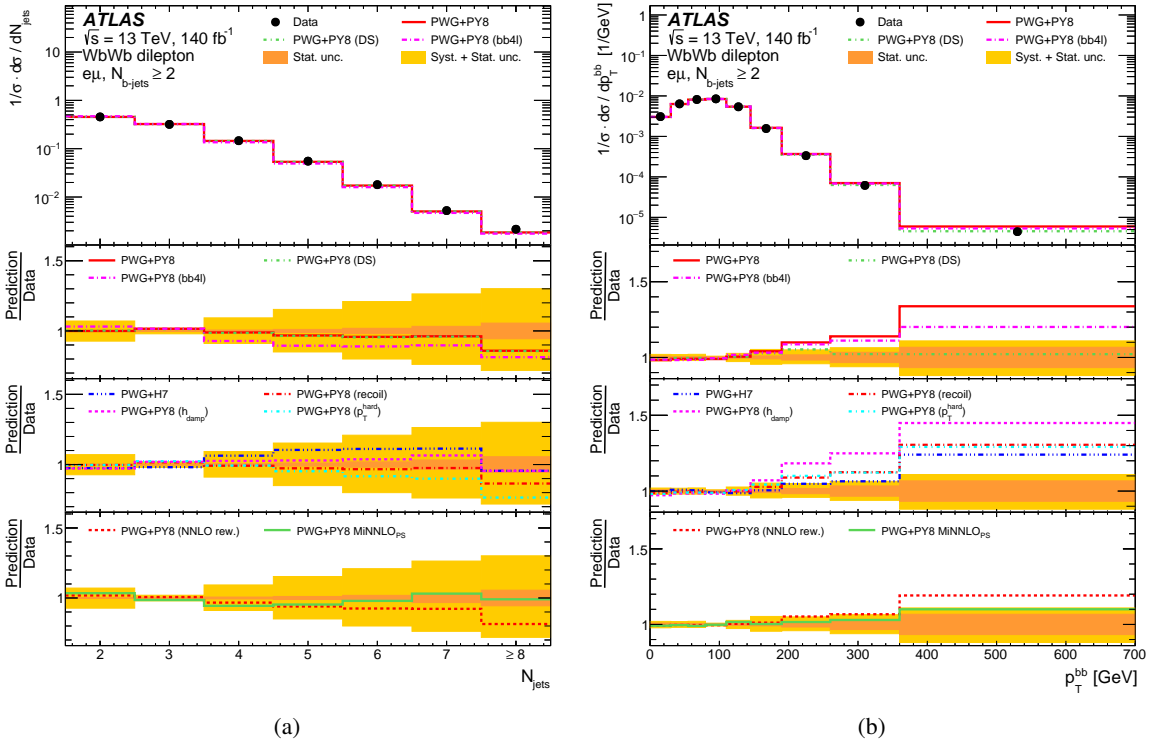


Figure 11: Relative differential cross-section measurement as a function of the (a) N_{jets} and (b) p_{T}^{bb} variables. The cross-section is unfolded to particle-level in the fiducial phase space. The measurement is compared with predictions provided by Powheg+Pythia 8 with different schemes for computing the $t\bar{t}/tW$ interference, with predictions obtained with different NLO+PS MC generators and predictions where the $t\bar{t}$ component is simulated with an NNLO+PS MC generator or corrected to NNLO. The lower panels show the ratios of the predictions to the data with the bands showing the statistical and total uncertainties in the data.

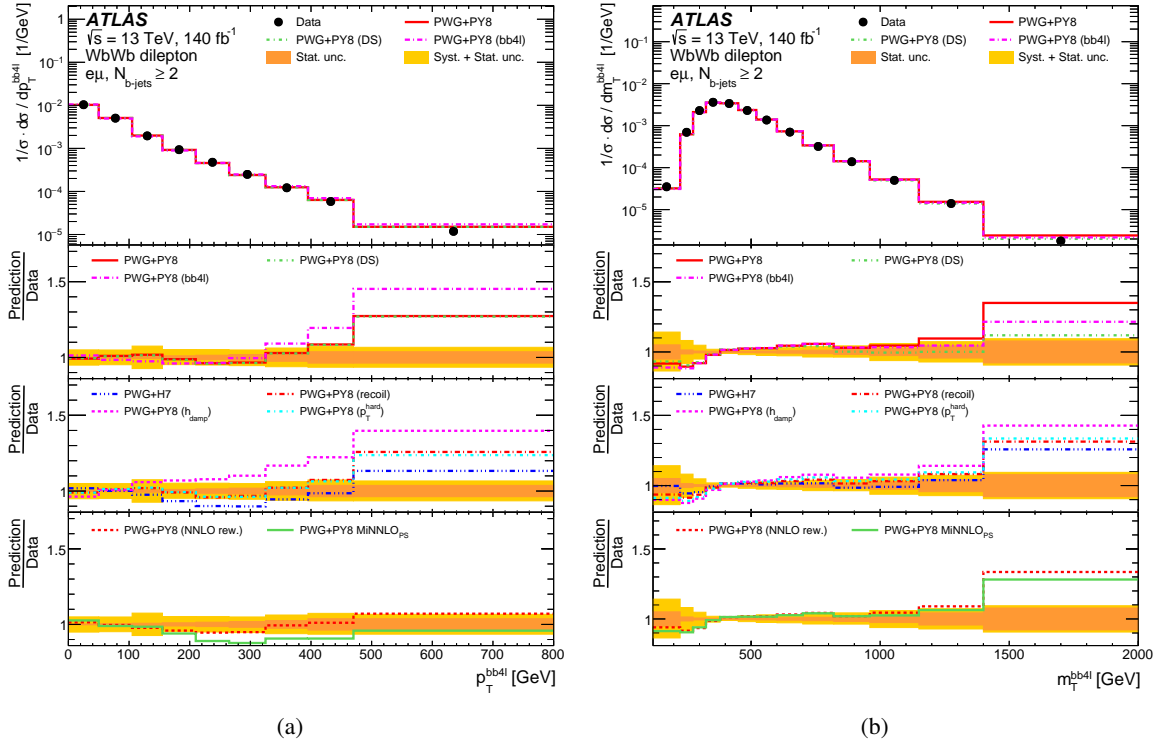


Figure 12: Relative differential cross-section measurement as a function of the (a) p_T^{bb4l} and (b) m_T^{bb4l} variables. The cross-section is unfolded to particle-level in the fiducial phase space. The measurement is compared with predictions provided by Powheg+Pythia 8 with different schemes for computing the $t\bar{t}/tW$ interference, with predictions obtained with different NLO+PS MC generators and predictions where the $t\bar{t}$ component is simulated with an NNLO+PS MC generator or corrected to NNLO. The lower panels show the ratios of the predictions to the data with the bands showing the statistical and total uncertainties in the data.

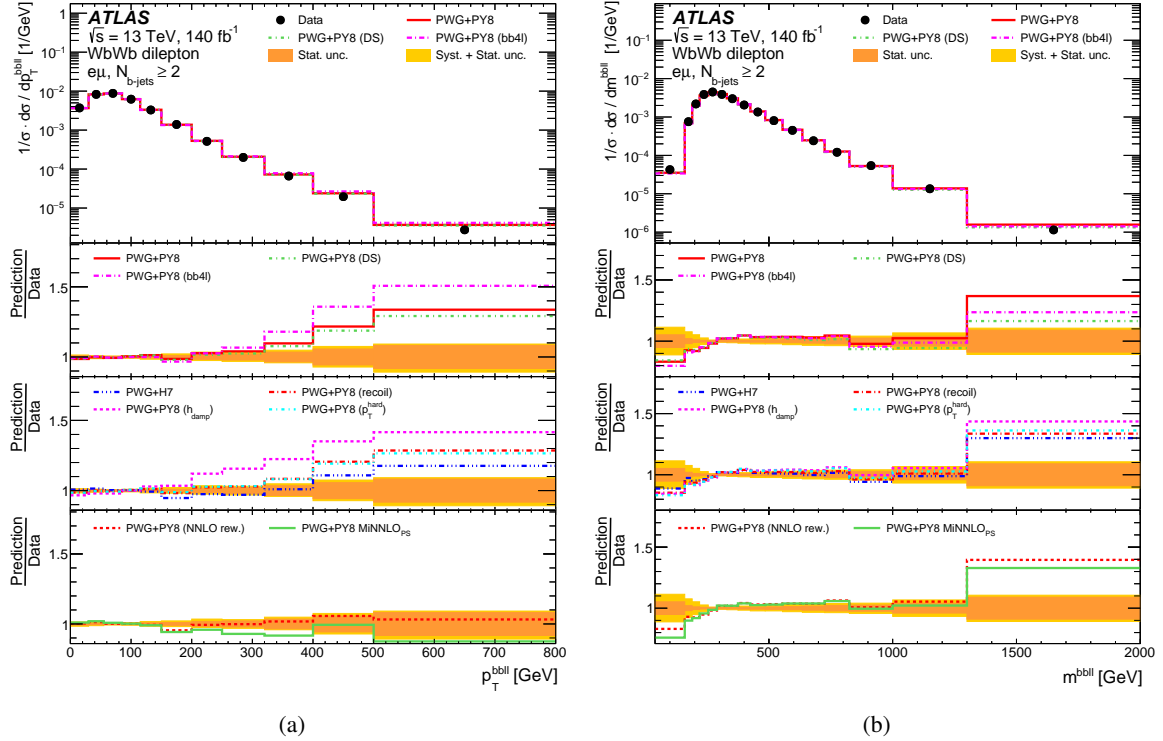


Figure 13: Relative differential cross-section measurement as a function of the (a) p_T^{bbll} and (b) m^{bbll} variables. The cross-section is unfolded to particle-level in the fiducial phase space. The measurement is compared with predictions provided by Powheg+Pythia 8 with different schemes for computing the $t\bar{t}/tW$ interference, with predictions obtained with different NLO+PS MC generators and predictions where the $t\bar{t}$ component is simulated with an NNLO+PS MC generator or corrected to NNLO. The lower panels show the ratios of the predictions to the data with the bands showing the statistical and total uncertainties in the data.

6.4 Integrated fiducial cross-section

The integrated fiducial cross-section is measured in both phase spaces, by applying the unfolding procedure described in Section 5 to a single-bin distribution. In this case, the unfolding matrix is a 1×1 matrix, and the unfolding procedure from Eq. (2) is equivalent to a simple division of the acceptance-corrected, background-subtracted reconstructed event count in data by the efficiency.

The integrated fiducial cross-sections in the two phase spaces are measured to be

2b-exclusive region $\sigma_{\text{fid}} = 5.77 \pm 0.01 \text{ (stat.)} {}^{+0.27}_{-0.29} \text{ (syst.)} \pm 0.05 \text{ (lumi.) pb;}$

2b-inclusive region $\sigma_{\text{fid}} = 5.97 \pm 0.01 \text{ (stat.)} {}^{+0.27}_{-0.30} \text{ (syst.)} \pm 0.05 \text{ (lumi.) pb.}$

As shown in Table 6, the measurements in both the 2b-inclusive and exclusive phase spaces are limited by the uncertainties in the signal modelling and flavour-tagging efficiency. Other significant sources of uncertainties are related to the lepton isolation and jet energy scale.

The measured cross-sections are compared with theoretical predictions from different MC generators in Figure 14. All the $t\bar{t}$ and tW theoretical predictions are normalised to the NNLO+NNLL and NLO+NNLL cross-sections respectively, as described in Section 3.1.1. All differences among the predictions are thus due to how differently the MC generators model the acceptance of the fiducial phase spaces relative to the full phase space, which encompasses the entire kinematic region predicted by the theoretical models. The

Table 6: Summary of all the uncertainty sources for the total cross-section in the fiducial phase spaces. Only uncertainty classes contributing more than 0.1% are shown.

Phase space	$e\mu, N_{b\text{-jets}} = 2$	$e\mu, N_{b\text{-jets}} \geq 2$
Fiducial cross-section [pb]	5.77	5.97
Total Uncertainty [%]	${}^{+4.6}_{-5.2}$	${}^{+4.6}_{-5.1}$
Statistical [%]	± 0.2	± 0.2
Systematic [%]	${}^{+4.5}_{-5.2}$	${}^{+4.6}_{-5.1}$
Jets [%]	${}^{+1.6}_{-1.8}$	${}^{+1.8}_{-1.9}$
Pile-up [%]	± 0.6	${}^{+0.5}_{-0.6}$
Flavour tagging [%]	± 2.9	± 3.0
Background [%]	± 0.3	± 0.3
Leptons and E_T^{miss} [%]	± 1.8	± 1.8
Luminosity [%]	± 0.8	± 0.8
$t\bar{t}$ modelling [%]	± 0.7	± 0.7
tW modelling [%]	± 0.1	± 0.1
Generator parameters [%]	${}^{+1.9}_{-2.9}$	${}^{+1.7}_{-2.7}$
Parton shower [%]	± 1.0	± 0.8
Hard scattering [%]	± 0.7	± 0.7

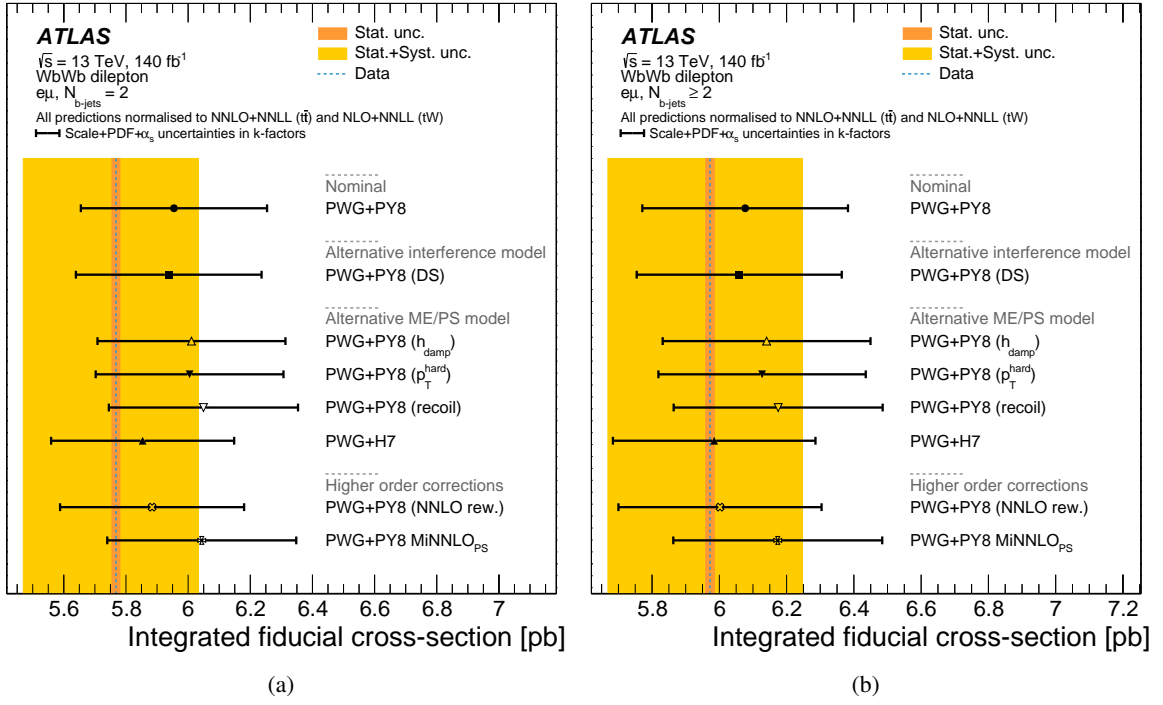


Figure 14: Integrated fiducial cross-section measurement in (a) the $2b$ -exclusive and (b) the $2b$ -inclusive regions. The measured cross-sections are compared with theoretical predictions from different MC generators. All the $t\bar{t}$ and tW theoretical predictions are normalised to the NNLO+NNLL and NLO+NNLL cross-sections respectively.

effect of the theoretical uncertainties, namely scale, PDF and α_s , on the modelling of the fiducial acceptance is negligible and the dominant source of uncertainty in the predicted fiducial cross-section is due to the correction terms used to correct the NLO cross-sections from the generators to the higher-order predictions (k -factors). All the predictions are compatible with the measurement within the quoted uncertainty.

7 Conclusions

This study presents the results of a differential cross-section measurement in the $WbWb$ final state using data collected by the ATLAS detector at the LHC at a centre-of-mass energy of $\sqrt{s} = 13 \text{ TeV}$, corresponding to an integrated luminosity of 140 fb^{-1} . The analysis focuses on the fiducial phase spaces defined by requiring at least or exactly two b -tagged jets and two leptons with opposite charges and different flavours.

The differential cross-section as a function of the variable most sensitive to the $t\bar{t}$ and tW interference, m_{minimax}^{bl} , is measured in the $2b$ -exclusive region. The results are compared with different schemes to model the interference, with the DR approach showing the best agreement with the data, although it still fails to accurately describe the data in the extreme tail of the distribution. The sample simulating the full $bb4l$ final state shows larger differences in this region, but a full assessment would require further exploration of theoretical uncertainties. This measurement provides critical input for refining future versions of the $bb4l$ generator as well as enabling improvements in the modelling of the $t\bar{t}$ and tW interference effects.

In the $2b$ -inclusive region, the differential cross-sections are measured as a function of kinematic variables related to the leptons, jets, and combinations of the two b -jets (bb system), the two b -jets and the two charged leptons ($bbll$ system), and the two b -jets and all charged and neutral leptons ($bb4l$ system). The results indicate that none of the considered NLO+PS predictions, including the $bb4l$ sample, is able to simultaneously describe all observables in the fiducial phase space. This finding is consistent with previous measurements in both the dilepton and semileptonic final states. The best-performing predictions are from the nominal PowHEG+PYTHIA 8, in particular after the inclusion of higher-order corrections to the $t\bar{t}$ sample via the NNLO reweighting and, to a minor extent, MiNNLO_{PS}, and PowHEG+HERWIG 7 models. However, it is important to emphasise that the PowHEG+PYTHIA 8 predictions benefit from tuning to data, particularly for the N_{jets} and $p_T(t\bar{t})$ distributions, while the PowHEG+PYTHIA 8 MiNNLO_{PS} and $bb4l$ predictions represent theoretical predictions without such tuning. Finally, models with alternative h_{damp} and $p_{T,\text{hard}}$ variations are only compatible with a single observable.

The integrated fiducial cross-sections are also measured in the $2b$ -exclusive and $2b$ -inclusive regions. The measured cross-sections are found to be 5.77 ± 0.01 (stat.) $^{+0.27}_{-0.30}$ (syst.) pb and 5.97 ± 0.01 (stat.) $^{+0.28}_{-0.31}$ (syst.) pb, respectively. These measurements are primarily limited by uncertainties in the signal modelling and flavour-tagging efficiency, followed by other sources such as lepton isolation and jet energy scale.

This measurement represents a significant improvement with respect to previous publications, as the uncertainty is reduced by a factor of two, allowing for better discrimination between models. The sensitivity for most observables is currently limited primarily by uncertainties in signal modelling, including those related to the treatment of $t\bar{t}/tW$ interference, and by statistical uncertainties in the tails of the distributions. Further improvements are expected with the data collected during the LHC Run 3 and through the use of new MC simulations optimised based on these measurements.

In conclusion, the results of this study provide valuable insights into the modelling of the $WbWb$ final state in the fiducial phase space. The observed discrepancies between the measured cross-sections and theoretical predictions highlight the need for further improvements in the modelling of this process. While this analysis employs separate samples to model the $t\bar{t}$ and tW components of the $WbWb$ final state, it also provides a valuable opportunity to improve and tune the MC simulations that model the full $WbWb$ final state. Such improvements are crucial, as a full simulation of the $WbWb$ final state, with a complete set of systematic uncertainties, would allow for a more accurate disentanglement of the $t\bar{t}$ and tW contributions, thereby reducing the corresponding uncertainties.

Acknowledgements

We thank CERN for the very successful operation of the LHC and its injectors, as well as the support staff at CERN and at our institutions worldwide without whom ATLAS could not be operated efficiently.

The crucial computing support from all WLCG partners is acknowledged gratefully, in particular from CERN, the ATLAS Tier-1 facilities at TRIUMF/SFU (Canada), NDGF (Denmark, Norway, Sweden), CC-IN2P3 (France), KIT/GridKA (Germany), INFN-CNAF (Italy), NL-T1 (Netherlands), PIC (Spain), RAL (UK) and BNL (USA), the Tier-2 facilities worldwide and large non-WLCG resource providers. Major contributors of computing resources are listed in Ref. [114].

We gratefully acknowledge the support of ANPCyT, Argentina; YerPhI, Armenia; ARC, Australia; BMWFW and FWF, Austria; ANAS, Azerbaijan; CNPq and FAPESP, Brazil; NSERC, NRC and CFI, Canada; CERN;

ANID, Chile; CAS, MOST and NSFC, China; Minciencias, Colombia; MEYS CR, Czech Republic; DNRF and DNSRC, Denmark; IN2P3-CNRS and CEA-DRF/IRFU, France; SRNSFG, Georgia; BMBF, HGF and MPG, Germany; GSRI, Greece; RGC and Hong Kong SAR, China; ICHEP and Academy of Sciences and Humanities, Israel; INFN, Italy; MEXT and JSPS, Japan; CNRST, Morocco; NWO, Netherlands; RCN, Norway; MNiSW, Poland; FCT, Portugal; MNE/IFA, Romania; MSTDI, Serbia; MSSR, Slovakia; ARIS and MVZI, Slovenia; DSi/NRF, South Africa; MICIU/AEI, Spain; SRC and Wallenberg Foundation, Sweden; SERI, SNSF and Cantons of Bern and Geneva, Switzerland; NSTC, Taipei; TENMAK, Türkiye; STFC/UKRI, United Kingdom; DOE and NSF, United States of America.

Individual groups and members have received support from BCKDF, CANARIE, CRC and DRAC, Canada; CERN-CZ, FORTE and PRIMUS, Czech Republic; COST, ERC, ERDF, Horizon 2020, ICSC-NextGenerationEU and Marie Skłodowska-Curie Actions, European Union; Investissements d'Avenir Labex, Investissements d'Avenir Idex and ANR, France; DFG and AvH Foundation, Germany; Herakleitos, Thales and Aristeia programmes co-financed by EU-ESF and the Greek NSRF, Greece; BSF-NSF and MINERVA, Israel; NCN and NAWA, Poland; La Caixa Banking Foundation, CERCA Programme Generalitat de Catalunya and PROMETEO and GenT Programmes Generalitat Valenciana, Spain; Göran Gustafssons Stiftelse, Sweden; The Royal Society and Leverhulme Trust, United Kingdom.

In addition, individual members wish to acknowledge support from Armenia: Yerevan Physics Institute (FAPERJ); CERN: European Organization for Nuclear Research (CERN DOCT); Chile: Agencia Nacional de Investigación y Desarrollo (FONDECYT 1230812, FONDECYT 1240864); China: Chinese Ministry of Science and Technology (MOST-2023YFA1605700, MOST-2023YFA1609300), National Natural Science Foundation of China (NSFC - 12175119, NSFC 12275265); Czech Republic: Czech Science Foundation (GACR - 24-11373S), Ministry of Education Youth and Sports (ERC-CZ-LL2327, FORTE CZ.02.01.01/00/22_008/0004632), PRIMUS Research Programme (PRIMUS/21/SCI/017); EU: H2020 European Research Council (ERC - 101002463); European Union: European Research Council (BARD No. 101116429, ERC - 948254, ERC 101089007), European Regional Development Fund (SMASH COFUND 101081355, SLO ERDF), Horizon 2020 Framework Programme (MUCCA - CHIST-ERA-19-XAI-00), European Union, Future Artificial Intelligence Research (FAIR-NextGenerationEU PE00000013), Horizon 2020 (EuroHPC - EHPC-DEV-2024D11-051), Italian Center for High Performance Computing, Big Data and Quantum Computing (ICSC, NextGenerationEU); France: Agence Nationale de la Recherche (ANR-21-CE31-0022, ANR-22-EDIR-0002); Germany: Baden-Württemberg Stiftung (BW Stiftung-Postdoc Elite-programme), Deutsche Forschungsgemeinschaft (DFG - 469666862, DFG - CR 312/5-2); China: Research Grants Council (GRF); Italy: Istituto Nazionale di Fisica Nucleare (ICSC, NextGenerationEU), Ministero dell'Università e della Ricerca (NextGenEU I53D23000820006 M4C2.1.1); Japan: Japan Society for the Promotion of Science (JSPS KAKENHI JP22H01227, JSPS KAKENHI JP22H04944, JSPS KAKENHI JP22KK0227, JSPS KAKENHI JP23KK0245, JSPS KAKENHI JP24K23939); Norway: Research Council of Norway (RCN-314472); Poland: Ministry of Science and Higher Education (IDUB AGH, POB8, D4 no 9722), Polish National Science Centre (NCN 2021/42/E/ST2/00350, NCN OPUS 2023/51/B/ST2/02507, NCN OPUS nr 2022/47/B/ST2/03059, NCN UMO-2019/34/E/ST2/00393, UMO-2022/47/O/ST2/00148, UMO-2023/49/B/ST2/04085, UMO-2023/51/B/ST2/00920, UMO-2024/53/N/ST2/00869); Portugal: Foundation for Science and Technology (FCT); Spain: Ministry of Science and Innovation (MCIN & NextGenEU PCI2022-135018-2, MICIN & FEDER PID2021-125273NB, RYC2019-028510-I, RYC2020-030254-I, RYC2021-031273-I, RYC2022-038164-I); Sweden: Carl Trygger Foundation (Carl Trygger Foundation CTS 22:2312), Swedish Research Council (Swedish Research Council 2023-04654, VR 2021-03651, VR 2022-03845, VR 2022-04683, VR 2023-03403, VR 2024-05451), Knut and Alice Wallenberg Foundation (KAW 2018.0458, KAW 2022.0358, KAW 2023.0366); Switzerland: Swiss National Science Foundation (SNSF - PCEFP2_194658); United Kingdom: Leverhulme Trust (Leverhulme

Trust RPG-2020-004), Royal Society (NIF-R1-231091); United States of America: U.S. Department of Energy (ECA DE-AC02-76SF00515), Neubauer Family Foundation.

References

- [1] L. Evans and P. Bryant, *LHC Machine*, [JINST **3** \(2008\) S08001](#).
- [2] ATLAS Collaboration, *Measurements of top-quark pair differential and double-differential cross-sections in the $\ell+jets$ channel with pp collisions at $\sqrt{s} = 13\text{ TeV}$ using the ATLAS detector*, [Eur. Phys. J. C **79** \(2019\) 1028](#), arXiv: [1908.07305 \[hep-ex\]](#), Erratum: [Eur. Phys. J. C **80** \(2020\) 1092](#).
- [3] ATLAS Collaboration, *Inclusive and differential cross-sections for dilepton $t\bar{t}$ production measured in $\sqrt{s} = 13\text{ TeV}$ pp collisions with the ATLAS detector*, [JHEP **07** \(2023\) 141](#), arXiv: [2303.15340 \[hep-ex\]](#).
- [4] ATLAS Collaboration, *Measurement of differential cross-sections in $t\bar{t}$ and $t\bar{t}+jets$ production in the lepton+jets final state in pp collisions at $\sqrt{s} = 13\text{ TeV}$ using 140fb^{-1} of ATLAS data*, [JHEP **08** \(2024\) 182](#), arXiv: [2406.19701 \[hep-ex\]](#).
- [5] CMS Collaboration, *Measurement of differential $t\bar{t}$ production cross sections in the full kinematic range using lepton+jets events from proton–proton collisions at $\sqrt{s} = 13\text{ TeV}$* , [Phys. Rev. D **104** \(2021\) 092013](#), arXiv: [2108.02803 \[hep-ex\]](#).
- [6] CMS Collaboration, *Measurement of $t\bar{t}$ normalised multi-differential cross sections in pp collisions at $\sqrt{s} = 13\text{ TeV}$, and simultaneous determination of the strong coupling strength, top quark pole mass, and parton distribution functions*, [Eur. Phys. J. C **80** \(2020\) 658](#), arXiv: [1904.05237 \[hep-ex\]](#).
- [7] M. Beneke, P. Falgari, S. Klein and C. Schwinn, *Hadronic top-quark pair production with NNLL threshold resummation*, [Nucl. Phys. B **855** \(2012\) 695](#), arXiv: [1109.1536 \[hep-ph\]](#).
- [8] M. Cacciari, M. Czakon, M. Mangano, A. Mitov and P. Nason, *Top-pair production at hadron colliders with next-to-next-to-leading logarithmic soft-gluon resummation*, [Phys. Lett. B **710** \(2012\) 612](#), arXiv: [1111.5869 \[hep-ph\]](#).
- [9] P. Bärnreuther, M. Czakon and A. Mitov, *Percent-Level-Precision Physics at the Tevatron: Next-to-Next-to-Leading Order QCD Corrections to $q\bar{q} \rightarrow t\bar{t} + X$* , [Phys. Rev. Lett. **109** \(2012\) 132001](#), arXiv: [1204.5201 \[hep-ph\]](#).
- [10] M. Czakon and A. Mitov, *NNLO corrections to top-pair production at hadron colliders: the all-fermionic scattering channels*, [JHEP **12** \(2012\) 054](#), arXiv: [1207.0236 \[hep-ph\]](#).
- [11] M. Czakon and A. Mitov, *NNLO corrections to top pair production at hadron colliders: the quark-gluon reaction*, [JHEP **01** \(2013\) 080](#), arXiv: [1210.6832 \[hep-ph\]](#).
- [12] M. Czakon, P. Fiedler and A. Mitov, *Total Top-Quark Pair-Production Cross Section at Hadron Colliders Through $O(\alpha_S^4)$* , [Phys. Rev. Lett. **110** \(2013\) 252004](#), arXiv: [1303.6254 \[hep-ph\]](#).
- [13] M. Czakon and A. Mitov, *Top++: A program for the calculation of the top-pair cross-section at hadron colliders*, [Comput. Phys. Commun. **185** \(2014\) 2930](#), arXiv: [1112.5675 \[hep-ph\]](#).

- [14] S. Catani, S. Devoto, M. Grazzini, S. Kallweit and J. Mazzitelli, *Top-quark pair production at the LHC: Fully differential QCD predictions at NNLO*, *JHEP* **07** (2019) 100, arXiv: [1906.06535 \[hep-ph\]](#).
- [15] C. D. White, S. Frixione, E. Laenen and F. Maltoni, *Isolating Wt production at the LHC*, *JHEP* **11** (2009) 074, arXiv: [0908.0631 \[hep-ph\]](#).
- [16] S. Frixione, E. Laenen, P. Motylinski, C. White and B. R. Webber, *Single-top hadroproduction in association with a W boson*, *JHEP* **07** (2008) 029, arXiv: [0805.3067 \[hep-ph\]](#).
- [17] W. Hollik, J. M. Lindert and D. Pagani, *NLO corrections to squark-squark production and decay at the LHC*, *JHEP* **03** (2013) 139, arXiv: [1207.1071 \[hep-ph\]](#).
- [18] F. Demartin, B. Maier, F. Maltoni, K. Mawatari and M. Zaro, *tWH associated production at the LHC*, *Eur. Phys. J. C* **77** (2017) 34, arXiv: [1607.05862 \[hep-ph\]](#).
- [19] ATLAS Collaboration, *Studies on top-quark Monte Carlo modelling for Top2016*, ATL-PHYS-PUB-2016-020, 2016, URL: <https://cds.cern.ch/record/2216168>.
- [20] V. Ravindran, J. Smith and W. L. Van Neerven, *Next-to-leading order QCD corrections to differential distributions of Higgs boson production in hadron-hadron collisions*, *Nucl. Phys. B* **634** (2002) 247, arXiv: [hep-ph/0201114](#).
- [21] A. Denner, S. Dittmaier, S. Kallweit and S. Pozzorini, *NLO QCD corrections to off-shell top-antitop production with leptonic decays at hadron colliders*, *JHEP* **10** (2012) 110, arXiv: [1207.5018 \[hep-ph\]](#).
- [22] G. Bevilacqua, M. Czakon, A. van Hameren, C. G. Papadopoulos and M. Worek, *Complete off-shell effects in top quark pair hadroproduction with leptonic decay at next-to-leading order*, *JHEP* **02** (2011) 083, arXiv: [1012.4230 \[hep-ph\]](#).
- [23] F. Cascioli, S. Kallweit, P. Maierhöfer and S. Pozzorini, *A unified NLO description of top-pair and associated Wt production*, *Eur. Phys. J. C* **74** (2014) 2783, arXiv: [1312.0546 \[hep-ph\]](#).
- [24] R. Frederix, *Top Quark Induced Backgrounds to Higgs Production in the $WW^{(*)} \rightarrow llvv$ Decay Channel at Next-to-Leading-Order in QCD*, *Phys. Rev. Lett.* **112** (2014) 082002, arXiv: [1311.4893 \[hep-ph\]](#).
- [25] T. Ježo, J. M. Lindert, P. Nason, C. Oleari and S. Pozzorini, *An NLO+PS generator for t̄t and Wt production and decay including non-resonant and interference effects*, *Eur. Phys. J. C* **76** (2016) 691, arXiv: [1607.04538 \[hep-ph\]](#).
- [26] ATLAS Collaboration, *Probing the Quantum Interference between Singly and Doubly Resonant Top-Quark Production in pp Collisions at $\sqrt{s} = 13$ TeV with the ATLAS Detector*, *Phys. Rev. Lett.* **121** (2018) 152002, arXiv: [1806.04667 \[hep-ex\]](#).
- [27] ATLAS Collaboration, *The ATLAS Experiment at the CERN Large Hadron Collider*, *JINST* **3** (2008) S08003.
- [28] ATLAS Collaboration, *ATLAS Insertable B-Layer: Technical Design Report*, ATLAS-TDR-19; CERN-LHCC-2010-013, 2010, URL: <https://cds.cern.ch/record/1291633>, Addendum: ATLAS-TDR-19-ADD-1; CERN-LHCC-2012-009, 2012, URL: <https://cds.cern.ch/record/1451888>.

- [29] B. Abbott et al., *Production and integration of the ATLAS Insertable B-Layer*, JINST **13** (2018) T05008, arXiv: [1803.00844 \[physics.ins-det\]](#).
- [30] G. Avoni et al., *The new LUCID-2 detector for luminosity measurement and monitoring in ATLAS*, JINST **13** (2018) P07017.
- [31] ATLAS Collaboration, *Performance of the ATLAS trigger system in 2015*, Eur. Phys. J. C **77** (2017) 317, arXiv: [1611.09661 \[hep-ex\]](#).
- [32] ATLAS Collaboration, *Software and computing for Run 3 of the ATLAS experiment at the LHC*, Eur. Phys. J. C **85** (2025) 234, arXiv: [2404.06335 \[hep-ex\]](#).
- [33] ATLAS Collaboration, *ATLAS data quality operations and performance for 2015–2018 data-taking*, JINST **15** (2020) P04003, arXiv: [1911.04632 \[physics.ins-det\]](#).
- [34] ATLAS Collaboration, *Luminosity determination in $p p$ collisions at $\sqrt{s} = 13$ TeV using the ATLAS detector at the LHC*, Eur. Phys. J. C **83** (2023) 982, arXiv: [2212.09379 \[hep-ex\]](#).
- [35] ATLAS Collaboration, *The ATLAS Simulation Infrastructure*, Eur. Phys. J. C **70** (2010) 823, arXiv: [1005.4568 \[physics.ins-det\]](#).
- [36] S. Agostinelli et al., *GEANT4 – a simulation toolkit*, Nucl. Instrum. Meth. A **506** (2003) 250.
- [37] ATLAS Collaboration, *Performance of the Fast ATLAS Tracking Simulation (FATRAS) and the ATLAS Fast Calorimeter Simulation (FastCaloSim) with single particles*, ATL-SOFT-PUB-2014-001, 2014, URL: <https://cds.cern.ch/record/1669341>.
- [38] T. Sjöstrand, S. Mrenna and P. Skands, *A brief introduction to PYTHIA 8.1*, Comput. Phys. Commun. **178** (2008) 852, arXiv: [0710.3820 \[hep-ph\]](#).
- [39] NNPDF Collaboration, R. D. Ball et al., *Parton distributions with LHC data*, Nucl. Phys. B **867** (2013) 244, arXiv: [1207.1303 \[hep-ph\]](#).
- [40] ATLAS Collaboration, *The Pythia 8 A3 tune description of ATLAS minimum bias and inelastic measurements incorporating the Donnachie–Landshoff diffractive model*, ATL-PHYS-PUB-2016-017, 2016, URL: <https://cds.cern.ch/record/2206965>.
- [41] ATLAS Collaboration, *Measurement of the Inelastic Proton–Proton Cross Section at $\sqrt{s} = 13$ TeV with the ATLAS Detector at the LHC*, Phys. Rev. Lett. **117** (2016) 182002, arXiv: [1606.02625 \[hep-ex\]](#).
- [42] ATLAS Collaboration, *ATLAS Pythia 8 tunes to 7 TeV data*, ATL-PHYS-PUB-2014-021, 2014, URL: <https://cds.cern.ch/record/1966419>.
- [43] D. J. Lange, *The EvtGen particle decay simulation package*, Nucl. Instrum. Meth. A **462** (2001) 152.
- [44] J. Bellm et al., *Herwig 7.0/Herwig++ 3.0 release note*, Eur. Phys. J. C **76** (2016) 196, arXiv: [1512.01178 \[hep-ph\]](#).
- [45] M. Bähr et al., *Herwig++ physics and manual*, Eur. Phys. J. C **58** (2008) 639, arXiv: [0803.0883 \[hep-ph\]](#).
- [46] ATLAS Collaboration, *Studies of $t\bar{t}/tW$ interference effects in $b\bar{b}\ell^+\ell^- v\bar{v}'$ final states with Powheg and MADGRAPH5_AMC@NLO setups*, ATL-PHYS-PUB-2021-042, 2021, URL: <https://cds.cern.ch/record/2792254>.

- [47] S. Frixione, G. Ridolfi and P. Nason,
A positive-weight next-to-leading-order Monte Carlo for heavy flavour hadroproduction,
JHEP **09** (2007) 126, arXiv: [0707.3088 \[hep-ph\]](#).
- [48] P. Nason, *A new method for combining NLO QCD with shower Monte Carlo algorithms*,
JHEP **11** (2004) 040, arXiv: [hep-ph/0409146](#).
- [49] S. Frixione, P. Nason and C. Oleari,
Matching NLO QCD computations with parton shower simulations: the POWHEG method,
JHEP **11** (2007) 070, arXiv: [0709.2092 \[hep-ph\]](#).
- [50] S. Alioli, P. Nason, C. Oleari and E. Re, *A general framework for implementing NLO calculations in shower Monte Carlo programs: the POWHEG BOX*, **JHEP** **06** (2010) 043,
arXiv: [1002.2581 \[hep-ph\]](#).
- [51] T. Sjöstrand et al., *An introduction to PYTHIA 8.2*, **Comput. Phys. Commun.** **191** (2015) 159,
arXiv: [1410.3012 \[hep-ph\]](#).
- [52] NNPDF Collaboration, R. D. Ball et al., *Parton distributions for the LHC run II*,
JHEP **04** (2015) 040, arXiv: [1410.8849 \[hep-ph\]](#).
- [53] C. Bierlich et al., *A comprehensive guide to the physics and usage of PYTHIA 8.3*,
SciPost Phys. Codeb. (2022) 8, arXiv: [2203.11601 \[hep-ph\]](#).
- [54] H. Brooks and P. Skands, *Coherent showers in decays of colored resonances*,
Phys. Rev. D **100** (2019) 076006, arXiv: [1907.08980 \[hep-ph\]](#).
- [55] R. D. Ball et al., *The PDF4LHC21 combination of global PDF fits for the LHC Run III*,
J. Phys. G **49** (2022) 080501, arXiv: [2203.05506 \[hep-ph\]](#).
- [56] S. Bailey, T. Cridge, L. A. Harland-Lang, A. D. Martin and R. S. Thorne,
Parton distributions from LHC, HERA, Tevatron and fixed target data: MSHT20 PDFs,
Eur. Phys. J. C **81** (2021) 341, arXiv: [2012.04684 \[hep-ph\]](#).
- [57] T.-J. Hou et al.,
New CTEQ global analysis of quantum chromodynamics with high-precision data from the LHC,
Phys. Rev. D **103** (2021) 014013, arXiv: [1912.10053 \[hep-ph\]](#).
- [58] R. D. Ball et al., *Parton distributions from high-precision collider data*,
Eur. Phys. J. C **77** (2017) 663, arXiv: [1706.00428 \[hep-ph\]](#).
- [59] E. Re,
Single-top Wt-channel production matched with parton showers using the POWHEG method,
Eur. Phys. J. C **71** (2011) 1547, arXiv: [1009.2450 \[hep-ph\]](#).
- [60] N. Kidonakis and N. Yamanaka,
Higher-order corrections for tW production at high-energy hadron colliders, **JHEP** **05** (2021) 278,
arXiv: [2102.11300 \[hep-ph\]](#).
- [61] L. A. Harland-Lang, A. D. Martin, P. Motylinski and R. S. Thorne,
Parton distributions in the LHC era: MMHT 2014 PDFs, **Eur. Phys. J. C** **75** (2015) 204,
arXiv: [1412.3989 \[hep-ph\]](#).
- [62] S. Höche, S. Mrenna, S. Payne, C. T. Preuss and P. Skands,
A Study of QCD Radiation in VBF Higgs Production with Vincia and Pythia,
SciPost Phys. **12** (2022) 010, arXiv: [2106.10987 \[hep-ph\]](#).

- [63] ATLAS Collaboration, *Studies on the improvement of the matching uncertainty definition in top-quark processes simulated with PowHEG+PYTHIA8*, ATL-PHYS-PUB-2023-029, 2013, URL: <https://cds.cern.ch/record/2872787>.
- [64] ATLAS Collaboration, *Measurement of the top-quark mass using a leptonic invariant mass in pp collisions at $\sqrt{s} = 13$ TeV with the ATLAS detector*, JHEP **06** (2023) 019, arXiv: [2209.00583 \[hep-ex\]](#).
- [65] T. Ježo, J. M. Lindert, N. Moretti and S. Pozzorini, *New NLOPS predictions for $t\bar{t} + b$ -jet production at the LHC*, Eur. Phys. J. C **78** (2018) 502, arXiv: [1802.00426 \[hep-ph\]](#).
- [66] T. Ježo and P. Nason, *On the Treatment of Resonances in Next-to-Leading Order Calculations Matched to a Parton Shower*, JHEP **12** (2015) 065, arXiv: [1509.09071 \[hep-ph\]](#).
- [67] T. Ježo, J. M. Lindert and S. Pozzorini, *Resonance-aware NLOPS matching for off-shell $t\bar{t} + tW$ production with semileptonic decays*, JHEP **10** (2023) 008, arXiv: [2307.15653 \[hep-ph\]](#).
- [68] M. Czakon et al., *Top-pair production at the LHC through NNLO QCD and NLO EW*, JHEP **10** (2017) 186, arXiv: [1705.04105 \[hep-ph\]](#).
- [69] M. Grazzini, S. Kallweit and M. Wiesemann, *Fully differential NNLO computations with MATRIX*, Eur. Phys. J. C **78** (2018) 537, arXiv: [1711.06631 \[hep-ph\]](#).
- [70] J. Mazzitelli et al., *Next-to-Next-to-Leading Order Event Generation for Top-Quark Pair Production*, Phys. Rev. Lett. **127** (2021) 062001, arXiv: [2012.14267 \[hep-ph\]](#).
- [71] E. Bothmann et al., *Event generation with Sherpa 2.2*, SciPost Phys. **7** (2019) 034, arXiv: [1905.09127 \[hep-ph\]](#).
- [72] T. Gleisberg and S. Höche, *Comix, a new matrix element generator*, JHEP **12** (2008) 039, arXiv: [0808.3674 \[hep-ph\]](#).
- [73] F. Buccioni et al., *OpenLoops 2*, Eur. Phys. J. C **79** (2019) 866, arXiv: [1907.13071 \[hep-ph\]](#).
- [74] F. Cascioli, P. Maierhöfer and S. Pozzorini, *Scattering Amplitudes with Open Loops*, Phys. Rev. Lett. **108** (2012) 111601, arXiv: [1111.5206 \[hep-ph\]](#).
- [75] A. Denner, S. Dittmaier and L. Hofer, *COLLIER: A fortran-based complex one-loop library in extended regularizations*, Comput. Phys. Commun. **212** (2017) 220, arXiv: [1604.06792 \[hep-ph\]](#).
- [76] S. Schumann and F. Krauss, *A parton shower algorithm based on Catani–Seymour dipole factorisation*, JHEP **03** (2008) 038, arXiv: [0709.1027 \[hep-ph\]](#).
- [77] S. Höche, F. Krauss, M. Schönher and F. Siegert, *A critical appraisal of NLO+PS matching methods*, JHEP **09** (2012) 049, arXiv: [1111.1220 \[hep-ph\]](#).
- [78] S. Höche, F. Krauss, M. Schönher and F. Siegert, *QCD matrix elements + parton showers. The NLO case*, JHEP **04** (2013) 027, arXiv: [1207.5030 \[hep-ph\]](#).
- [79] S. Catani, F. Krauss, B. R. Webber and R. Kuhn, *QCD Matrix Elements + Parton Showers*, JHEP **11** (2001) 063, arXiv: [hep-ph/0109231](#).

- [80] S. Höche, F. Krauss, S. Schumann and F. Siegert, *QCD matrix elements and truncated showers*, JHEP **05** (2009) 053, arXiv: [0903.1219 \[hep-ph\]](#).
- [81] C. Anastasiou, L. Dixon, K. Melnikov and F. Petriello, *High-precision QCD at hadron colliders: Electroweak gauge boson rapidity distributions at next-to-next-to leading order*, Phys. Rev. D **69** (2004) 094008, arXiv: [hep-ph/0312266](#).
- [82] J. Alwall et al., *The automated computation of tree-level and next-to-leading order differential cross sections, and their matching to parton shower simulations*, JHEP **07** (2014) 079, arXiv: [1405.0301 \[hep-ph\]](#).
- [83] H. B. Hartanto, B. Jäger, L. Reina and D. Wackerlo, *Higgs boson production in association with top quarks in the POWHEG BOX*, Phys. Rev. D **91** (2015) 094003, arXiv: [1501.04498 \[hep-ph\]](#).
- [84] ATLAS Collaboration, *Performance of electron and photon triggers in ATLAS during LHC Run 2*, Eur. Phys. J. C **80** (2020) 47, arXiv: [1909.00761 \[hep-ex\]](#).
- [85] ATLAS Collaboration, *Performance of the ATLAS muon triggers in Run 2*, JINST **15** (2020) P09015, arXiv: [2004.13447 \[physics.ins-det\]](#).
- [86] ATLAS Collaboration, *Electron and photon performance measurements with the ATLAS detector using the 2015–2017 LHC proton–proton collision data*, JINST **14** (2019) P12006, arXiv: [1908.00005 \[hep-ex\]](#).
- [87] ATLAS Collaboration, *Electron and photon efficiencies in LHC Run 2 with the ATLAS experiment*, JHEP **05** (2024) 162, arXiv: [2308.13362 \[hep-ex\]](#).
- [88] ATLAS Collaboration, *Evidence for the associated production of the Higgs boson and a top quark pair with the ATLAS detector*, Phys. Rev. D **97** (2018) 072003, arXiv: [1712.08891 \[hep-ex\]](#).
- [89] ATLAS Collaboration, *Muon reconstruction and identification efficiency in ATLAS using the full Run 2 pp collision data set at $\sqrt{s} = 13$ TeV*, Eur. Phys. J. C **81** (2021) 578, arXiv: [2012.00578 \[hep-ex\]](#).
- [90] ATLAS Collaboration, *Studies of the muon momentum calibration and performance of the ATLAS detector with pp collisions at $\sqrt{s} = 13$ TeV*, Eur. Phys. J. C **83** (2023) 686, arXiv: [2212.07338 \[hep-ex\]](#).
- [91] M. Cacciari, G. P. Salam and G. Soyez, *The anti- k_t jet clustering algorithm*, JHEP **04** (2008) 063, arXiv: [0802.1189 \[hep-ph\]](#).
- [92] M. Cacciari, G. P. Salam and G. Soyez, *FastJet user manual*, Eur. Phys. J. C **72** (2012) 1896, arXiv: [1111.6097 \[hep-ph\]](#).
- [93] ATLAS Collaboration, *Jet reconstruction and performance using particle flow with the ATLAS Detector*, Eur. Phys. J. C **77** (2017) 466, arXiv: [1703.10485 \[hep-ex\]](#).
- [94] ATLAS Collaboration, *Performance of pile-up mitigation techniques for jets in pp collisions at $\sqrt{s} = 8$ TeV using the ATLAS detector*, Eur. Phys. J. C **76** (2016) 581, arXiv: [1510.03823 \[hep-ex\]](#).
- [95] ATLAS Collaboration, *Jet energy scale and resolution measured in proton–proton collisions at $\sqrt{s} = 13$ TeV with the ATLAS detector*, Eur. Phys. J. C **81** (2021) 689, arXiv: [2007.02645 \[hep-ex\]](#).

- [96] ATLAS Collaboration, *ATLAS flavour-tagging algorithms for the LHC Run 2 pp collision dataset*, *Eur. Phys. J. C* **83** (2023) 681, arXiv: [2211.16345 \[physics.data-an\]](#).
- [97] ATLAS Collaboration, *ATLAS b-jet identification performance and efficiency measurement with $t\bar{t}$ events in pp collisions at $\sqrt{s} = 13$ TeV*, *Eur. Phys. J. C* **79** (2019) 970, arXiv: [1907.05120 \[hep-ex\]](#).
- [98] ATLAS Collaboration, *The performance of missing transverse momentum reconstruction and its significance with the ATLAS detector using 140fb^{-1} of $\sqrt{s} = 13$ TeV pp collisions*, (2024), arXiv: [2402.05858 \[hep-ex\]](#).
- [99] CMS Collaboration, *Measurements of $t\bar{t}$ differential cross sections in proton–proton collisions at $\sqrt{s} = 13$ TeV using events containing two leptons*, *JHEP* **02** (2019) 149, arXiv: [1811.06625 \[hep-ex\]](#).
- [100] ATLAS Collaboration, *Measurement of $t\bar{t}$ production in association with additional b-jets in the $e\mu$ final state in proton–proton collisions at $\sqrt{s} = 13$ TeV with the ATLAS detector*, *JHEP* **01** (2025) 068, arXiv: [2407.13473 \[hep-ex\]](#).
- [101] M. Cacciari, G. P. Salam and G. Soyez, *The Catchment Area of Jets*, *JHEP* **04** (2008) 005, arXiv: [0802.1188 \[hep-ph\]](#).
- [102] G. D’Agostini, *A multidimensional unfolding method based on Bayes’ theorem*, *Nucl. Instrum. Meth. A* **362** (1995) 487.
- [103] T. Adye, ‘Unfolding algorithms and tests using RooUnfold’, *Proceedings, 2011 Workshop on Statistical Issues Related to Discovery Claims in Search Experiments and Unfolding (PHYSTAT 2011)* (CERN, Geneva, Switzerland, 17th–20th Jan. 2011) 313, arXiv: [1105.1160 \[physics.data-an\]](#).
- [104] ATLAS Collaboration, *Measurement of the c-jet mistagging efficiency in $t\bar{t}$ events using pp collision data at $\sqrt{s} = 13$ TeV collected with the ATLAS detector*, *Eur. Phys. J. C* **82** (2022) 95, arXiv: [2109.10627 \[hep-ex\]](#).
- [105] ATLAS Collaboration, *Calibration of the light-flavour jet mistagging efficiency of the b-tagging algorithms with Z+jets events using 139fb^{-1} of ATLAS proton–proton collision data at $\sqrt{s} = 13$ TeV*, *Eur. Phys. J. C* **83** (2023) 728, arXiv: [2301.06319 \[hep-ex\]](#).
- [106] ATLAS Collaboration, *Studies on top-quark Monte Carlo modelling with Sherpa and MG5_aMC@NLO*, ATL-PHYS-PUB-2017-007, 2017, URL: <https://cds.cern.ch/record/2261938>.
- [107] ATLAS Collaboration, *Measurement of the top quark mass in the $t\bar{t} \rightarrow \text{lepton+jets}$ channel from $\sqrt{s} = 8$ TeV ATLAS data and combination with previous results*, *Eur. Phys. J. C* **79** (2019) 290, arXiv: [1810.01772 \[hep-ex\]](#).
- [108] CMS Collaboration, *Measurement of the top quark mass using proton–proton data at $\sqrt{s} = 7$ and 8 TeV*, *Phys. Rev. D* **93** (2016) 072004, arXiv: [1509.04044 \[hep-ex\]](#).
- [109] J. Butterworth et al., *PDF4LHC recommendations for LHC Run II*, *J. Phys. G* **43** (2016) 023001, arXiv: [1510.03865 \[hep-ph\]](#).
- [110] ATLAS Collaboration, *ATLAS simulation of boson plus jets processes in Run 2*, ATL-PHYS-PUB-2017-006, 2017, URL: <https://cds.cern.ch/record/2261937>.

- [111] ATLAS Collaboration, *Measurement of $W^\pm Z$ production cross sections and gauge boson polarisation in pp collisions at $\sqrt{s} = 13$ TeV with the ATLAS detector*, *Eur. Phys. J. C* **79** (2019) 535, arXiv: [1902.05759 \[hep-ex\]](https://arxiv.org/abs/1902.05759).
- [112] D. de Florian et al., *Handbook of LHC Higgs Cross Sections: 4. Deciphering the Nature of the Higgs Sector*, (2017), arXiv: [1610.07922 \[hep-ph\]](https://arxiv.org/abs/1610.07922).
- [113] E. Maguire, L. Heinrich and G. Watt, *HEPData: a repository for high energy physics data*, *J. Phys. Conf. Ser.* **898** (2017) 102006, ed. by R. Mount and C. Tull, arXiv: [1704.05473 \[hep-ex\]](https://arxiv.org/abs/1704.05473).
- [114] ATLAS Collaboration, *ATLAS Computing Acknowledgements*, ATL-SOFT-PUB-2025-001, 2025, URL: <https://cds.cern.ch/record/2922210>.

The ATLAS Collaboration

G. Aad [ID¹⁰⁴](#), E. Aakvaag [ID¹⁷](#), B. Abbott [ID¹²³](#), S. Abdelhameed [ID^{119a}](#), K. Abeling [ID⁵⁵](#), N.J. Abicht [ID⁴⁹](#), S.H. Abidi [ID³⁰](#), M. Aboelela [ID⁴⁵](#), A. Aboulhorma [ID^{36e}](#), H. Abramowicz [ID¹⁵⁷](#), Y. Abulaiti [ID¹²⁰](#), B.S. Acharya [ID^{69a,69b,n}](#), A. Ackermann [ID^{63a}](#), C. Adam Bourdarios [ID⁴](#), L. Adamczyk [ID^{86a}](#), S.V. Addepalli [ID¹⁴⁹](#), M.J. Addison [ID¹⁰³](#), J. Adelman [ID¹¹⁸](#), A. Adiguzel [ID^{22c}](#), T. Adye [ID¹³⁷](#), A.A. Affolder [ID¹³⁹](#), Y. Afik [ID⁴⁰](#), M.N. Agaras [ID¹³](#), A. Aggarwal [ID¹⁰²](#), C. Agheorghiesei [ID^{28c}](#), F. Ahmadov [ID^{39,ae}](#), S. Ahuja [ID⁹⁷](#), X. Ai [ID^{143b}](#), G. Aielli [ID^{76a,76b}](#), A. Aikot [ID¹⁶⁹](#), M. Ait Tamlihat [ID^{36e}](#), B. Aitbenchikh [ID^{36a}](#), M. Akbiyik [ID¹⁰²](#), T.P.A. Åkesson [ID¹⁰⁰](#), A.V. Akimov [ID¹⁵¹](#), D. Akiyama [ID¹⁷⁴](#), N.N. Akolkar [ID²⁵](#), S. Aktas [ID^{22a}](#), G.L. Alberghi [ID^{24b}](#), J. Albert [ID¹⁷¹](#), P. Albicocco [ID⁵³](#), G.L. Albouy [ID⁶⁰](#), S. Alderweireldt [ID⁵²](#), Z.L. Alegria [ID¹²⁴](#), M. Aleksa [ID³⁷](#), I.N. Aleksandrov [ID³⁹](#), C. Alexa [ID^{28b}](#), T. Alexopoulos [ID¹⁰](#), F. Alfonsi [ID^{24b}](#), M. Algren [ID⁵⁶](#), M. Alhroob [ID¹⁷³](#), B. Ali [ID¹³⁵](#), H.M.J. Ali [ID^{93,x}](#), S. Ali [ID³²](#), S.W. Alibocus [ID⁹⁴](#), M. Aliev [ID^{34c}](#), G. Alimonti [ID^{71a}](#), W. Alkakhi [ID⁵⁵](#), C. Allaire [ID⁶⁶](#), B.M.M. Allbrooke [ID¹⁵²](#), J.S. Allen [ID¹⁰³](#), J.F. Allen [ID⁵²](#), P.P. Allport [ID²¹](#), A. Aloisio [ID^{72a,72b}](#), F. Alonso [ID⁹²](#), C. Alpigiani [ID¹⁴²](#), Z.M.K. Alsolami [ID⁹³](#), A. Alvarez Fernandez [ID¹⁰²](#), M. Alves Cardoso [ID⁵⁶](#), M.G. Alvaggi [ID^{72a,72b}](#), M. Aly [ID¹⁰³](#), Y. Amaral Coutinho [ID^{83b}](#), A. Ambler [ID¹⁰⁶](#), C. Amelung [ID³⁷](#), M. Amerl [ID¹⁰³](#), C.G. Ames [ID¹¹¹](#), T. Amezza [ID¹³⁰](#), D. Amidei [ID¹⁰⁸](#), B. Amini [ID⁵⁴](#), K. Amirie [ID¹⁶¹](#), A. Amirkhanov [ID³⁹](#), S.P. Amor Dos Santos [ID^{133a}](#), K.R. Amos [ID¹⁶⁹](#), D. Amperiadou [ID¹⁵⁸](#), S. An [ID⁸⁴](#), C. Anastopoulos [ID¹⁴⁵](#), T. Andeen [ID¹¹](#), J.K. Anders [ID⁹⁴](#), A.C. Anderson [ID⁵⁹](#), A. Andreazza [ID^{71a,71b}](#), S. Angelidakis [ID⁹](#), A. Angerami [ID⁴²](#), A.V. Anisenkov [ID³⁹](#), A. Annovi [ID^{74a}](#), C. Antel [ID⁵⁶](#), E. Antipov [ID¹⁵¹](#), M. Antonelli [ID⁵³](#), F. Anulli [ID^{75a}](#), M. Aoki [ID⁸⁴](#), T. Aoki [ID¹⁵⁹](#), M.A. Aparo [ID¹⁵²](#), L. Aperio Bella [ID⁴⁸](#), M. Apicella [ID³¹](#), C. Appelt [ID¹⁵⁷](#), A. Apyan [ID²⁷](#), S.J. Arbiol Val [ID⁸⁷](#), C. Arcangeletti [ID⁵³](#), A.T.H. Arce [ID⁵¹](#), J-F. Arguin [ID¹¹⁰](#), S. Argyropoulos [ID¹⁵⁸](#), J.-H. Arling [ID⁴⁸](#), O. Arnaez [ID⁴](#), H. Arnold [ID¹⁵¹](#), G. Artoni [ID^{75a,75b}](#), H. Asada [ID¹¹³](#), K. Asai [ID¹²¹](#), S. Asai [ID¹⁵⁹](#), S. Asatryan [ID¹⁷⁹](#), N.A. Asbah [ID³⁷](#), R.A. Ashby Pickering [ID¹⁷³](#), A.M. Aslam [ID⁹⁷](#), K. Assamagan [ID³⁰](#), R. Astalos [ID^{29a}](#), K.S.V. Astrand [ID¹⁰⁰](#), S. Atashi [ID¹⁶⁵](#), R.J. Atkin [ID^{34a}](#), H. Atmani [ID^{36f}](#), P.A. Atmasiddha [ID¹³¹](#), K. Augsten [ID¹³⁵](#), A.D. Auriol [ID⁴¹](#), V.A. Astrup [ID¹⁰³](#), G. Avolio [ID³⁷](#), K. Axiotis [ID⁵⁶](#), G. Azuelos [ID^{110,ai}](#), D. Babal [ID^{29b}](#), H. Bachacou [ID¹³⁸](#), K. Bachas [ID^{158,r}](#), A. Bachiu [ID³⁵](#), E. Bachmann [ID⁵⁰](#), M.J. Backes [ID^{63a}](#), A. Badea [ID⁴⁰](#), T.M. Baer [ID¹⁰⁸](#), P. Bagnaia [ID^{75a,75b}](#), M. Bahmani [ID¹⁹](#), D. Bahner [ID⁵⁴](#), K. Bai [ID¹²⁶](#), J.T. Baines [ID¹³⁷](#), L. Baines [ID⁹⁶](#), O.K. Baker [ID¹⁷⁸](#), E. Bakos [ID¹⁶](#), D. Bakshi Gupta [ID⁸](#), L.E. Balabram Filho [ID^{83b}](#), V. Balakrishnan [ID¹²³](#), R. Balasubramanian [ID⁴](#), E.M. Baldin [ID³⁸](#), P. Balek [ID^{86a}](#), E. Ballabene [ID^{24b,24a}](#), F. Balli [ID¹³⁸](#), L.M. Baltes [ID^{63a}](#), W.K. Balunas [ID³³](#), J. Balz [ID¹⁰²](#), I. Bamwidhi [ID^{119b}](#), E. Banas [ID⁸⁷](#), M. Bandiermonte [ID¹³²](#), A. Bandyopadhyay [ID²⁵](#), S. Bansal [ID²⁵](#), L. Barak [ID¹⁵⁷](#), M. Barakat [ID⁴⁸](#), E.L. Barberio [ID¹⁰⁷](#), D. Barberis [ID^{18b}](#), M. Barbero [ID¹⁰⁴](#), M.Z. Barel [ID¹¹⁷](#), T. Barillari [ID¹¹²](#), M-S. Barisits [ID³⁷](#), T. Barklow [ID¹⁴⁹](#), P. Baron [ID¹³⁶](#), D.A. Baron Moreno [ID¹⁰³](#), A. Baroncelli [ID⁶²](#), A.J. Barr [ID¹²⁹](#), J.D. Barr [ID⁹⁸](#), F. Barreiro [ID¹⁰¹](#), J. Barreiro Guimaraes da Costa [ID¹⁴](#), M.G. Barros Teixeira [ID^{133a}](#), S. Barsov [ID³⁸](#), F. Bartels [ID^{63a}](#), R. Bartoldus [ID¹⁴⁹](#), A.E. Barton [ID⁹³](#), P. Bartos [ID^{29a}](#), A. Basan [ID¹⁰²](#), M. Baselga [ID⁴⁹](#), S. Bashiri [ID⁸⁷](#), A. Bassalat [ID^{66,b}](#), M.J. Basso [ID^{162a}](#), S. Bataju [ID⁴⁵](#), R. Bate [ID¹⁷⁰](#), R.L. Bates [ID⁵⁹](#), S. Batlamous [ID¹⁰¹](#), M. Battaglia [ID¹³⁹](#), D. Battulga [ID¹⁹](#), M. Baucé [ID^{75a,75b}](#), M. Bauer [ID⁷⁹](#), P. Bauer [ID²⁵](#), L.T. Bayer [ID⁴⁸](#), L.T. Bazzano Hurrell [ID³¹](#), J.B. Beacham [ID¹¹²](#), T. Beau [ID¹³⁰](#), J.Y. Beauchamp [ID⁹²](#), P.H. Beauchemin [ID¹⁶⁴](#), P. Bechtle [ID²⁵](#), H.P. Beck [ID^{20,q}](#), K. Becker [ID¹⁷³](#), A.J. Beddall [ID⁸²](#), V.A. Bednyakov [ID³⁹](#), C.P. Bee [ID¹⁵¹](#), L.J. Beemster [ID¹⁶](#), M. Begalli [ID^{83d}](#), M. Begel [ID³⁰](#), J.K. Behr [ID⁴⁸](#), J.F. Beirer [ID³⁷](#), F. Beisiegel [ID²⁵](#), M. Belfkir [ID^{119b}](#), G. Bella [ID¹⁵⁷](#), L. Bellagamba [ID^{24b}](#), A. Bellerive [ID³⁵](#), C.D. Bellgraph [ID⁶⁸](#), P. Bellos [ID²¹](#), K. Beloborodov [ID³⁸](#), D. Benchekroun [ID^{36a}](#), F. Bendebba [ID^{36a}](#), Y. Benhammou [ID¹⁵⁷](#),

K.C. Benkendorfer [ID⁶¹](#), L. Beresford [ID⁴⁸](#), M. Beretta [ID⁵³](#), E. Bergeaas Kuutmann [ID¹⁶⁷](#), N. Berger [ID⁴](#),
 B. Bergmann [ID¹³⁵](#), J. Beringer [ID^{18a}](#), G. Bernardi [ID⁵](#), C. Bernius [ID¹⁴⁹](#), F.U. Bernlochner [ID²⁵](#),
 F. Bernon [ID³⁷](#), A. Berrocal Guardia [ID¹³](#), T. Berry [ID⁹⁷](#), P. Berta [ID¹³⁶](#), A. Berthold [ID⁵⁰](#), A. Berti [ID^{133a}](#),
 R. Bertrand [ID¹⁰⁴](#), S. Bethke [ID¹¹²](#), A. Betti [ID^{75a,75b}](#), A.J. Bevan [ID⁹⁶](#), L. Bezio [ID⁵⁶](#), N.K. Bhalla [ID⁵⁴](#),
 S. Bharthuar [ID¹¹²](#), S. Bhatta [ID¹⁵¹](#), P. Bhattacharai [ID¹⁴⁹](#), Z.M. Bhatti [ID¹²⁰](#), K.D. Bhide [ID⁵⁴](#),
 V.S. Bhopatkar [ID¹²⁴](#), R.M. Bianchi [ID¹³²](#), G. Bianco [ID^{24b,24a}](#), O. Biebel [ID¹¹¹](#), M. Biglietti [ID^{77a}](#),
 C.S. Billingsley [ID⁴⁵](#), Y. Bimgni [ID^{36f}](#), M. Bindl [ID⁵⁵](#), A. Bingham [ID¹⁷⁷](#), A. Bingul [ID^{22b}](#), C. Bini [ID^{75a,75b}](#),
 G.A. Bird [ID³³](#), M. Birman [ID¹⁷⁵](#), M. Biros [ID¹³⁶](#), S. Biryukov [ID¹⁵²](#), T. Bisanz [ID⁴⁹](#), E. Bisceglie [ID^{24b,24a}](#),
 J.P. Biswal [ID¹³⁷](#), D. Biswas [ID¹⁴⁷](#), I. Bloch [ID⁴⁸](#), A. Blue [ID⁵⁹](#), U. Blumenschein [ID⁹⁶](#), J. Blumenthal [ID¹⁰²](#),
 V.S. Bobrovnikov [ID³⁹](#), L. Boccardo [ID^{57b,57a}](#), M. Boehler [ID⁵⁴](#), B. Boehm [ID¹⁷²](#), D. Bogavac [ID¹³](#),
 A.G. Bogdanchikov [ID³⁸](#), L.S. Boggia [ID¹³⁰](#), V. Boisvert [ID⁹⁷](#), P. Bokan [ID³⁷](#), T. Bold [ID^{86a}](#), M. Bomben [ID⁵](#),
 M. Bona [ID⁹⁶](#), M. Boonekamp [ID¹³⁸](#), A.G. Borbely [ID⁵⁹](#), I.S. Bordulev [ID³⁸](#), G. Borissov [ID⁹³](#),
 D. Bortoletto [ID¹²⁹](#), D. Boscherini [ID^{24b}](#), M. Bosman [ID¹³](#), K. Bouaouda [ID^{36a}](#), N. Bouchhar [ID¹⁶⁹](#),
 L. Boudet [ID⁴](#), J. Boudreau [ID¹³²](#), E.V. Bouhova-Thacker [ID⁹³](#), D. Boumediene [ID⁴¹](#), R. Bouquet [ID^{57b,57a}](#),
 A. Boveia [ID¹²²](#), J. Boyd [ID³⁷](#), D. Boye [ID³⁰](#), I.R. Boyko [ID³⁹](#), L. Bozianu [ID⁵⁶](#), J. Bracinik [ID²¹](#),
 N. Brahimi [ID⁴](#), G. Brandt [ID¹⁷⁷](#), O. Brandt [ID³³](#), B. Brau [ID¹⁰⁵](#), J.E. Brau [ID¹²⁶](#), R. Brener [ID¹⁷⁵](#),
 L. Brenner [ID¹¹⁷](#), R. Brenner [ID¹⁶⁷](#), S. Bressler [ID¹⁷⁵](#), G. Brianti [ID^{78a,78b}](#), D. Britton [ID⁵⁹](#), D. Britzger [ID¹¹²](#),
 I. Brock [ID²⁵](#), R. Brock [ID¹⁰⁹](#), G. Brooijmans [ID⁴²](#), A.J. Brooks [ID⁶⁸](#), E.M. Brooks [ID^{162b}](#), E. Brost [ID³⁰](#),
 L.M. Brown [ID^{171,162a}](#), L.E. Bruce [ID⁶¹](#), T.L. Bruckler [ID¹²⁹](#), P.A. Bruckman de Renstrom [ID⁸⁷](#),
 B. Brüers [ID⁴⁸](#), A. Bruni [ID^{24b}](#), G. Bruni [ID^{24b}](#), D. Brunner [ID^{47a,47b}](#), M. Bruschi [ID^{24b}](#), N. Bruscino [ID^{75a,75b}](#),
 T. Buanes [ID¹⁷](#), Q. Buat [ID¹⁴²](#), D. Buchin [ID¹¹²](#), A.G. Buckley [ID⁵⁹](#), O. Bulekov [ID⁸²](#), B.A. Bullard [ID¹⁴⁹](#),
 S. Burdin [ID⁹⁴](#), C.D. Burgard [ID⁴⁹](#), A.M. Burger [ID⁹¹](#), B. Burghgrave [ID⁸](#), O. Burlayenko [ID⁵⁴](#),
 J. Burleson [ID¹⁶⁸](#), J.C. Burzynski [ID¹⁴⁸](#), E.L. Busch [ID⁴²](#), V. Büscher [ID¹⁰²](#), P.J. Bussey [ID⁵⁹](#), J.M. Butler [ID²⁶](#),
 C.M. Buttar [ID⁵⁹](#), J.M. Butterworth [ID⁹⁸](#), W. Buttinger [ID¹³⁷](#), C.J. Buxo Vazquez [ID¹⁰⁹](#), A.R. Buzykaev [ID³⁹](#),
 S. Cabrera Urbán [ID¹⁶⁹](#), L. Cadamuro [ID⁶⁶](#), D. Caforio [ID⁵⁸](#), H. Cai [ID¹³²](#), Y. Cai [ID^{24b,114c,24a}](#), Y. Cai [ID^{114a}](#),
 V.M.M. Cairo [ID³⁷](#), O. Cakir [ID^{3a}](#), N. Calace [ID³⁷](#), P. Calafiura [ID^{18a}](#), G. Calderini [ID¹³⁰](#), P. Calfayan [ID³⁵](#),
 G. Callea [ID⁵⁹](#), L.P. Caloba [ID^{83b}](#), D. Calvet [ID⁴¹](#), S. Calvet [ID⁴¹](#), R. Camacho Toro [ID¹³⁰](#), S. Camarda [ID³⁷](#),
 D. Camarero Munoz [ID²⁷](#), P. Camarri [ID^{76a,76b}](#), C. Camincher [ID¹⁷¹](#), M. Campanelli [ID⁹⁸](#), A. Camplani [ID⁴³](#),
 V. Canale [ID^{72a,72b}](#), A.C. Canbay [ID^{3a}](#), E. Canonero [ID⁹⁷](#), J. Cantero [ID¹⁶⁹](#), Y. Cao [ID¹⁶⁸](#), F. Capocasa [ID²⁷](#),
 M. Capua [ID^{44b,44a}](#), A. Carbone [ID^{71a,71b}](#), R. Cardarelli [ID^{76a}](#), J.C.J. Cardenas [ID⁸](#), M.P. Cardiff [ID²⁷](#),
 G. Carducci [ID^{44b,44a}](#), T. Carli [ID³⁷](#), G. Carlino [ID^{72a}](#), J.I. Carlotto [ID¹³](#), B.T. Carlson [ID^{132,s}](#),
 E.M. Carlson [ID¹⁷¹](#), J. Carmignani [ID⁹⁴](#), L. Carminati [ID^{71a,71b}](#), A. Carnelli [ID⁴](#), M. Carnesale [ID³⁷](#),
 S. Caron [ID¹¹⁶](#), E. Carquin [ID^{140f}](#), I.B. Carr [ID¹⁰⁷](#), S. Carrá [ID^{73a,73b}](#), G. Carratta [ID^{24b,24a}](#), A.M. Carroll [ID¹²⁶](#),
 M.P. Casado [ID^{13,i}](#), P. Casolario [ID^{72a,72b}](#), M. Caspar [ID⁴⁸](#), F.L. Castillo [ID⁴](#), L. Castillo Garcia [ID¹³](#),
 V. Castillo Gimenez [ID¹⁶⁹](#), N.F. Castro [ID^{133a,133e}](#), A. Catinaccio [ID³⁷](#), J.R. Catmore [ID¹²⁸](#), T. Cavaliere [ID⁴](#),
 V. Cavaliere [ID³⁰](#), L.J. Caviedes Betancourt [ID^{23b}](#), E. Celebi [ID⁸²](#), S. Celli [ID³⁷](#), V. Cepaitis [ID⁵⁶](#),
 K. Cerny [ID¹²⁵](#), A.S. Cerqueira [ID^{83a}](#), A. Cerri [ID^{74a,74b,al}](#), L. Cerrito [ID^{76a,76b}](#), F. Cerutti [ID^{18a}](#),
 B. Cervato [ID^{71a,71b}](#), A. Cervelli [ID^{24b}](#), G. Cesarin [ID⁵³](#), S.A. Cetin [ID⁸²](#), P.M. Chabrillat [ID¹³⁰](#),
 R. Chakkappai [ID⁶⁶](#), S. Chakraborty [ID¹⁷³](#), J. Chan [ID^{18a}](#), W.Y. Chan [ID¹⁵⁹](#), J.D. Chapman [ID³³](#),
 E. Chapon [ID¹³⁸](#), B. Chargeishvili [ID^{155b}](#), D.G. Charlton [ID²¹](#), C. Chauhan [ID¹³⁶](#), Y. Che [ID^{114a}](#),
 S. Chekanov [ID⁶](#), S.V. Chekulaev [ID^{162a}](#), G.A. Chelkov [ID^{39,a}](#), B. Chen [ID¹⁵⁷](#), B. Chen [ID¹⁷¹](#), H. Chen [ID^{114a}](#),
 H. Chen [ID³⁰](#), J. Chen [ID^{144a}](#), J. Chen [ID¹⁴⁸](#), M. Chen [ID¹²⁹](#), S. Chen [ID⁸⁹](#), S.J. Chen [ID^{114a}](#), X. Chen [ID^{144a}](#),
 X. Chen [ID^{15,ah}](#), Z. Chen [ID⁶²](#), C.L. Cheng [ID¹⁷⁶](#), H.C. Cheng [ID^{64a}](#), S. Cheong [ID¹⁴⁹](#), A. Cheplakov [ID³⁹](#),
 E. Cherepanova [ID¹¹⁷](#), R. Cherkaoui El Moursli [ID^{36e}](#), E. Cheu [ID⁷](#), K. Cheung [ID⁶⁵](#), L. Chevalier [ID¹³⁸](#),
 V. Chiarella [ID⁵³](#), G. Chiarelli [ID^{74a}](#), G. Chiodini [ID^{70a}](#), A.S. Chisholm [ID²¹](#), A. Chitan [ID^{28b}](#),
 M. Chitishvili [ID¹⁶⁹](#), M.V. Chizhov [ID^{39,t}](#), K. Choi [ID¹¹](#), Y. Chou [ID¹⁴²](#), E.Y.S. Chow [ID¹¹⁶](#), K.L. Chu [ID¹⁷⁵](#),
 M.C. Chu [ID^{64a}](#), X. Chu [ID^{14,114c}](#), Z. Chubinidze [ID⁵³](#), J. Chudoba [ID¹³⁴](#), J.J. Chwastowski [ID⁸⁷](#),

D. Cieri [ID¹¹²](#), K.M. Ciesla [ID^{86a}](#), V. Cindro [ID⁹⁵](#), A. Ciocio [ID^{18a}](#), F. Cirotto [ID^{72a,72b}](#), Z.H. Citron [ID¹⁷⁵](#), M. Citterio [ID^{71a}](#), D.A. Ciubotaru [ID^{28b}](#), A. Clark [ID⁵⁶](#), P.J. Clark [ID⁵²](#), N. Clarke Hall [ID⁹⁸](#), C. Clarry [ID¹⁶¹](#), S.E. Clawson [ID⁴⁸](#), C. Clement [ID^{47a,47b}](#), Y. Coadou [ID¹⁰⁴](#), M. Cobal [ID^{69a,69c}](#), A. Coccaro [ID^{57b}](#), R.F. Coelho Barrue [ID^{133a}](#), R. Coelho Lopes De Sa [ID¹⁰⁵](#), S. Coelli [ID^{71a}](#), L.S. Colangeli [ID¹⁶¹](#), B. Cole [ID⁴²](#), P. Collado Soto [ID¹⁰¹](#), J. Collot [ID⁶⁰](#), R. Coluccia [ID^{70a,70b}](#), P. Conde Muñoz [ID^{133a,133g}](#), M.P. Connell [ID^{34c}](#), S.H. Connell [ID^{34c}](#), E.I. Conroy [ID¹²⁹](#), M. Contreras Cossio [ID¹¹](#), F. Conventi [ID^{72a,aj}](#), H.G. Cooke [ID²¹](#), A.M. Cooper-Sarkar [ID¹²⁹](#), L. Corazzina [ID^{75a,75b}](#), F.A. Corchia [ID^{24b,24a}](#), A. Cordeiro Oudot Choi [ID¹⁴²](#), L.D. Corpe [ID⁴¹](#), M. Corradi [ID^{75a,75b}](#), F. Corriveau [ID^{106,ac}](#), A. Cortes-Gonzalez [ID¹⁵⁹](#), M.J. Costa [ID¹⁶⁹](#), F. Costanza [ID⁴](#), D. Costanzo [ID¹⁴⁵](#), B.M. Cote [ID¹²²](#), J. Couthures [ID⁴](#), G. Cowan [ID⁹⁷](#), K. Cranmer [ID¹⁷⁶](#), L. Cremer [ID⁴⁹](#), D. Cremonini [ID^{24b,24a}](#), S. Crépé-Renaudin [ID⁶⁰](#), F. Crescioli [ID¹³⁰](#), T. Cresta [ID^{73a,73b}](#), M. Cristinziani [ID¹⁴⁷](#), M. Cristoforetti [ID^{78a,78b}](#), V. Croft [ID¹¹⁷](#), J.E. Crosby [ID¹²⁴](#), G. Crosetti [ID^{44b,44a}](#), A. Cueto [ID¹⁰¹](#), H. Cui [ID⁹⁸](#), Z. Cui [ID⁷](#), W.R. Cunningham [ID⁵⁹](#), F. Curcio [ID¹⁶⁹](#), J.R. Curran [ID⁵²](#), M.J. Da Cunha Sargedas De Sousa [ID^{57b,57a}](#), J.V. Da Fonseca Pinto [ID^{83b}](#), C. Da Via [ID¹⁰³](#), W. Dabrowski [ID^{86a}](#), T. Dado [ID³⁷](#), S. Dahbi [ID¹⁵⁴](#), T. Dai [ID¹⁰⁸](#), D. Dal Santo [ID²⁰](#), C. Dallapiccola [ID¹⁰⁵](#), M. Dam [ID⁴³](#), G. D'amen [ID³⁰](#), V. D'Amico [ID¹¹¹](#), J. Damp [ID¹⁰²](#), J.R. Dandoy [ID³⁵](#), D. Dannheim [ID³⁷](#), G. D'anniballe [ID^{74a,74b}](#), M. Danninger [ID¹⁴⁸](#), V. Dao [ID¹⁵¹](#), G. Darbo [ID^{57b}](#), S.J. Das [ID³⁰](#), F. Dattola [ID⁴⁸](#), S. D'Auria [ID^{71a,71b}](#), A. D'Avanzo [ID^{72a,72b}](#), T. Davidek [ID¹³⁶](#), J. Davidson [ID¹⁷³](#), I. Dawson [ID⁹⁶](#), K. De [ID⁸](#), C. De Almeida Rossi [ID¹⁶¹](#), R. De Asmundis [ID^{72a}](#), N. De Biase [ID⁴⁸](#), S. De Castro [ID^{24b,24a}](#), N. De Groot [ID¹¹⁶](#), P. de Jong [ID¹¹⁷](#), H. De la Torre [ID¹¹⁸](#), A. De Maria [ID^{114a}](#), A. De Salvo [ID^{75a}](#), U. De Sanctis [ID^{76a,76b}](#), F. De Santis [ID^{70a,70b}](#), A. De Santo [ID¹⁵²](#), J.B. De Vivie De Regie [ID⁶⁰](#), J. Debevc [ID⁹⁵](#), D.V. Dedovich [ID³⁹](#), J. Degens [ID⁹⁴](#), A.M. Deiana [ID⁴⁵](#), J. Del Peso [ID¹⁰¹](#), L. Delagrange [ID¹³⁰](#), F. Deliot [ID¹³⁸](#), C.M. Delitzsch [ID⁴⁹](#), M. Della Pietra [ID^{72a,72b}](#), D. Della Volpe [ID⁵⁶](#), A. Dell'Acqua [ID³⁷](#), L. Dell'Asta [ID^{71a,71b}](#), M. Delmastro [ID⁴](#), C.C. Delogu [ID¹⁰²](#), P.A. Delsart [ID⁶⁰](#), S. Demers [ID¹⁷⁸](#), M. Demichev [ID³⁹](#), S.P. Denisov [ID³⁸](#), H. Denizli [ID^{22a,m}](#), L. D'Eramo [ID⁴¹](#), D. Derendarz [ID⁸⁷](#), F. Derue [ID¹³⁰](#), P. Dervan [ID⁹⁴](#), A.M. Desai [ID¹](#), K. Desch [ID²⁵](#), F.A. Di Bello [ID^{57b,57a}](#), A. Di Ciaccio [ID^{76a,76b}](#), L. Di Ciaccio [ID⁴](#), A. Di Domenico [ID^{75a,75b}](#), C. Di Donato [ID^{72a,72b}](#), A. Di Girolamo [ID³⁷](#), G. Di Gregorio [ID³⁷](#), A. Di Luca [ID^{78a,78b}](#), B. Di Micco [ID^{77a,77b}](#), R. Di Nardo [ID^{77a,77b}](#), K.F. Di Petrillo [ID⁴⁰](#), M. Diamantopoulou [ID³⁵](#), F.A. Dias [ID¹¹⁷](#), M.A. Diaz [ID^{140a,140b}](#), A.R. Didenko [ID³⁹](#), M. Didenko [ID¹⁶⁹](#), S.D. Diefenbacher [ID^{18a}](#), E.B. Diehl [ID¹⁰⁸](#), S. Díez Cornell [ID⁴⁸](#), C. Diez Pardos [ID¹⁴⁷](#), C. Dimitriadi [ID¹⁵⁰](#), A. Dimitrievska [ID²¹](#), A. Dimri [ID¹⁵¹](#), J. Dingfelder [ID²⁵](#), T. Dingley [ID¹²⁹](#), I-M. Dinu [ID^{28b}](#), S.J. Dittmeier [ID^{63b}](#), F. Dittus [ID³⁷](#), M. Divisek [ID¹³⁶](#), B. Dixit [ID⁹⁴](#), F. Djama [ID¹⁰⁴](#), T. Djobava [ID^{155b}](#), C. Doglioni [ID^{103,100}](#), A. Dohnalova [ID^{29a}](#), Z. Dolezal [ID¹³⁶](#), K. Domijan [ID^{86a}](#), K.M. Dona [ID⁴⁰](#), M. Donadelli [ID^{83d}](#), B. Dong [ID¹⁰⁹](#), J. Donini [ID⁴¹](#), A. D'Onofrio [ID^{72a,72b}](#), M. D'Onofrio [ID⁹⁴](#), J. Dopke [ID¹³⁷](#), A. Doria [ID^{72a}](#), N. Dos Santos Fernandes [ID^{133a}](#), P. Dougan [ID¹⁰³](#), M.T. Dova [ID⁹²](#), A.T. Doyle [ID⁵⁹](#), M.A. Draguet [ID¹²⁹](#), M.P. Drescher [ID⁵⁵](#), E. Dreyer [ID¹⁷⁵](#), I. Drivas-koulouris [ID¹⁰](#), M. Drnevich [ID¹²⁰](#), M. Drozdova [ID⁵⁶](#), D. Du [ID⁶²](#), T.A. du Pree [ID¹¹⁷](#), Z. Duan [ID^{114a}](#), M. Dubau [ID⁴](#), F. Dubinin [ID³⁹](#), M. Dubovsky [ID^{29a}](#), E. Duchovni [ID¹⁷⁵](#), G. Duckeck [ID¹¹¹](#), P.K. Duckett [ID⁹⁸](#), O.A. Ducu [ID^{28b}](#), D. Duda [ID⁵²](#), A. Dudarev [ID³⁷](#), E.R. Duden [ID²⁷](#), M. D'uffizi [ID¹⁰³](#), L. Duflot [ID⁶⁶](#), M. Dührssen [ID³⁷](#), I. Duminica [ID^{28g}](#), A.E. Dumitriu [ID^{28b}](#), M. Dunford [ID^{63a}](#), S. Dungs [ID⁴⁹](#), K. Dunne [ID^{47a,47b}](#), A. Duperrin [ID¹⁰⁴](#), H. Duran Yildiz [ID^{3a}](#), M. Düren [ID⁵⁸](#), A. Durglishvili [ID^{155b}](#), D. Duvnjak [ID³⁵](#), G.I. Dyckes [ID^{18a}](#), M. Dyndal [ID^{86a}](#), B.S. Dziedzic [ID³⁷](#), Z.O. Earnshaw [ID¹⁵²](#), G.H. Eberwein [ID¹²⁹](#), B. Eckerova [ID^{29a}](#), S. Eggebrecht [ID⁵⁵](#), E. Egidio Purcino De Souza [ID^{83e}](#), G. Eigen [ID¹⁷](#), K. Einsweiler [ID^{18a}](#), T. Ekelof [ID¹⁶⁷](#), P.A. Ekman [ID¹⁰⁰](#), S. El Farkh [ID^{36b}](#), Y. El Ghazali [ID⁶²](#), H. El Jarrari [ID³⁷](#), A. El Moussaoui [ID^{36a}](#), V. Ellajosyula [ID¹⁶⁷](#), M. Ellert [ID¹⁶⁷](#), F. Ellinghaus [ID¹⁷⁷](#), N. Ellis [ID³⁷](#), J. Elmsheuser [ID³⁰](#), M. Elsawy [ID^{119a}](#), M. Elsing [ID³⁷](#), D. Emeliyanov [ID¹³⁷](#), Y. Enari [ID⁸⁴](#), I. Ene [ID^{18a}](#), S. Epari [ID¹¹⁰](#), D. Ernani Martins Neto [ID⁸⁷](#), F. Ernst [ID³⁷](#), M. Errenst [ID¹⁷⁷](#), M. Escalier [ID⁶⁶](#), C. Escobar [ID¹⁶⁹](#), E. Etzion [ID¹⁵⁷](#), G. Evans [ID^{133a,133b}](#), H. Evans [ID⁶⁸](#), L.S. Evans [ID⁹⁷](#), A. Ezhilov [ID³⁸](#),

S. Ezzarqtouni [ID^{36a}](#), F. Fabbri [ID^{24b,24a}](#), L. Fabbri [ID^{24b,24a}](#), G. Facini [ID⁹⁸](#), V. Fadeyev [ID¹³⁹](#), R.M. Fakhrutdinov [ID³⁸](#), D. Fakoudis [ID¹⁰²](#), S. Falciano [ID^{75a}](#), L.F. Falda Ulhoa Coelho [ID^{133a}](#), F. Fallavollita [ID¹¹²](#), G. Falsetti [ID^{44b,44a}](#), J. Faltova [ID¹³⁶](#), C. Fan [ID¹⁶⁸](#), K.Y. Fan [ID^{64b}](#), Y. Fan [ID¹⁴](#), Y. Fang [ID^{14,114c}](#), M. Fanti [ID^{71a,71b}](#), M. Faraj [ID^{69a,69b}](#), Z. Farazpay [ID⁹⁹](#), A. Farbin [ID⁸](#), A. Farilla [ID^{77a}](#), T. Farooque [ID¹⁰⁹](#), J.N. Farr [ID¹⁷⁸](#), S.M. Farrington [ID^{137,52}](#), F. Fassi [ID^{36e}](#), D. Fassouliotis [ID⁹](#), M. Faucci Giannelli [ID^{76b}](#), L. Fayard [ID⁶⁶](#), P. Federic [ID¹³⁶](#), P. Federicova [ID¹³⁴](#), O.L. Fedin [ID^{38,a}](#), M. Feickert [ID¹⁷⁶](#), L. Feligioni [ID¹⁰⁴](#), D.E. Fellers [ID^{18a}](#), C. Feng [ID^{143a}](#), Z. Feng [ID¹¹⁷](#), M.J. Fenton [ID¹⁶⁵](#), L. Ferencz [ID⁴⁸](#), B. Fernandez Barbadillo [ID⁹³](#), P. Fernandez Martinez [ID⁶⁷](#), M.J.V. Fernoux [ID¹⁰⁴](#), J. Ferrando [ID⁹³](#), A. Ferrari [ID¹⁶⁷](#), P. Ferrari [ID^{117,116}](#), R. Ferrari [ID^{73a}](#), D. Ferrere [ID⁵⁶](#), C. Ferretti [ID¹⁰⁸](#), M.P. Fewell [ID¹](#), D. Fiacco [ID^{75a,75b}](#), F. Fiedler [ID¹⁰²](#), P. Fiedler [ID¹³⁵](#), S. Filimonov [ID³⁹](#), M.S. Filip [ID^{28b,u}](#), A. Filipčič [ID⁹⁵](#), E.K. Filmer [ID^{162a}](#), F. Filthaut [ID¹¹⁶](#), M.C.N. Fiolhais [ID^{133a,133c,c}](#), L. Fiorini [ID¹⁶⁹](#), W.C. Fisher [ID¹⁰⁹](#), T. Fitschen [ID¹⁰³](#), P.M. Fitzhugh [ID¹³⁸](#), I. Fleck [ID¹⁴⁷](#), P. Fleischmann [ID¹⁰⁸](#), T. Flick [ID¹⁷⁷](#), M. Flores [ID^{34d,ag}](#), L.R. Flores Castillo [ID^{64a}](#), L. Flores Sanz De Acedo [ID³⁷](#), F.M. Follega [ID^{78a,78b}](#), N. Fomin [ID³³](#), J.H. Foo [ID¹⁶¹](#), A. Formica [ID¹³⁸](#), A.C. Forti [ID¹⁰³](#), E. Fortin [ID³⁷](#), A.W. Fortman [ID^{18a}](#), L. Foster [ID^{18a}](#), L. Fountas [ID^{9,j}](#), D. Fournier [ID⁶⁶](#), H. Fox [ID⁹³](#), P. Francavilla [ID^{74a,74b}](#), S. Francescato [ID⁶¹](#), S. Franchellucci [ID⁵⁶](#), M. Franchini [ID^{24b,24a}](#), S. Franchino [ID^{63a}](#), D. Francis [ID³⁷](#), L. Franco [ID¹¹⁶](#), V. Franco Lima [ID³⁷](#), L. Franconi [ID⁴⁸](#), M. Franklin [ID⁶¹](#), G. Frattari [ID²⁷](#), Y.Y. Frid [ID¹⁵⁷](#), J. Friend [ID⁵⁹](#), N. Fritzsche [ID³⁷](#), A. Froch [ID⁵⁶](#), D. Froidevaux [ID³⁷](#), J.A. Frost [ID¹²⁹](#), Y. Fu [ID¹⁰⁹](#), S. Fuenzalida Garrido [ID^{140f}](#), M. Fujimoto [ID¹⁰⁴](#), K.Y. Fung [ID^{64a}](#), E. Furtado De Simas Filho [ID^{83e}](#), M. Furukawa [ID¹⁵⁹](#), J. Fuster [ID¹⁶⁹](#), A. Gaa [ID⁵⁵](#), A. Gabrielli [ID^{24b,24a}](#), A. Gabrielli [ID¹⁶¹](#), P. Gadow [ID³⁷](#), G. Gagliardi [ID^{57b,57a}](#), L.G. Gagnon [ID^{18a}](#), S. Gaid [ID^{88b}](#), S. Galantzan [ID¹⁵⁷](#), J. Gallagher [ID¹](#), E.J. Gallas [ID¹²⁹](#), A.L. Gallen [ID¹⁶⁷](#), B.J. Gallop [ID¹³⁷](#), K.K. Gan [ID¹²²](#), S. Ganguly [ID¹⁵⁹](#), Y. Gao [ID⁵²](#), A. Garabaglu [ID¹⁴²](#), F.M. Garay Walls [ID^{140a,140b}](#), C. García [ID¹⁶⁹](#), A. Garcia Alonso [ID¹¹⁷](#), A.G. Garcia Caffaro [ID¹⁷⁸](#), J.E. García Navarro [ID¹⁶⁹](#), M. Garcia-Sciveres [ID^{18a}](#), G.L. Gardner [ID¹³¹](#), R.W. Gardner [ID⁴⁰](#), N. Garelli [ID¹⁶⁴](#), R.B. Garg [ID¹⁴⁹](#), J.M. Gargan [ID⁵²](#), C.A. Garner [ID¹⁶¹](#), C.M. Garvey [ID^{34a}](#), V.K. Gassmann [ID¹⁶⁴](#), G. Gaudio [ID^{73a}](#), V. Gautam [ID¹³](#), P. Gauzzi [ID^{75a,75b}](#), J. Gavranovic [ID⁹⁵](#), I.L. Gavrilenco [ID^{133a}](#), A. Gavriluk [ID³⁸](#), C. Gay [ID¹⁷⁰](#), G. Gaycken [ID¹²⁶](#), E.N. Gazis [ID¹⁰](#), A. Gekow [ID¹²²](#), C. Gemme [ID^{57b}](#), M.H. Genest [ID⁶⁰](#), A.D. Gentry [ID¹¹⁵](#), S. George [ID⁹⁷](#), T. Geralis [ID⁴⁶](#), A.A. Gerwin [ID¹²³](#), P. Gessinger-Befurt [ID³⁷](#), M.E. Geyik [ID¹⁷⁷](#), M. Ghani [ID¹⁷³](#), K. Ghorbanian [ID⁹⁶](#), A. Ghosal [ID¹⁴⁷](#), A. Ghosh [ID¹⁶⁵](#), A. Ghosh [ID⁷](#), B. Giacobbe [ID^{24b}](#), S. Giagu [ID^{75a,75b}](#), T. Giani [ID¹¹⁷](#), A. Giannini [ID⁶²](#), S.M. Gibson [ID⁹⁷](#), M. Gignac [ID¹³⁹](#), D.T. Gil [ID^{86b}](#), A.K. Gilbert [ID^{86a}](#), B.J. Gilbert [ID⁴²](#), D. Gillberg [ID³⁵](#), G. Gilles [ID¹¹⁷](#), D.M. Gingrich [ID^{2,ai}](#), M.P. Giordani [ID^{69a,69c}](#), P.F. Giraud [ID¹³⁸](#), G. Giugliarelli [ID^{69a,69c}](#), D. Giugni [ID^{71a}](#), F. Giulì [ID^{76a,76b}](#), I. Gkialas [ID^{9,j}](#), L.K. Gladilin [ID³⁸](#), C. Glasman [ID¹⁰¹](#), M. Glazewska [ID²⁰](#), R.M. Gleason [ID¹⁶⁵](#), G. Glemža [ID⁴⁸](#), M. Glisic [ID¹²⁶](#), I. Gnesi [ID^{44b}](#), Y. Go [ID³⁰](#), M. Goblirsch-Kolb [ID³⁷](#), B. Gocke [ID⁴⁹](#), D. Godin [ID¹¹⁰](#), B. Gokturk [ID^{22a}](#), S. Goldfarb [ID¹⁰⁷](#), T. Golling [ID⁵⁶](#), M.G.D. Gololo [ID^{34c}](#), D. Golubkov [ID³⁸](#), J.P. Gombas [ID¹⁰⁹](#), A. Gomes [ID^{133a,133b}](#), G. Gomes Da Silva [ID¹⁴⁷](#), A.J. Gomez Delegido [ID¹⁶⁹](#), R. Gonçalo [ID^{133a}](#), L. Gonella [ID²¹](#), A. Gongadze [ID^{155c}](#), F. Gonnella [ID²¹](#), J.L. Gonski [ID¹⁴⁹](#), R.Y. González Andana [ID⁵²](#), S. González de la Hoz [ID¹⁶⁹](#), M.V. Gonzalez Rodrigues [ID⁴⁸](#), R. Gonzalez Suarez [ID¹⁶⁷](#), S. Gonzalez-Sevilla [ID⁵⁶](#), L. Goossens [ID³⁷](#), B. Gorini [ID³⁷](#), E. Gorini [ID^{70a,70b}](#), A. Gorišek [ID⁹⁵](#), T.C. Gosart [ID¹³¹](#), A.T. Goshaw [ID⁵¹](#), M.I. Gostkin [ID³⁹](#), S. Goswami [ID¹²⁴](#), C.A. Gottardo [ID³⁷](#), S.A. Gotz [ID¹¹¹](#), M. Gouighri [ID^{36b}](#), A.G. Goussiou [ID¹⁴²](#), N. Govender [ID^{34c}](#), R.P. Grabarczyk [ID¹²⁹](#), I. Grabowska-Bold [ID^{86a}](#), K. Graham [ID³⁵](#), E. Gramstad [ID¹²⁸](#), S. Grancagnolo [ID^{70a,70b}](#), C.M. Grant ¹, P.M. Gravila [ID^{28f}](#), F.G. Gravili [ID^{70a,70b}](#), H.M. Gray [ID^{18a}](#), M. Greco [ID¹¹²](#), M.J. Green [ID¹](#), C. Grefe [ID²⁵](#), A.S. Grefsrud [ID¹⁷](#), I.M. Gregor [ID⁴⁸](#), K.T. Greif [ID¹⁶⁵](#), P. Grenier [ID¹⁴⁹](#), S.G. Grewe [ID¹¹²](#), A.A. Grillo [ID¹³⁹](#), K. Grimm [ID³²](#), S. Grinstein [ID^{13,y}](#), J.-F. Grivaz [ID⁶⁶](#), E. Gross [ID¹⁷⁵](#), J. Grosse-Knetter [ID⁵⁵](#), L. Guan [ID¹⁰⁸](#), G. Guerrieri [ID³⁷](#), R. Guevara [ID¹²⁸](#), R. Gugel [ID¹⁰²](#), J.A.M. Guhit [ID¹⁰⁸](#), A. Guida [ID¹⁹](#), E. Guilloton [ID¹⁷³](#), S. Guindon [ID³⁷](#), F. Guo [ID^{14,114c}](#), J. Guo [ID^{144a}](#),

L. Guo **id**⁴⁸, L. Guo **id**^{114b,w}, Y. Guo **id**¹⁰⁸, A. Gupta **id**⁴⁹, R. Gupta **id**¹³², S. Gupta **id**²⁷, S. Gurbuz **id**²⁵,
 S.S. Gurdasani **id**⁴⁸, G. Gustavino **id**^{75a,75b}, P. Gutierrez **id**¹²³, L.F. Gutierrez Zagazeta **id**¹³¹,
 M. Gutsche **id**⁵⁰, C. Gutschow **id**⁹⁸, C. Gwenlan **id**¹²⁹, C.B. Gwilliam **id**⁹⁴, E.S. Haaland **id**¹²⁸,
 A. Haas **id**¹²⁰, M. Habedank **id**⁵⁹, C. Haber **id**^{18a}, H.K. Hadavand **id**⁸, A. Haddad **id**⁴¹, A. Hadef **id**⁵⁰,
 A.I. Hagan **id**⁹³, J.J. Hahn **id**¹⁴⁷, E.H. Haines **id**⁹⁸, M. Haleem **id**¹⁷², J. Haley **id**¹²⁴, G.D. Hallewell **id**¹⁰⁴,
 L. Halser **id**²⁰, K. Hamano **id**¹⁷¹, M. Hamer **id**²⁵, S.E.D. Hammoud **id**⁶⁶, E.J. Hampshire **id**⁹⁷,
 J. Han **id**^{143a}, L. Han **id**^{114a}, L. Han **id**⁶², S. Han **id**^{18a}, K. Hanagaki **id**⁸⁴, M. Hance **id**¹³⁹, D.A. Hangal **id**⁴²,
 H. Hanif **id**¹⁴⁸, M.D. Hank **id**¹³¹, J.B. Hansen **id**⁴³, P.H. Hansen **id**⁴³, D. Harada **id**⁵⁶, T. Harenberg **id**¹⁷⁷,
 S. Harkusha **id**¹⁷⁹, M.L. Harris **id**¹⁰⁵, Y.T. Harris **id**²⁵, J. Harrison **id**¹³, N.M. Harrison **id**¹²²,
 P.F. Harrison¹⁷³, M.L.E. Hart **id**⁹⁸, N.M. Hartman **id**¹¹², N.M. Hartmann **id**¹¹¹, R.Z. Hasan **id**^{97,137},
 Y. Hasegawa **id**¹⁴⁶, F. Haslbeck **id**¹²⁹, S. Hassan **id**¹⁷, R. Hauser **id**¹⁰⁹, M. Havierenik **id**¹³⁶,
 C.M. Hawkes **id**²¹, R.J. Hawkings **id**³⁷, Y. Hayashi **id**¹⁵⁹, D. Hayden **id**¹⁰⁹, C. Hayes **id**¹⁰⁸,
 R.L. Hayes **id**¹¹⁷, C.P. Hays **id**¹²⁹, J.M. Hays **id**⁹⁶, H.S. Hayward **id**⁹⁴, M. He **id**^{14,114c}, Y. He **id**⁴⁸,
 Y. He **id**⁹⁸, N.B. Heatley **id**⁹⁶, V. Hedberg **id**¹⁰⁰, C. Heidegger **id**⁵⁴, K.K. Heidegger **id**⁵⁴, J. Heilman **id**³⁵,
 S. Heim **id**⁴⁸, T. Heim **id**^{18a}, J.G. Heinlein **id**¹³¹, J.J. Heinrich **id**¹²⁶, L. Heinrich **id**¹¹², J. Hejbal **id**¹³⁴,
 M. Helbig **id**⁵⁰, A. Held **id**¹⁷⁶, S. Hellesund **id**¹⁷, C.M. Helling **id**¹⁷⁰, S. Hellman **id**^{47a,47b},
 A.M. Henriques Correia³⁷, H. Herde **id**¹⁰⁰, Y. Hernández Jiménez **id**¹⁵¹, L.M. Herrmann **id**²⁵,
 T. Herrmann **id**⁵⁰, G. Herten **id**⁵⁴, R. Hertenberger **id**¹¹¹, L. Hervas **id**³⁷, M.E. Hesping **id**¹⁰²,
 N.P. Hessey **id**^{162a}, J. Hessler **id**¹¹², M. Hidaoui **id**^{36b}, N. Hidic **id**¹³⁶, E. Hill **id**¹⁶¹, T.S. Hillersoy **id**¹⁷,
 S.J. Hillier **id**²¹, J.R. Hinds **id**¹⁰⁹, F. Hinterkeuser **id**²⁵, M. Hirose **id**¹²⁷, S. Hirose **id**¹⁶³,
 D. Hirschbuehl **id**¹⁷⁷, T.G. Hitchings **id**¹⁰³, B. Hiti **id**⁹⁵, J. Hobbs **id**¹⁵¹, R. Hobincu **id**^{28e}, N. Hod **id**¹⁷⁵,
 A.M. Hodges **id**¹⁶⁸, M.C. Hodgkinson **id**¹⁴⁵, B.H. Hodgkinson **id**¹²⁹, A. Hoecker **id**³⁷, D.D. Hofer **id**¹⁰⁸,
 J. Hofer **id**¹⁶⁹, M. Holzbock **id**³⁷, L.B.A.H. Hommels **id**³³, V. Homsak **id**¹²⁹, B.P. Honan **id**¹⁰³,
 J.J. Hong **id**⁶⁸, T.M. Hong **id**¹³², B.H. Hooberman **id**¹⁶⁸, W.H. Hopkins **id**⁶, M.C. Hoppesch **id**¹⁶⁸,
 Y. Horii **id**¹¹³, M.E. Horstmann **id**¹¹², S. Hou **id**¹⁵⁴, M.R. Housenga **id**¹⁶⁸, A.S. Howard **id**⁹⁵,
 J. Howarth **id**⁵⁹, J. Hoya **id**⁶, M. Hrabovsky **id**¹²⁵, T. Hryna'ova **id**⁴, P.J. Hsu **id**⁶⁵, S.-C. Hsu **id**¹⁴²,
 T. Hsu **id**⁶⁶, M. Hu **id**^{18a}, Q. Hu **id**⁶², S. Huang **id**³³, X. Huang **id**^{14,114c}, Y. Huang **id**¹³⁶, Y. Huang **id**^{114b},
 Y. Huang **id**¹⁰², Y. Huang **id**¹⁴, Z. Huang **id**⁶⁶, Z. Hubacek **id**¹³⁵, M. Huebner **id**²⁵, F. Huegging **id**²⁵,
 T.B. Huffman **id**¹²⁹, M. Hufnagel Maranha De Faria **id**^{83a}, C.A. Hugli **id**⁴⁸, M. Huhtinen **id**³⁷,
 S.K. Huiberts **id**¹⁷, R. Hulskens **id**¹⁰⁶, C.E. Hultquist **id**^{18a}, N. Huseynov **id**^{12,g}, J. Huston **id**¹⁰⁹, J. Huth **id**⁶¹,
 R. Hyneman **id**⁷, G. Iacobucci **id**⁵⁶, G. Iakovidis **id**³⁰, L. Iconomidou-Fayard **id**⁶⁶, J.P. Iddon **id**³⁷,
 P. Iengo **id**^{72a,72b}, R. Iguchi **id**¹⁵⁹, Y. Iiyama **id**¹⁵⁹, T. Iizawa **id**¹⁵⁹, Y. Ikegami **id**⁸⁴, D. Iliadis **id**¹⁵⁸,
 N. Ilic **id**¹⁶¹, H. Imam **id**^{36a}, G. Inacio Goncalves **id**^{83d}, S.A. Infante Cabanas **id**^{140c},
 T. Ingebretsen Carlson **id**^{47a,47b}, J.M. Inglis **id**⁹⁶, G. Introzzi **id**^{73a,73b}, M. Iodice **id**^{77a}, V. Ippolito **id**^{75a,75b},
 R.K. Irwin **id**⁹⁴, M. Ishino **id**¹⁵⁹, W. Islam **id**¹⁷⁶, C. Issever **id**¹⁹, S. Istin **id**^{22a,an}, K. Itabashi **id**⁸⁴,
 H. Ito **id**¹⁷⁴, R. Iuppa **id**^{78a,78b}, A. Ivina **id**¹⁷⁵, V. Izzo **id**^{72a}, P. Jacka **id**¹³⁴, P. Jackson **id**¹, P. Jain **id**⁴⁸,
 K. Jakobs **id**⁵⁴, T. Jakoubek **id**¹⁷⁵, J. Jamieson **id**⁵⁹, W. Jang **id**¹⁵⁹, S. Jankovych **id**¹³⁶, M. Javurkova **id**¹⁰⁵,
 P. Jawahar **id**¹⁰³, L. Jeanty **id**¹²⁶, J. Jejelava **id**^{155a,af}, P. Jenni **id**^{54,f}, C.E. Jessiman **id**³⁵, C. Jia **id**^{143a},
 H. Jia **id**¹⁷⁰, J. Jia **id**¹⁵¹, X. Jia **id**^{14,114c}, Z. Jia **id**^{114a}, C. Jiang **id**⁵², Q. Jiang **id**^{64b}, S. Jiggins **id**⁴⁸,
 M. Jimenez Ortega **id**¹⁶⁹, J. Jimenez Pena **id**¹³, S. Jin **id**^{114a}, A. Jinaru **id**^{28b}, O. Jinnouchi **id**¹⁴¹,
 P. Johansson **id**¹⁴⁵, K.A. Johns **id**⁷, J.W. Johnson **id**¹³⁹, F.A. Jolly **id**⁴⁸, D.M. Jones **id**¹⁵², E. Jones **id**⁴⁸,
 K.S. Jones⁸, P. Jones **id**³³, R.W.L. Jones **id**⁹³, T.J. Jones **id**⁹⁴, H.L. Joos **id**^{55,37}, R. Joshi **id**¹²²,
 J. Jovicevic **id**¹⁶, X. Ju **id**^{18a}, J.J. Junggeburth **id**³⁷, T. Junkermann **id**^{63a}, A. Juste Rozas **id**^{13,y},
 M.K. Juzek **id**⁸⁷, S. Kabana **id**^{140e}, A. Kaczmarska **id**⁸⁷, M. Kado **id**¹¹², H. Kagan **id**¹²², M. Kagan **id**¹⁴⁹,
 A. Kahn **id**¹³¹, C. Kahra **id**¹⁰², T. Kaji **id**¹⁵⁹, E. Kajomovitz **id**¹⁵⁶, N. Kakati **id**¹⁷⁵, N. Kakoty **id**¹³,
 I. Kalaitzidou **id**⁵⁴, S. Kandel **id**⁸, N.J. Kang **id**¹³⁹, D. Kar **id**^{34g}, K. Karava **id**¹²⁹, E. Karentzos **id**²⁵,
 O. Karkout **id**¹¹⁷, S.N. Karpov **id**³⁹, Z.M. Karpova **id**³⁹, V. Kartvelishvili **id**⁹³, A.N. Karyukhin **id**³⁸,

E. Kasimi [ID¹⁵⁸](#), J. Katzy [ID⁴⁸](#), S. Kaur [ID³⁵](#), K. Kawade [ID¹⁴⁶](#), M.P. Kawale [ID¹²³](#), C. Kawamoto [ID⁸⁹](#), T. Kawamoto [ID⁶²](#), E.F. Kay [ID³⁷](#), F.I. Kaya [ID¹⁶⁴](#), S. Kazakos [ID¹⁰⁹](#), V.F. Kazanin [ID³⁸](#), J.M. Keaveney [ID^{34a}](#), R. Keeler [ID¹⁷¹](#), G.V. Kehris [ID⁶¹](#), J.S. Keller [ID³⁵](#), J.J. Kempster [ID¹⁵²](#), O. Kepka [ID¹³⁴](#), J. Kerr [ID^{162b}](#), B.P. Kerridge [ID¹³⁷](#), B.P. Kerševan [ID⁹⁵](#), L. Keszeghova [ID^{29a}](#), R.A. Khan [ID¹³²](#), A. Khanov [ID¹²⁴](#), A.G. Kharlamov [ID³⁸](#), T. Kharlamova [ID³⁸](#), E.E. Khoda [ID¹⁴²](#), M. Kholodenko [ID^{133a}](#), T.J. Khoo [ID¹⁹](#), G. Khoriauli [ID¹⁷²](#), Y. Khoulaki [ID^{36a}](#), J. Khubua [ID^{155b,*}](#), Y.A.R. Khwaira [ID¹³⁰](#), B. Kibirige [ID^{34g}](#), D. Kim [ID⁶](#), D.W. Kim [ID^{47a,47b}](#), Y.K. Kim [ID⁴⁰](#), N. Kimura [ID⁹⁸](#), M.K. Kingston [ID⁵⁵](#), A. Kirchhoff [ID⁵⁵](#), C. Kirfel [ID²⁵](#), F. Kirfel [ID²⁵](#), J. Kirk [ID¹³⁷](#), A.E. Kiryunin [ID¹¹²](#), S. Kita [ID¹⁶³](#), O. Kivernyk [ID²⁵](#), M. Klassen [ID¹⁶⁴](#), C. Klein [ID³⁵](#), L. Klein [ID¹⁷²](#), M.H. Klein [ID⁴⁵](#), S.B. Klein [ID⁵⁶](#), U. Klein [ID⁹⁴](#), A. Klimentov [ID³⁰](#), T. Klioutchnikova [ID³⁷](#), P. Kluit [ID¹¹⁷](#), S. Kluth [ID¹¹²](#), E. Knerner [ID⁷⁹](#), T.M. Knight [ID¹⁶¹](#), A. Knue [ID⁴⁹](#), M. Kobel [ID⁵⁰](#), D. Kobylanski [ID¹⁷⁵](#), S.F. Koch [ID¹²⁹](#), M. Kocian [ID¹⁴⁹](#), P. Kodyš [ID¹³⁶](#), D.M. Koeck [ID¹²⁶](#), T. Koffas [ID³⁵](#), O. Kolay [ID⁵⁰](#), I. Koletsou [ID⁴](#), T. Komarek [ID⁸⁷](#), K. Köneke [ID⁵⁵](#), A.X.Y. Kong [ID¹](#), T. Kono [ID¹²¹](#), N. Konstantinidis [ID⁹⁸](#), P. Kontaxakis [ID⁵⁶](#), B. Konya [ID¹⁰⁰](#), R. Kopeliansky [ID⁴²](#), S. Koperny [ID^{86a}](#), K. Korcyl [ID⁸⁷](#), K. Kordas [ID^{158,d}](#), A. Korn [ID⁹⁸](#), S. Korn [ID⁵⁵](#), I. Korolkov [ID¹³](#), N. Korotkova [ID³⁸](#), B. Kortman [ID¹¹⁷](#), O. Kortner [ID¹¹²](#), S. Kortner [ID¹¹²](#), W.H. Kostecka [ID¹¹⁸](#), M. Kostov [ID^{29a}](#), V.V. Kostyukhin [ID¹⁴⁷](#), A. Kotsokechagia [ID³⁷](#), A. Kotwal [ID⁵¹](#), A. Koulouris [ID³⁷](#), A. Kourkoumeli-Charalampidi [ID^{73a,73b}](#), C. Kourkoumelis [ID⁹](#), E. Kourlitis [ID¹¹²](#), O. Kovanda [ID¹²⁶](#), R. Kowalewski [ID¹⁷¹](#), W. Kozanecki [ID¹²⁶](#), A.S. Kozhin [ID³⁸](#), V.A. Kramarenko [ID³⁸](#), G. Kramberger [ID⁹⁵](#), P. Kramer [ID²⁵](#), M.W. Krasny [ID¹³⁰](#), A. Krasznahorkay [ID¹⁰⁵](#), A.C. Kraus [ID¹¹⁸](#), J.W. Kraus [ID¹⁷⁷](#), J.A. Kremer [ID⁴⁸](#), N.B. Krengel [ID¹⁴⁷](#), T. Kresse [ID⁵⁰](#), L. Kretschmann [ID¹⁷⁷](#), J. Kretzschmar [ID⁹⁴](#), K. Kreul [ID¹⁹](#), P. Krieger [ID¹⁶¹](#), K. Krizka [ID²¹](#), K. Kroeninger [ID⁴⁹](#), H. Kroha [ID¹¹²](#), J. Kroll [ID¹³⁴](#), J. Kroll [ID¹³¹](#), K.S. Krowpman [ID¹⁰⁹](#), U. Kruchonak [ID³⁹](#), H. Krüger [ID²⁵](#), N. Krumnack ⁸¹, M.C. Kruse [ID⁵¹](#), O. Kuchinskaja [ID³⁹](#), S. Kuday [ID^{3a}](#), S. Kuehn [ID³⁷](#), R. Kuesters [ID⁵⁴](#), T. Kuhl [ID⁴⁸](#), V. Kukhtin [ID³⁹](#), Y. Kulchitsky [ID³⁹](#), S. Kuleshov [ID^{140d,140b}](#), J. Kull [ID¹](#), E.V. Kumar [ID¹¹¹](#), M. Kumar [ID^{34g}](#), N. Kumari [ID⁴⁸](#), P. Kumari [ID^{162b}](#), A. Kupco [ID¹³⁴](#), T. Kupfer ⁴⁹, A. Kupich [ID³⁸](#), O. Kuprash [ID⁵⁴](#), H. Kurashige [ID⁸⁵](#), L.L. Kurchaninov [ID^{162a}](#), O. Kurdysh [ID⁴](#), Y.A. Kurochkin [ID³⁸](#), A. Kurova [ID³⁸](#), M. Kuze [ID¹⁴¹](#), A.K. Kvam [ID¹⁰⁵](#), J. Kvita [ID¹²⁵](#), N.G. Kyriacou [ID¹⁰⁸](#), C. Lacasta [ID¹⁶⁹](#), F. Lacava [ID^{75a,75b}](#), H. Lacker [ID¹⁹](#), D. Lacour [ID¹³⁰](#), N.N. Lad [ID⁹⁸](#), E. Ladygin [ID³⁹](#), A. Lafarge [ID⁴¹](#), B. Laforge [ID¹³⁰](#), T. Lagouri [ID¹⁷⁸](#), F.Z. Lahbabi [ID^{36a}](#), S. Lai [ID⁵⁵](#), J.E. Lambert [ID¹⁷¹](#), S. Lammers [ID⁶⁸](#), W. Lampl [ID⁷](#), C. Lampoudis [ID^{158,d}](#), G. Lamprinoudis [ID¹⁰²](#), A.N. Lancaster [ID¹¹⁸](#), E. Lançon [ID³⁰](#), U. Landgraf [ID⁵⁴](#), M.P.J. Landon [ID⁹⁶](#), V.S. Lang [ID⁵⁴](#), O.K.B. Langrekken [ID¹²⁸](#), A.J. Lankford [ID¹⁶⁵](#), F. Lanni [ID³⁷](#), K. Lantzsch [ID²⁵](#), A. Lanza [ID^{73a}](#), M. Lanzac Berrocal [ID¹⁶⁹](#), J.F. Laporte [ID¹³⁸](#), T. Lari [ID^{71a}](#), D. Larsen [ID¹⁷](#), L. Larson [ID¹¹](#), F. Lasagni Manghi [ID^{24b}](#), M. Lassnig [ID³⁷](#), S.D. Lawlor [ID¹⁴⁵](#), R. Lazaridou ¹⁷³, M. Lazzaroni [ID^{71a,71b}](#), H.D.M. Le [ID¹⁰⁹](#), E.M. Le Boulicaut [ID¹⁷⁸](#), L.T. Le Pottier [ID^{18a}](#), B. Leban [ID^{24b,24a}](#), F. Ledroit-Guillon [ID⁶⁰](#), T.F. Lee [ID^{162b}](#), L.L. Leeuw [ID^{34c}](#), M. Lefebvre [ID¹⁷¹](#), C. Leggett [ID^{18a}](#), G. Lehmann Miotto [ID³⁷](#), M. Leigh [ID⁵⁶](#), W.A. Leight [ID¹⁰⁵](#), W. Leinonen [ID¹¹⁶](#), A. Leisos [ID^{158,v}](#), M.A.L. Leite [ID^{83c}](#), C.E. Leitgeb [ID¹⁹](#), R. Leitner [ID¹³⁶](#), K.J.C. Leney [ID⁴⁵](#), T. Lenz [ID²⁵](#), S. Leone [ID^{74a}](#), C. Leonidopoulos [ID⁵²](#), A. Leopold [ID¹⁵⁰](#), J.H. Lepage Bourbonnais [ID³⁵](#), R. Les [ID¹⁰⁹](#), C.G. Lester [ID³³](#), M. Levchenko [ID³⁸](#), J. Levêque [ID⁴](#), L.J. Levinson [ID¹⁷⁵](#), G. Levrini [ID^{24b,24a}](#), M.P. Lewicki [ID⁸⁷](#), C. Lewis [ID¹⁴²](#), D.J. Lewis [ID⁴](#), L. Lewitt [ID¹⁴⁵](#), A. Li [ID³⁰](#), B. Li [ID^{143a}](#), C. Li ¹⁰⁸, C-Q. Li [ID¹¹²](#), H. Li [ID^{143a}](#), H. Li [ID¹⁰³](#), H. Li [ID¹⁵](#), H. Li [ID⁶²](#), H. Li [ID^{143a}](#), J. Li [ID^{144a}](#), K. Li [ID¹⁴](#), L. Li [ID^{144a}](#), R. Li [ID¹⁷⁸](#), S. Li [ID^{14,114c}](#), S. Li [ID^{144b,144a}](#), T. Li [ID⁵](#), X. Li [ID¹⁰⁶](#), Z. Li [ID¹⁵⁹](#), Z. Li [ID^{14,114c}](#), Z. Li [ID⁶²](#), S. Liang [ID^{14,114c}](#), Z. Liang [ID¹⁴](#), M. Liberatore [ID¹³⁸](#), B. Liberti [ID^{76a}](#), K. Lie [ID^{64c}](#), J. Lieber Marin [ID^{83e}](#), H. Lien [ID⁶⁸](#), H. Lin [ID¹⁰⁸](#), S.F. Lin [ID¹⁵¹](#), L. Linden [ID¹¹¹](#), R.E. Lindley [ID⁷](#), J.H. Lindon [ID³⁷](#), J. Ling [ID⁶¹](#), E. Lipeles [ID¹³¹](#), A. Lipniacka [ID¹⁷](#), A. Lister [ID¹⁷⁰](#), J.D. Little [ID⁶⁸](#), B. Liu [ID¹⁴](#), B.X. Liu [ID^{114b}](#), D. Liu [ID^{144b,144a}](#), D. Liu [ID¹³⁹](#), E.H.L. Liu [ID²¹](#), J.K.K. Liu [ID¹²⁰](#), K. Liu [ID^{144b}](#), K. Liu [ID^{144b,144a}](#), M. Liu [ID⁶²](#), M.Y. Liu [ID⁶²](#), P. Liu [ID¹⁴](#), Q. Liu [ID^{144b,142,144a}](#), X. Liu [ID⁶²](#), X. Liu [ID^{143a}](#), Y. Liu [ID^{114b,114c}](#), Y.L. Liu [ID^{143a}](#), Y.W. Liu [ID⁶²](#),

Z. Liu [ID^{66,1}](#), S.L. Lloyd [ID⁹⁶](#), E.M. Lobodzinska [ID⁴⁸](#), P. Loch [ID⁷](#), E. Lodhi [ID¹⁶¹](#), T. Lohse [ID¹⁹](#), K. Lohwasser [ID¹⁴⁵](#), E. Loiacono [ID⁴⁸](#), J.D. Lomas [ID²¹](#), J.D. Long [ID⁴²](#), I. Longarini [ID¹⁶⁵](#), R. Longo [ID¹⁶⁸](#), A. Lopez Solis [ID¹³](#), N.A. Lopez-canelas [ID⁷](#), N. Lorenzo Martinez [ID⁴](#), A.M. Lory [ID¹¹¹](#), M. Losada [ID^{119a}](#), G. Löschecke Centeno [ID¹⁵²](#), X. Lou [ID^{47a,47b}](#), X. Lou [ID^{14,114c}](#), A. Lounis [ID⁶⁶](#), P.A. Love [ID⁹³](#), M. Lu [ID⁶⁶](#), S. Lu [ID¹³¹](#), Y.J. Lu [ID¹⁵⁴](#), H.J. Lubatti [ID¹⁴²](#), C. Luci [ID^{75a,75b}](#), F.L. Lucio Alves [ID^{114a}](#), F. Luehring [ID⁶⁸](#), B.S. Lunday [ID¹³¹](#), O. Lundberg [ID¹⁵⁰](#), J. Lunde [ID³⁷](#), N.A. Luongo [ID⁶](#), M.S. Lutz [ID³⁷](#), A.B. Lux [ID²⁶](#), D. Lynn [ID³⁰](#), R. Lysak [ID¹³⁴](#), V. Lysenko [ID¹³⁵](#), E. Lytken [ID¹⁰⁰](#), V. Lyubushkin [ID³⁹](#), T. Lyubushkina [ID³⁹](#), M.M. Lyukova [ID¹⁵¹](#), M.Firdaus M. Soberi [ID⁵²](#), H. Ma [ID³⁰](#), K. Ma [ID⁶²](#), L.L. Ma [ID^{143a}](#), W. Ma [ID⁶²](#), Y. Ma [ID¹²⁴](#), J.C. MacDonald [ID¹⁰²](#), P.C. Machado De Abreu Farias [ID^{83e}](#), R. Madar [ID⁴¹](#), T. Madula [ID⁹⁸](#), J. Maeda [ID⁸⁵](#), T. Maeno [ID³⁰](#), P.T. Mafa [ID^{34c,k}](#), H. Maguire [ID¹⁴⁵](#), V. Maiboroda [ID⁶⁶](#), A. Maio [ID^{133a,133b,133d}](#), K. Maj [ID^{86a}](#), O. Majersky [ID⁴⁸](#), S. Majewski [ID¹²⁶](#), R. Makhmanazarov [ID³⁸](#), N. Makovec [ID⁶⁶](#), V. Maksimovic [ID¹⁶](#), B. Malaescu [ID¹³⁰](#), J. Malamant [ID¹²⁸](#), Pa. Malecki [ID⁸⁷](#), V.P. Maleev [ID³⁸](#), F. Malek [ID^{60,p}](#), M. Mali [ID⁹⁵](#), D. Malito [ID⁹⁷](#), U. Mallik [ID^{80,*}](#), A. Maloizel [ID⁵](#), S. Maltezos [ID¹⁰](#), A. Malvezzi Lopes [ID^{83d}](#), S. Malyukov [ID³⁹](#), J. Mamuzic [ID¹³](#), G. Mancini [ID⁵³](#), M.N. Mancini [ID²⁷](#), G. Manco [ID^{73a,73b}](#), J.P. Mandalia [ID⁹⁶](#), S.S. Mandarry [ID¹⁵²](#), I. Mandić [ID⁹⁵](#), L. Manhaes de Andrade Filho [ID^{83a}](#), I.M. Maniatis [ID¹⁷⁵](#), J. Manjarres Ramos [ID⁹¹](#), D.C. Mankad [ID¹⁷⁵](#), A. Mann [ID¹¹¹](#), T. Manoussos [ID³⁷](#), M.N. Mantinan [ID⁴⁰](#), S. Manzoni [ID³⁷](#), L. Mao [ID^{144a}](#), X. Mapekula [ID^{34c}](#), A. Marantis [ID¹⁵⁸](#), R.R. Marcelo Gregorio [ID⁹⁶](#), G. Marchiori [ID⁵](#), M. Marcisovsky [ID¹³⁴](#), C. Marcon [ID^{71a}](#), E. Maricic [ID¹⁶](#), M. Marinescu [ID⁴⁸](#), S. Marium [ID⁴⁸](#), M. Marjanovic [ID¹²³](#), A. Markhoos [ID⁵⁴](#), M. Markovitch [ID⁶⁶](#), M.K. Maroun [ID¹⁰⁵](#), G.T. Marsden [ID¹⁰³](#), E.J. Marshall [ID⁹³](#), Z. Marshall [ID^{18a}](#), S. Marti-Garcia [ID¹⁶⁹](#), J. Martin [ID⁹⁸](#), T.A. Martin [ID¹³⁷](#), V.J. Martin [ID⁵²](#), B. Martin dit Latour [ID¹⁷](#), L. Martinelli [ID^{75a,75b}](#), M. Martinez [ID^{13,y}](#), P. Martinez Agullo [ID¹⁶⁹](#), V.I. Martinez Outschoorn [ID¹⁰⁵](#), P. Martinez Suarez [ID¹³](#), S. Martin-Haugh [ID¹³⁷](#), G. Martinovicova [ID¹³⁶](#), V.S. Martoiu [ID^{28b}](#), A.C. Martyniuk [ID⁹⁸](#), A. Marzin [ID³⁷](#), D. Mascione [ID^{78a,78b}](#), L. Masetti [ID¹⁰²](#), J. Masik [ID¹⁰³](#), A.L. Maslennikov [ID³⁹](#), S.L. Mason [ID⁴²](#), P. Massarotti [ID^{72a,72b}](#), P. Mastrandrea [ID^{74a,74b}](#), A. Mastroberardino [ID^{44b,44a}](#), T. Masubuchi [ID¹²⁷](#), T.T. Mathew [ID¹²⁶](#), J. Matousek [ID¹³⁶](#), D.M. Mattern [ID⁴⁹](#), J. Maurer [ID^{28b}](#), T. Maurin [ID⁵⁹](#), A.J. Maury [ID⁶⁶](#), B. Maček [ID⁹⁵](#), C. Mavungu Tsava [ID¹⁰⁴](#), D.A. Maximov [ID³⁸](#), A.E. May [ID¹⁰³](#), E. Mayer [ID⁴¹](#), R. Mazini [ID^{34g}](#), I. Maznas [ID¹¹⁸](#), S.M. Mazza [ID¹³⁹](#), E. Mazzeo [ID³⁷](#), J.P. Mc Gowen [ID¹⁷¹](#), S.P. Mc Kee [ID¹⁰⁸](#), C.A. Mc Lean [ID⁶](#), C.C. McCracken [ID¹⁷⁰](#), E.F. McDonald [ID¹⁰⁷](#), A.E. McDougall [ID¹¹⁷](#), L.F. McElhinney [ID⁹³](#), J.A. McFayden [ID¹⁵²](#), R.P. McGovern [ID¹³¹](#), R.P. Mckenzie [ID^{34g}](#), T.C. McLachlan [ID⁴⁸](#), D.J. McLaughlin [ID⁹⁸](#), S.J. McMahon [ID¹³⁷](#), C.M. Mcpartland [ID⁹⁴](#), R.A. McPherson [ID^{171,ac}](#), S. Mehlhase [ID¹¹¹](#), A. Mehta [ID⁹⁴](#), D. Melini [ID¹⁶⁹](#), B.R. Mellado Garcia [ID^{34g}](#), A.H. Melo [ID⁵⁵](#), F. Meloni [ID⁴⁸](#), A.M. Mendes Jacques Da Costa [ID¹⁰³](#), L. Meng [ID⁹³](#), S. Menke [ID¹¹²](#), M. Mentink [ID³⁷](#), E. Meoni [ID^{44b,44a}](#), G. Mercado [ID¹¹⁸](#), S. Merianos [ID¹⁵⁸](#), C. Merlassino [ID^{69a,69c}](#), C. Meroni [ID^{71a,71b}](#), J. Metcalfe [ID⁶](#), A.S. Mete [ID⁶](#), E. Meuser [ID¹⁰²](#), C. Meyer [ID⁶⁸](#), J-P. Meyer [ID¹³⁸](#), Y. Miao [ID^{114a}](#), R.P. Middleton [ID¹³⁷](#), M. Mihovilovic [ID⁶⁶](#), L. Mijović [ID⁵²](#), G. Mikenberg [ID¹⁷⁵](#), M. Mikestikova [ID¹³⁴](#), M. Mikuž [ID⁹⁵](#), H. Mildner [ID¹⁰²](#), A. Milic [ID³⁷](#), D.W. Miller [ID⁴⁰](#), E.H. Miller [ID¹⁴⁹](#), L.S. Miller [ID³⁵](#), A. Milov [ID¹⁷⁵](#), D.A. Milstead [ID^{47a,47b}](#), T. Min [ID^{114a}](#), A.A. Minaenko [ID³⁸](#), I.A. Minashvili [ID^{155b}](#), A.I. Mincer [ID¹²⁰](#), B. Mindur [ID^{86a}](#), M. Mineev [ID³⁹](#), Y. Mino [ID⁸⁹](#), L.M. Mir [ID¹³](#), M. Miralles Lopez [ID⁵⁹](#), M. Mironova [ID^{18a}](#), M.C. Missio [ID¹¹⁶](#), A. Mitra [ID¹⁷³](#), V.A. Mitsou [ID¹⁶⁹](#), Y. Mitsumori [ID¹¹³](#), O. Miu [ID¹⁶¹](#), P.S. Miyagawa [ID⁹⁶](#), T. Mkrtchyan [ID^{63a}](#), M. Mlinarevic [ID⁹⁸](#), T. Mlinarevic [ID⁹⁸](#), M. Mlynarikova [ID³⁷](#), S. Mobius [ID²⁰](#), M.H. Mohamed Farook [ID¹¹⁵](#), S. Mohapatra [ID⁴²](#), S. Mohiuddin [ID¹²⁴](#), G. Mokgatitswane [ID^{34g}](#), L. Moleri [ID¹⁷⁵](#), U. Molinatti [ID¹²⁹](#), L.G. Mollier [ID²⁰](#), B. Mondal [ID¹⁴⁷](#), S. Mondal [ID¹³⁵](#), K. Mönig [ID⁴⁸](#), E. Monnier [ID¹⁰⁴](#), L. Monsonis Romero [ID¹⁶⁹](#), J. Montejo Berlingen [ID¹³](#), A. Montella [ID^{47a,47b}](#), M. Montella [ID¹²²](#), F. Montereali [ID^{77a,77b}](#), F. Monticelli [ID⁹²](#), S. Monzani [ID^{69a,69c}](#), A. Morancho Tarda [ID⁴³](#), N. Morange [ID⁶⁶](#), A.L. Moreira De Carvalho [ID⁴⁸](#), M. Moreno Llácer [ID¹⁶⁹](#), C. Moreno Martinez [ID⁵⁶](#), J.M. Moreno Perez [ID^{23b}](#),

P. Morettini [ID^{57b}](#), S. Morgenstern [ID³⁷](#), M. Morii [ID⁶¹](#), M. Morinaga [ID¹⁵⁹](#), M. Moritsu [ID⁹⁰](#),
 F. Morodei [ID^{75a,75b}](#), P. Moschovakos [ID³⁷](#), B. Moser [ID⁵⁴](#), M. Mosidze [ID^{155b}](#), T. Moskalets [ID⁴⁵](#),
 P. Moskvitina [ID¹¹⁶](#), J. Moss [ID³²](#), P. Moszkowicz [ID^{86a}](#), A. Moussa [ID^{36d}](#), Y. Moyal [ID¹⁷⁵](#),
 H. Moyano Gomez [ID¹³](#), E.J.W. Moyse [ID¹⁰⁵](#), O. Mtintsilana [ID^{34g}](#), S. Muanza [ID¹⁰⁴](#), M. Mucha²⁵,
 J. Mueller [ID¹³²](#), R. Müller [ID³⁷](#), G.A. Mullier [ID¹⁶⁷](#), A.J. Mullin³³, J.J. Mullin⁵¹, A.C. Mullins⁴⁵,
 A.E. Mulski [ID⁶¹](#), D.P. Mungo [ID¹⁶¹](#), D. Munoz Perez [ID¹⁶⁹](#), F.J. Munoz Sanchez [ID¹⁰³](#),
 W.J. Murray [ID^{173,137}](#), M. Muškinja [ID⁹⁵](#), C. Mwewa [ID⁴⁸](#), A.G. Myagkov [ID^{38,a}](#), A.J. Myers [ID⁸](#),
 G. Myers [ID¹⁰⁸](#), M. Myska [ID¹³⁵](#), B.P. Nachman [ID^{18a}](#), K. Nagai [ID¹²⁹](#), K. Nagano [ID⁸⁴](#), R. Nagasaka¹⁵⁹,
 J.L. Nagle [ID^{30,ak}](#), E. Nagy [ID¹⁰⁴](#), A.M. Nairz [ID³⁷](#), Y. Nakahama [ID⁸⁴](#), K. Nakamura [ID⁸⁴](#), K. Nakkalil [ID⁵](#),
 A. Nandi [ID^{63b}](#), H. Nanjo [ID¹²⁷](#), E.A. Narayanan [ID⁴⁵](#), Y. Narukawa [ID¹⁵⁹](#), I. Naryshkin [ID³⁸](#),
 L. Nasella [ID^{71a,71b}](#), S. Nasri [ID^{119b}](#), C. Nass [ID²⁵](#), G. Navarro [ID^{23a}](#), J. Navarro-Gonzalez [ID¹⁶⁹](#),
 A. Nayaz [ID¹⁹](#), P.Y. Nechaeva [ID³⁸](#), S. Nechaeva [ID^{24b,24a}](#), F. Nechansky [ID¹³⁴](#), L. Nedic [ID¹²⁹](#), T.J. Neep [ID²¹](#),
 A. Negri [ID^{73a,73b}](#), M. Negrini [ID^{24b}](#), C. Nellist [ID¹¹⁷](#), C. Nelson [ID¹⁰⁶](#), K. Nelson [ID¹⁰⁸](#), S. Nemecek [ID¹³⁴](#),
 M. Nessi [ID^{37,h}](#), M.S. Neubauer [ID¹⁶⁸](#), J. Newell [ID⁹⁴](#), P.R. Newman [ID²¹](#), Y.W.Y. Ng [ID¹⁶⁸](#), B. Ngair [ID^{119a}](#),
 H.D.N. Nguyen [ID¹¹⁰](#), J.D. Nichols [ID¹²³](#), R.B. Nickerson [ID¹²⁹](#), R. Nicolaïdou [ID¹³⁸](#), J. Nielsen [ID¹³⁹](#),
 M. Niemeyer [ID⁵⁵](#), J. Niermann [ID³⁷](#), N. Nikiforou [ID³⁷](#), V. Nikolaenko [ID^{38,a}](#), I. Nikolic-Audit [ID¹³⁰](#),
 P. Nilsson [ID³⁰](#), I. Ninca [ID⁴⁸](#), G. Ninio [ID¹⁵⁷](#), A. Nisati [ID^{75a}](#), N. Nishu [ID²](#), R. Nisius [ID¹¹²](#),
 N. Nitika [ID^{69a,69c}](#), J-E. Nitschke [ID⁵⁰](#), E.K. Nkademeng [ID^{34b}](#), T. Nobe [ID¹⁵⁹](#), T. Nommensen [ID¹⁵³](#),
 M.B. Norfolk [ID¹⁴⁵](#), B.J. Norman [ID³⁵](#), M. Noury [ID^{36a}](#), J. Novak [ID⁹⁵](#), T. Novak [ID⁹⁵](#), R. Novotny [ID¹³⁵](#),
 L. Nozka [ID¹²⁵](#), K. Ntekas [ID¹⁶⁵](#), N.M.J. Nunes De Moura Junior [ID^{83b}](#), J. Ocariz [ID¹³⁰](#), A. Ochi [ID⁸⁵](#),
 I. Ochoa [ID^{133a}](#), S. Oerdekk [ID^{48,z}](#), J.T. Offermann [ID⁴⁰](#), A. Ogrodnik [ID¹³⁶](#), A. Oh [ID¹⁰³](#), C.C. Ohm [ID¹⁵⁰](#),
 H. Oide [ID⁸⁴](#), M.L. Ojeda [ID³⁷](#), Y. Okumura [ID¹⁵⁹](#), L.F. Oleiro Seabra [ID^{133a}](#), I. Oleksiyuk [ID⁵⁶](#),
 G. Oliveira Correa [ID¹³](#), D. Oliveira Damazio [ID³⁰](#), J.L. Oliver [ID¹⁶⁵](#), Ö.O. Öncel [ID⁵⁴](#), A.P. O'Neill [ID²⁰](#),
 A. Onofre [ID^{133a,133e,e}](#), P.U.E. Onyisi [ID¹¹](#), M.J. Oreglia [ID⁴⁰](#), D. Orestano [ID^{77a,77b}](#), R. Orlandini [ID^{77a,77b}](#),
 R.S. Orr [ID¹⁶¹](#), L.M. Osojnak [ID¹³¹](#), Y. Osumi [ID¹¹³](#), G. Otero y Garzon [ID³¹](#), H. Otono [ID⁹⁰](#),
 G.J. Ottino [ID^{18a}](#), M. Ouchrif [ID^{36d}](#), F. Ould-Saada [ID¹²⁸](#), T. Ovsianikova [ID¹⁴²](#), M. Owen [ID⁵⁹](#),
 R.E. Owen [ID¹³⁷](#), V.E. Ozcan [ID^{22a}](#), F. Ozturk [ID⁸⁷](#), N. Ozturk [ID⁸](#), S. Ozturk [ID⁸²](#), H.A. Pacey [ID¹²⁹](#),
 K. Pachal [ID^{162a}](#), A. Pacheco Pages [ID¹³](#), C. Padilla Aranda [ID¹³](#), G. Padovano [ID^{75a,75b}](#),
 S. Pagan Griso [ID^{18a}](#), G. Palacino [ID⁶⁸](#), A. Palazzo [ID^{70a,70b}](#), J. Pampel [ID²⁵](#), J. Pan [ID¹⁷⁸](#), T. Pan [ID^{64a}](#),
 D.K. Panchal [ID¹¹](#), C.E. Pandini [ID⁶⁰](#), J.G. Panduro Vazquez [ID¹³⁷](#), H.D. Pandya [ID¹](#), H. Pang [ID¹³⁸](#),
 P. Pani [ID⁴⁸](#), G. Panizzo [ID^{69a,69c}](#), L. Panwar [ID¹³⁰](#), L. Paolozzi [ID⁵⁶](#), S. Parajuli [ID¹⁶⁸](#), A. Paramonov [ID⁶](#),
 C. Paraskevopoulos [ID⁵³](#), D. Paredes Hernandez [ID^{64b}](#), A. Parieti [ID^{73a,73b}](#), K.R. Park [ID⁴²](#), T.H. Park [ID¹¹²](#),
 F. Parodi [ID^{57b,57a}](#), J.A. Parsons [ID⁴²](#), U. Parzefall [ID⁵⁴](#), B. Pascual Dias [ID⁴¹](#), L. Pascual Dominguez [ID¹⁰¹](#),
 E. Pasqualucci [ID^{75a}](#), S. Passaggio [ID^{57b}](#), F. Pastore [ID⁹⁷](#), P. Patel [ID⁸⁷](#), U.M. Patel [ID⁵¹](#), J.R. Pater [ID¹⁰³](#),
 T. Pauly [ID³⁷](#), F. Pauwels [ID¹³⁶](#), C.I. Pazos [ID¹⁶⁴](#), M. Pedersen [ID¹²⁸](#), R. Pedro [ID^{133a}](#), S.V. Peleganchuk [ID³⁸](#),
 O. Penc [ID³⁷](#), E.A. Pender [ID⁵²](#), S. Peng [ID¹⁵](#), G.D. Penn [ID¹⁷⁸](#), K.E. Penski [ID¹¹¹](#), M. Penzin [ID³⁸](#),
 B.S. Peralva [ID^{83d}](#), A.P. Pereira Peixoto [ID¹⁴²](#), L. Pereira Sanchez [ID¹⁴⁹](#), D.V. Perpelitsa [ID^{30,ak}](#),
 G. Perera [ID¹⁰⁵](#), E. Perez Codina [ID³⁷](#), M. Perganti [ID¹⁰](#), H. Pernegger [ID³⁷](#), S. Perrella [ID^{75a,75b}](#),
 O. Perrin [ID⁴¹](#), K. Peters [ID⁴⁸](#), R.F.Y. Peters [ID¹⁰³](#), B.A. Petersen [ID³⁷](#), T.C. Petersen [ID⁴³](#), E. Petit [ID¹⁰⁴](#),
 V. Petousis [ID¹³⁵](#), A.R. Petri [ID^{71a,71b}](#), C. Petridou [ID^{158,d}](#), T. Petru [ID¹³⁶](#), A. Petrukhin [ID¹⁴⁷](#), M. Pettee [ID^{18a}](#),
 A. Petukhov [ID⁸²](#), K. Petukhova [ID³⁷](#), R. Pezoa [ID^{140f}](#), L. Pezzotti [ID^{24b,24a}](#), G. Pezzullo [ID¹⁷⁸](#),
 L. Pfaffenbichler [ID³⁷](#), A.J. Pfleger [ID³⁷](#), T.M. Pham [ID¹⁷⁶](#), T. Pham [ID¹⁰⁷](#), P.W. Phillips [ID¹³⁷](#),
 G. Piacquadio [ID¹⁵¹](#), E. Pianori [ID^{18a}](#), F. Piazza [ID¹²⁶](#), R. Piegaia [ID³¹](#), D. Pietreanu [ID^{28b}](#),
 A.D. Pilkington [ID¹⁰³](#), M. Pinamonti [ID^{69a,69c}](#), J.L. Pinfold [ID²](#), B.C. Pinheiro Pereira [ID^{133a}](#),
 J. Pinol Bel [ID¹³](#), A.E. Pinto Pinoargote [ID¹³⁰](#), L. Pintucci [ID^{69a,69c}](#), K.M. Piper [ID¹⁵²](#), A. Pirttikoski [ID⁵⁶](#),
 D.A. Pizzi [ID³⁵](#), L. Pizzimento [ID^{64b}](#), A. Plebani [ID³³](#), M.-A. Pleier [ID³⁰](#), V. Pleskot [ID¹³⁶](#), E. Plotnikova³⁹,
 G. Poddar [ID⁹⁶](#), R. Poettgen [ID¹⁰⁰](#), L. Poggioli [ID¹³⁰](#), S. Polacek [ID¹³⁶](#), G. Polesello [ID^{73a}](#), A. Poley [ID¹⁴⁸](#),

A. Polini [ID^{24b}](#), C.S. Pollard [ID¹⁷³](#), Z.B. Pollock [ID¹²²](#), E. Pompa Pacchi [ID¹²³](#), N.I. Pond [ID⁹⁸](#),
 D. Ponomarenko [ID⁶⁸](#), L. Pontecorvo [ID³⁷](#), S. Popa [ID^{28a}](#), G.A. Popeneciu [ID^{28d}](#), A. Poreba [ID³⁷](#),
 D.M. Portillo Quintero [ID^{162a}](#), S. Pospisil [ID¹³⁵](#), M.A. Postill [ID¹⁴⁵](#), P. Postolache [ID^{28c}](#), K. Potamianos [ID¹⁷³](#),
 P.A. Potepa [ID^{86a}](#), I.N. Potrap [ID³⁹](#), C.J. Potter [ID³³](#), H. Potti [ID¹⁵³](#), J. Poveda [ID¹⁶⁹](#),
 M.E. Pozo Astigarraga [ID³⁷](#), R. Pozzi [ID³⁷](#), A. Prades Ibanez [ID^{76a,76b}](#), J. Pretel [ID¹⁷¹](#), D. Price [ID¹⁰³](#),
 M. Primavera [ID^{70a}](#), L. Primomo [ID^{69a,69c}](#), M.A. Principe Martin [ID¹⁰¹](#), R. Privara [ID¹²⁵](#), T. Procter [ID^{86b}](#),
 M.L. Proffitt [ID¹⁴²](#), N. Proklova [ID¹³¹](#), K. Prokofiev [ID^{64c}](#), G. Proto [ID¹¹²](#), J. Proudfoot [ID⁶](#),
 M. Przybycien [ID^{86a}](#), W.W. Przygoda [ID^{86b}](#), A. Psallidas [ID⁴⁶](#), J.E. Puddefoot [ID¹⁴⁵](#), D. Pudzha [ID⁵³](#),
 D. Pyatiizbyantseva [ID¹¹⁶](#), J. Qian [ID¹⁰⁸](#), R. Qian [ID¹⁰⁹](#), D. Qichen [ID¹⁰³](#), Y. Qin [ID¹³](#), T. Qiu [ID⁵²](#),
 A. Quadt [ID⁵⁵](#), M. Queitsch-Maitland [ID¹⁰³](#), G. Quetant [ID⁵⁶](#), R.P. Quinn [ID¹⁷⁰](#), G. Rabanal Bolanos [ID⁶¹](#),
 D. Rafanoharana [ID¹¹²](#), F. Raffaeli [ID^{76a,76b}](#), F. Ragusa [ID^{71a,71b}](#), J.L. Rainbolt [ID⁴⁰](#), J.A. Raine [ID⁵⁶](#),
 S. Rajagopalan [ID³⁰](#), E. Ramakoti [ID³⁹](#), L. Rambelli [ID^{57b,57a}](#), I.A. Ramirez-Berend [ID³⁵](#), K. Ran [ID^{48,114c}](#),
 D.S. Rankin [ID¹³¹](#), N.P. Rapheeja [ID^{34g}](#), H. Rasheed [ID^{28b}](#), D.F. Rassloff [ID^{63a}](#), A. Rastogi [ID^{18a}](#),
 S. Rave [ID¹⁰²](#), S. Ravera [ID^{57b,57a}](#), B. Ravina [ID³⁷](#), I. Ravinovich [ID¹⁷⁵](#), M. Raymond [ID³⁷](#), A.L. Read [ID¹²⁸](#),
 N.P. Readioff [ID¹⁴⁵](#), D.M. Rebuzzi [ID^{73a,73b}](#), A.S. Reed [ID¹¹²](#), K. Reeves [ID²⁷](#), J.A. Reidelsturz [ID¹⁷⁷](#),
 D. Reikher [ID¹²⁶](#), A. Rej [ID⁴⁹](#), C. Rembser [ID³⁷](#), H. Ren [ID⁶²](#), M. Renda [ID^{28b}](#), F. Renner [ID⁴⁸](#),
 A.G. Rennie [ID⁵⁹](#), A.L. Rescia [ID⁴⁸](#), S. Resconi [ID^{71a}](#), M. Ressegotti [ID^{57b,57a}](#), S. Rettie [ID³⁷](#),
 W.F. Rettie [ID³⁵](#), E. Reynolds [ID^{18a}](#), O.L. Rezanova [ID³⁹](#), P. Reznicek [ID¹³⁶](#), H. Riani [ID^{36d}](#), N. Ribaric [ID⁵¹](#),
 E. Ricci [ID^{78a,78b}](#), R. Richter [ID¹¹²](#), S. Richter [ID^{47a,47b}](#), E. Richter-Was [ID^{86b}](#), M. Ridel [ID¹³⁰](#),
 S. Ridouani [ID^{36d}](#), P. Rieck [ID¹²⁰](#), P. Riedler [ID³⁷](#), E.M. Riefel [ID^{47a,47b}](#), J.O. Rieger [ID¹¹⁷](#),
 M. Rijssenbeek [ID¹⁵¹](#), M. Rimoldi [ID³⁷](#), L. Rinaldi [ID^{24b,24a}](#), P. Rincke [ID^{167,55}](#), G. Ripellino [ID¹⁶⁷](#),
 I. Riu [ID¹³](#), J.C. Rivera Vergara [ID¹⁷¹](#), F. Rizatdinova [ID¹²⁴](#), E. Rizvi [ID⁹⁶](#), B.R. Roberts [ID^{18a}](#),
 S.S. Roberts [ID¹³⁹](#), D. Robinson [ID³³](#), M. Robles Manzano [ID¹⁰²](#), A. Robson [ID⁵⁹](#), A. Rocchi [ID^{76a,76b}](#),
 C. Roda [ID^{74a,74b}](#), S. Rodriguez Bosca [ID³⁷](#), Y. Rodriguez Garcia [ID^{23a}](#), A.M. Rodríguez Vera [ID¹¹⁸](#),
 S. Roe [ID³⁷](#), J.T. Roemer [ID³⁷](#), O. Røhne [ID¹²⁸](#), R.A. Rojas [ID³⁷](#), C.P.A. Roland [ID¹³⁰](#), A. Romaniouk [ID⁷⁹](#),
 E. Romano [ID^{73a,73b}](#), M. Romano [ID^{24b}](#), A.C. Romero Hernandez [ID¹⁶⁸](#), N. Rompotis [ID⁹⁴](#), L. Roos [ID¹³⁰](#),
 S. Rosati [ID^{75a}](#), B.J. Rosser [ID⁴⁰](#), E. Rossi [ID¹²⁹](#), E. Rossi [ID^{72a,72b}](#), L.P. Rossi [ID⁶¹](#), L. Rossini [ID⁵⁴](#),
 R. Rosten [ID¹²²](#), M. Rotaru [ID^{28b}](#), B. Rottler [ID⁵⁴](#), D. Rousseau [ID⁶⁶](#), D. Roussel [ID⁴⁸](#), S. Roy-Garand [ID¹⁶¹](#),
 A. Rozanov [ID¹⁰⁴](#), Z.M.A. Rozario [ID⁵⁹](#), Y. Rozen [ID¹⁵⁶](#), A. Rubio Jimenez [ID¹⁶⁹](#), V.H. Ruelas Rivera [ID¹⁹](#),
 T.A. Ruggeri [ID¹](#), A. Ruggiero [ID¹²⁹](#), A. Ruiz-Martinez [ID¹⁶⁹](#), A. Rummler [ID³⁷](#), Z. Rurikova [ID⁵⁴](#),
 N.A. Rusakovich [ID³⁹](#), H.L. Russell [ID¹⁷¹](#), G. Russo [ID^{75a,75b}](#), J.P. Rutherford [ID⁷](#),
 S. Rutherford Colmenares [ID³³](#), M. Rybar [ID¹³⁶](#), P. Rybczynski [ID^{86a}](#), A. Ryzhov [ID⁴⁵](#),
 J.A. Sabater Iglesias [ID⁵⁶](#), H.F.-W. Sadrozinski [ID¹³⁹](#), F. Safai Tehrani [ID^{75a}](#), S. Saha [ID¹](#), M. Sahinsoy [ID⁸²](#),
 B. Sahoo [ID¹⁷⁵](#), A. Saibel [ID¹⁶⁹](#), B.T. Saifuddin [ID¹²³](#), M. Saimpert [ID¹³⁸](#), G.T. Saito [ID^{83c}](#), M. Saito [ID¹⁵⁹](#),
 T. Saito [ID¹⁵⁹](#), A. Sala [ID^{71a,71b}](#), A. Salnikov [ID¹⁴⁹](#), J. Salt [ID¹⁶⁹](#), A. Salvador Salas [ID¹⁵⁷](#), F. Salvatore [ID¹⁵²](#),
 A. Salzburger [ID³⁷](#), D. Sammel [ID⁵⁴](#), E. Sampson [ID⁹³](#), D. Sampsonidis [ID^{158,d}](#), D. Sampsonidou [ID¹²⁶](#),
 J. Sánchez [ID¹⁶⁹](#), V. Sanchez Sebastian [ID¹⁶⁹](#), H. Sandaker [ID¹²⁸](#), C.O. Sander [ID⁴⁸](#), J.A. Sandesara [ID¹⁷⁶](#),
 M. Sandhoff [ID¹⁷⁷](#), C. Sandoval [ID^{23b}](#), L. Sanfilippo [ID^{63a}](#), D.P.C. Sankey [ID¹³⁷](#), T. Sano [ID⁸⁹](#),
 A. Sansoni [ID⁵³](#), L. Santi [ID³⁷](#), C. Santoni [ID⁴¹](#), H. Santos [ID^{133a,133b}](#), A. Santra [ID¹⁷⁵](#), E. Sanzani [ID^{24b,24a}](#),
 K.A. Saoucha [ID^{88b}](#), J.G. Saraiva [ID^{133a,133d}](#), J. Sardain [ID⁷](#), O. Sasaki [ID⁸⁴](#), K. Sato [ID¹⁶³](#), C. Sauer [ID³⁷](#),
 E. Sauvan [ID⁴](#), P. Savard [ID^{161,ai}](#), R. Sawada [ID¹⁵⁹](#), C. Sawyer [ID¹³⁷](#), L. Sawyer [ID⁹⁹](#), C. Sbarra [ID^{24b}](#),
 A. Sbrizzi [ID^{24b,24a}](#), T. Scanlon [ID⁹⁸](#), J. Schaarschmidt [ID¹⁴²](#), U. Schäfer [ID¹⁰²](#), A.C. Schaffer [ID^{66,45}](#),
 D. Schaile [ID¹¹¹](#), R.D. Schamberger [ID¹⁵¹](#), C. Scharf [ID¹⁹](#), M.M. Schefer [ID²⁰](#), V.A. Schegelsky [ID³⁸](#),
 D. Scheirich [ID¹³⁶](#), M. Schernau [ID^{140e}](#), C. Scheulen [ID⁵⁶](#), C. Schiavi [ID^{57b,57a}](#), M. Schioppa [ID^{44b,44a}](#),
 B. Schlag [ID¹⁴⁹](#), S. Schlenker [ID³⁷](#), J. Schmeing [ID¹⁷⁷](#), E. Schmidt [ID¹¹²](#), M.A. Schmidt [ID¹⁷⁷](#),
 K. Schmieden [ID¹⁰²](#), C. Schmitt [ID¹⁰²](#), N. Schmitt [ID¹⁰²](#), S. Schmitt [ID⁴⁸](#), N.A. Schneider [ID¹¹¹](#),
 L. Schoeffel [ID¹³⁸](#), A. Schoening [ID^{63b}](#), P.G. Scholer [ID³⁵](#), E. Schopf [ID¹⁴⁷](#), M. Schott [ID²⁵](#), S. Schramm [ID⁵⁶](#),

T. Schroer [ID⁵⁶](#), H.-C. Schultz-Coulon [ID^{63a}](#), M. Schumacher [ID⁵⁴](#), B.A. Schumm [ID¹³⁹](#), Ph. Schune [ID¹³⁸](#),
 H.R. Schwartz [ID¹³⁹](#), A. Schwartzman [ID¹⁴⁹](#), T.A. Schwarz [ID¹⁰⁸](#), Ph. Schwemling [ID¹³⁸](#),
 R. Schwienhorst [ID¹⁰⁹](#), F.G. Sciacca [ID²⁰](#), A. Sciandra [ID³⁰](#), G. Sciolla [ID²⁷](#), F. Scuri [ID^{74a}](#),
 C.D. Sebastiani [ID³⁷](#), K. Sedlaczek [ID¹¹⁸](#), S.C. Seidel [ID¹¹⁵](#), A. Seiden [ID¹³⁹](#), B.D. Seidlitz [ID⁴²](#),
 C. Seitz [ID⁴⁸](#), J.M. Seixas [ID^{83b}](#), G. Sekhniaidze [ID^{72a}](#), L. Selen [ID⁶⁰](#), N. Semprini-Cesari [ID^{24b,24a}](#),
 A. Semushin [ID¹⁷⁹](#), D. Sengupta [ID⁵⁶](#), V. Senthilkumar [ID¹⁶⁹](#), L. Serin [ID⁶⁶](#), M. Sessa [ID^{72a,72b}](#),
 H. Severini [ID¹²³](#), F. Sforza [ID^{57b,57a}](#), A. Sfyrla [ID⁵⁶](#), Q. Sha [ID¹⁴](#), E. Shabalina [ID⁵⁵](#), H. Shaddix [ID¹¹⁸](#),
 A.H. Shah [ID³³](#), R. Shaheen [ID¹⁵⁰](#), J.D. Shahinian [ID¹³¹](#), M. Shamim [ID³⁷](#), L.Y. Shan [ID¹⁴](#), M. Shapiro [ID^{18a}](#),
 A. Sharma [ID³⁷](#), A.S. Sharma [ID¹⁷⁰](#), P. Sharma [ID³⁰](#), P.B. Shatalov [ID³⁸](#), K. Shaw [ID¹⁵²](#), S.M. Shaw [ID¹⁰³](#),
 Q. Shen [ID^{144a}](#), D.J. Sheppard [ID¹⁴⁸](#), P. Sherwood [ID⁹⁸](#), L. Shi [ID⁹⁸](#), X. Shi [ID¹⁴](#), S. Shimizu [ID⁸⁴](#),
 C.O. Shimmin [ID¹⁷⁸](#), I.P.J. Shipsey [ID^{129,*}](#), S. Shirabe [ID⁹⁰](#), M. Shiyakova [ID^{39,aa}](#), M.J. Shochet [ID⁴⁰](#),
 D.R. Shope [ID¹²⁸](#), B. Shrestha [ID¹²³](#), S. Shrestha [ID^{122,am}](#), I. Shreyber [ID³⁹](#), M.J. Shroff [ID¹⁷¹](#), P. Sicho [ID¹³⁴](#),
 A.M. Sickles [ID¹⁶⁸](#), E. Sideras Haddad [ID^{34g,166}](#), A.C. Sidley [ID¹¹⁷](#), A. Sidoti [ID^{24b}](#), F. Siegert [ID⁵⁰](#),
 Dj. Sijacki [ID¹⁶](#), F. Sili [ID⁹²](#), J.M. Silva [ID⁵²](#), I. Silva Ferreira [ID^{83b}](#), M.V. Silva Oliveira [ID³⁰](#),
 S.B. Silverstein [ID^{47a}](#), S. Simion [ID⁶⁶](#), R. Simoniello [ID³⁷](#), E.L. Simpson [ID¹⁰³](#), H. Simpson [ID¹⁵²](#),
 L.R. Simpson [ID⁶](#), S. Simsek [ID⁸²](#), S. Sindhu [ID⁵⁵](#), P. Sinervo [ID¹⁶¹](#), S.N. Singh [ID²⁷](#), S. Singh [ID³⁰](#),
 S. Sinha [ID⁴⁸](#), S. Sinha [ID¹⁰³](#), M. Sioli [ID^{24b,24a}](#), K. Sioulas [ID⁹](#), I. Siral [ID³⁷](#), E. Sitnikova [ID⁴⁸](#),
 J. Sjölin [ID^{47a,47b}](#), A. Skaf [ID⁵⁵](#), E. Skorda [ID²¹](#), P. Skubic [ID¹²³](#), M. Slawinska [ID⁸⁷](#), I. Slazynk [ID¹⁷](#),
 I. Sliusar [ID¹²⁸](#), V. Smakhtin [ID¹⁷⁵](#), B.H. Smart [ID¹³⁷](#), S.Yu. Smirnov [ID^{140b}](#), Y. Smirnov [ID⁸²](#),
 L.N. Smirnova [ID^{38,a}](#), O. Smirnova [ID¹⁰⁰](#), A.C. Smith [ID⁴²](#), D.R. Smith [ID¹⁶⁵](#), J.L. Smith [ID¹⁰³](#),
 M.B. Smith [ID³⁵](#), R. Smith [ID¹⁴⁹](#), H. Smitmanns [ID¹⁰²](#), M. Smizanska [ID⁹³](#), K. Smolek [ID¹³⁵](#),
 P. Smolyanskiy [ID¹³⁵](#), A.A. Snesarev [ID³⁹](#), H.L. Snoek [ID¹¹⁷](#), S. Snyder [ID³⁰](#), R. Sobie [ID^{171,ac}](#),
 A. Soffer [ID¹⁵⁷](#), C.A. Solans Sanchez [ID³⁷](#), E.Yu. Soldatov [ID³⁹](#), U. Soldevila [ID¹⁶⁹](#), A.A. Solodkov [ID^{34g}](#),
 S. Solomon [ID²⁷](#), A. Soloshenko [ID³⁹](#), K. Solovieva [ID⁵⁴](#), O.V. Solovyanov [ID⁴¹](#), P. Sommer [ID⁵⁰](#),
 A. Sonay [ID¹³](#), A. Sopczak [ID¹³⁵](#), A.L. Sopio [ID⁵²](#), F. Sopkova [ID^{29b}](#), J.D. Sorenson [ID¹¹⁵](#),
 I.R. Sotarriva Alvarez [ID¹⁴¹](#), V. Sothilingam [ID^{63a}](#), O.J. Soto Sandoval [ID^{140c,140b}](#), S. Sottocornola [ID⁶⁸](#),
 R. Soualah [ID^{88a}](#), Z. Soumaimi [ID^{36e}](#), D. South [ID⁴⁸](#), N. Soybelman [ID¹⁷⁵](#), S. Spagnolo [ID^{70a,70b}](#),
 M. Spalla [ID¹¹²](#), D. Sperlich [ID⁵⁴](#), B. Spisso [ID^{72a,72b}](#), D.P. Spiteri [ID⁵⁹](#), L. Splendori [ID¹⁰⁴](#), M. Spousta [ID¹³⁶](#),
 E.J. Staats [ID³⁵](#), R. Stamen [ID^{63a}](#), E. Stancka [ID⁸⁷](#), W. Stanek-Maslouska [ID⁴⁸](#), M.V. Stange [ID⁵⁰](#),
 B. Stanislaus [ID^{18a}](#), M.M. Stanitzki [ID⁴⁸](#), B. Stapf [ID⁴⁸](#), E.A. Starchenko [ID³⁸](#), G.H. Stark [ID¹³⁹](#), J. Stark [ID⁹¹](#),
 P. Staroba [ID¹³⁴](#), P. Starovoitov [ID^{88b}](#), R. Staszewski [ID⁸⁷](#), G. Stavropoulos [ID⁴⁶](#), A. Stefl [ID³⁷](#),
 P. Steinberg [ID³⁰](#), B. Stelzer [ID^{148,162a}](#), H.J. Stelzer [ID¹³²](#), O. Stelzer-Chilton [ID^{162a}](#), H. Stenzel [ID⁵⁸](#),
 T.J. Stevenson [ID¹⁵²](#), G.A. Stewart [ID³⁷](#), J.R. Stewart [ID¹²⁴](#), M.C. Stockton [ID³⁷](#), G. Stoicea [ID^{28b}](#),
 M. Stolarski [ID^{133a}](#), S. Stonjek [ID¹¹²](#), A. Straessner [ID⁵⁰](#), J. Strandberg [ID¹⁵⁰](#), S. Strandberg [ID^{47a,47b}](#),
 M. Stratmann [ID¹⁷⁷](#), M. Strauss [ID¹²³](#), T. Strebler [ID¹⁰⁴](#), P. Strizenec [ID^{29b}](#), R. Ströhmer [ID¹⁷²](#),
 D.M. Strom [ID¹²⁶](#), R. Stroynowski [ID⁴⁵](#), A. Strubig [ID^{47a,47b}](#), S.A. Stucci [ID³⁰](#), B. Stugu [ID¹⁷](#), J. Stupak [ID¹²³](#),
 N.A. Styles [ID⁴⁸](#), D. Su [ID¹⁴⁹](#), S. Su [ID⁶²](#), X. Su [ID⁶²](#), D. Suchy [ID^{29a}](#), K. Sugizaki [ID¹³¹](#), V.V. Sulin [ID³⁸](#),
 M.J. Sullivan [ID⁹⁴](#), D.M.S. Sultan [ID¹²⁹](#), L. Sultanaliyeva [ID³⁸](#), S. Sultansoy [ID^{3b}](#), S. Sun [ID¹⁷⁶](#), W. Sun [ID¹⁴](#),
 O. Sunneborn Gudnadottir [ID¹⁶⁷](#), N. Sur [ID¹⁰⁰](#), M.R. Sutton [ID¹⁵²](#), H. Suzuki [ID¹⁶³](#), M. Svatos [ID¹³⁴](#),
 P.N. Swallow [ID³³](#), M. Swiatlowski [ID^{162a}](#), T. Swirski [ID¹⁷²](#), A. Swoboda [ID³⁷](#), I. Sykora [ID^{29a}](#),
 M. Sykora [ID¹³⁶](#), T. Sykora [ID¹³⁶](#), D. Ta [ID¹⁰²](#), K. Tackmann [ID^{48,z}](#), A. Taffard [ID¹⁶⁵](#), R. Tafirout [ID^{162a}](#),
 Y. Takubo [ID⁸⁴](#), M. Talby [ID¹⁰⁴](#), A.A. Talyshев [ID³⁸](#), K.C. Tam [ID^{64b}](#), N.M. Tamir [ID¹⁵⁷](#), A. Tanaka [ID¹⁵⁹](#),
 J. Tanaka [ID¹⁵⁹](#), R. Tanaka [ID⁶⁶](#), M. Tanasini [ID¹⁵¹](#), Z. Tao [ID¹⁷⁰](#), S. Tapia Araya [ID^{140f}](#), S. Tapprogge [ID¹⁰²](#),
 A. Tarek Abouelfadl Mohamed [ID¹⁰⁹](#), S. Tarem [ID¹⁵⁶](#), K. Tariq [ID¹⁴](#), G. Tarna [ID^{28b}](#), G.F. Tartarelli [ID^{71a}](#),
 M.J. Tartarin [ID⁹¹](#), P. Tas [ID¹³⁶](#), M. Tasevsky [ID¹³⁴](#), E. Tassi [ID^{44b,44a}](#), A.C. Tate [ID¹⁶⁸](#), G. Tateno [ID¹⁵⁹](#),
 Y. Tayalati [ID^{36e,ab}](#), G.N. Taylor [ID¹⁰⁷](#), W. Taylor [ID^{162b}](#), A.S. Tegetmeier [ID⁹¹](#), P. Teixeira-Dias [ID⁹⁷](#),
 J.J. Teoh [ID¹⁶¹](#), K. Terashi [ID¹⁵⁹](#), J. Terron [ID¹⁰¹](#), S. Terzo [ID¹³](#), M. Testa [ID⁵³](#), R.J. Teuscher [ID^{161,ac}](#),

A. Thaler [ID⁷⁹](#), O. Theiner [ID⁵⁶](#), T. Theveneaux-Pelzer [ID¹⁰⁴](#), D.W. Thomas [ID⁹⁷](#), J.P. Thomas [ID²¹](#), E.A. Thompson [ID^{18a}](#), P.D. Thompson [ID²¹](#), E. Thomson [ID¹³¹](#), R.E. Thornberry [ID⁴⁵](#), C. Tian [ID⁶²](#), Y. Tian [ID⁵⁶](#), V. Tikhomirov [ID³²](#), Yu.A. Tikhonov [ID³⁹](#), S. Timoshenko³⁸, D. Timoshyn [ID¹³⁶](#), E.X.L. Ting [ID¹](#), P. Tipton [ID¹⁷⁸](#), A. Tishelman-Charny [ID³⁰](#), K. Todome [ID¹⁴¹](#), S. Todorova-Nova [ID¹³⁶](#), S. Todt⁵⁰, L. Toffolin [ID^{69a,69c}](#), M. Togawa [ID⁸⁴](#), J. Tojo [ID⁹⁰](#), S. Tokár [ID^{29a}](#), O. Toldaiev [ID⁶⁸](#), G. Tolkachev [ID¹⁰⁴](#), M. Tomoto [ID^{84,113}](#), L. Tompkins [ID^{149,0}](#), E. Torrence [ID¹²⁶](#), H. Torres [ID⁹¹](#), E. Torró Pastor [ID¹⁶⁹](#), M. Toscani [ID³¹](#), C. Tosciri [ID⁴⁰](#), M. Tost [ID¹¹](#), D.R. Tovey [ID¹⁴⁵](#), T. Trefzger [ID¹⁷²](#), P.M. Tricarico [ID¹³](#), A. Tricoli [ID³⁰](#), I.M. Trigger [ID^{162a}](#), S. Trincaz-Duvold [ID¹³⁰](#), D.A. Trischuk [ID²⁷](#), A. Tropina³⁹, L. Truong [ID^{34c}](#), M. Trzebinski [ID⁸⁷](#), A. Trzupek [ID⁸⁷](#), F. Tsai [ID¹⁵¹](#), M. Tsai [ID¹⁰⁸](#), A. Tsiamis [ID¹⁵⁸](#), P.V. Tsiareshka³⁹, S. Tsigaridas [ID^{162a}](#), A. Tsirigotis [ID^{158,v}](#), V. Tsiskaridze [ID¹⁶¹](#), E.G. Tskhadadze [ID^{155a}](#), M. Tsopoulou [ID¹⁵⁸](#), Y. Tsujikawa [ID⁸⁹](#), I.I. Tsukerman [ID³⁸](#), V. Tsulaia [ID^{18a}](#), S. Tsuno [ID⁸⁴](#), K. Tsuri [ID¹²¹](#), D. Tsybychev [ID¹⁵¹](#), Y. Tu [ID^{64b}](#), A. Tudorache [ID^{28b}](#), V. Tudorache [ID^{28b}](#), S.B. Tuncay [ID¹²⁹](#), S. Turchikhin [ID^{57b,57a}](#), I. Turk Cakir [ID^{3a}](#), R. Turra [ID^{71a}](#), T. Turtuvshin [ID^{39,ad}](#), P.M. Tuts [ID⁴²](#), S. Tzamarias [ID^{158,d}](#), E. Tzovara [ID¹⁰²](#), Y. Uematsu [ID⁸⁴](#), F. Ukegawa [ID¹⁶³](#), P.A. Ulloa Poblete [ID^{140c,140b}](#), E.N. Umaka [ID³⁰](#), G. Unal [ID³⁷](#), A. Undrus [ID³⁰](#), G. Unel [ID¹⁶⁵](#), J. Urban [ID^{29b}](#), P. Urrejola [ID^{140a}](#), G. Usai [ID⁸](#), R. Ushioda [ID¹⁶⁰](#), M. Usman [ID¹¹⁰](#), F. Ustuner [ID⁵²](#), Z. Uysal [ID⁸²](#), V. Vacek [ID¹³⁵](#), B. Vachon [ID¹⁰⁶](#), T. Vafeiadis [ID³⁷](#), A. Vaitkus [ID⁹⁸](#), C. Valderanis [ID¹¹¹](#), E. Valdes Santurio [ID^{47a,47b}](#), M. Valente [ID³⁷](#), S. Valentini [ID^{24b,24a}](#), A. Valero [ID¹⁶⁹](#), E. Valiente Moreno [ID¹⁶⁹](#), A. Vallier [ID⁹¹](#), J.A. Valls Ferrer [ID¹⁶⁹](#), D.R. Van Arneman [ID¹¹⁷](#), T.R. Van Daalen [ID¹⁴²](#), A. Van Der Graaf [ID⁴⁹](#), H.Z. Van Der Schyf [ID^{34g}](#), P. Van Gemmeren [ID⁶](#), M. Van Rijnbach [ID³⁷](#), S. Van Stroud [ID⁹⁸](#), I. Van Vulpen [ID¹¹⁷](#), P. Vana [ID¹³⁶](#), M. Vanadia [ID^{76a,76b}](#), U.M. Vande Voorde [ID¹⁵⁰](#), W. Vandelli [ID³⁷](#), E.R. Vandewall [ID¹²⁴](#), D. Vannicola [ID¹⁵⁷](#), L. Vannoli [ID⁵³](#), R. Vari [ID^{75a}](#), M. Varma [ID¹⁷⁸](#), E.W. Varnes [ID⁷](#), C. Varni [ID^{18b}](#), D. Varouchas [ID⁶⁶](#), L. Varriale [ID¹⁶⁹](#), K.E. Varvell [ID¹⁵³](#), M.E. Vasile [ID^{28b}](#), L. Vaslin⁸⁴, M.D. Vassilev [ID¹⁴⁹](#), A. Vasyukov [ID³⁹](#), L.M. Vaughan [ID¹²⁴](#), R. Vavricka¹³⁶, T. Vazquez Schroeder [ID¹³](#), J. Veatch [ID³²](#), V. Vecchio [ID¹⁰³](#), M.J. Veen [ID¹⁰⁵](#), I. Velisek [ID³⁰](#), I. Velkovska [ID⁹⁵](#), L.M. Veloce [ID¹⁶¹](#), F. Veloso [ID^{133a,133c}](#), S. Veneziano [ID^{75a}](#), A. Ventura [ID^{70a,70b}](#), S. Ventura Gonzalez [ID¹³⁸](#), A. Verbytskyi [ID¹¹²](#), M. Verducci [ID^{74a,74b}](#), C. Vergis [ID⁹⁶](#), M. Verissimo De Araujo [ID^{83b}](#), W. Verkerke [ID¹¹⁷](#), J.C. Vermeulen [ID¹¹⁷](#), C. Vernieri [ID¹⁴⁹](#), M. Vessella [ID¹⁶⁵](#), M.C. Vetterli [ID^{148,ai}](#), A. Vgenopoulos [ID¹⁰²](#), N. Viaux Maira [ID^{140f}](#), T. Vickey [ID¹⁴⁵](#), O.E. Vickey Boeriu [ID¹⁴⁵](#), G.H.A. Viehhauser [ID¹²⁹](#), L. Vigani [ID^{63b}](#), M. Vigl [ID¹¹²](#), M. Villa [ID^{24b,24a}](#), M. Villaplana Perez [ID¹⁶⁹](#), E.M. Villhauer⁴⁰, E. Vilucchi [ID⁵³](#), M. Vincent [ID¹⁶⁹](#), M.G. Vincter [ID³⁵](#), A. Visibile¹¹⁷, C. Vittori [ID³⁷](#), I. Vivarelli [ID^{24b,24a}](#), E. Voevodina [ID¹¹²](#), F. Vogel [ID¹¹¹](#), J.C. Voigt [ID⁵⁰](#), P. Vokac [ID¹³⁵](#), Yu. Volkotrub [ID^{86b}](#), E. Von Toerne [ID²⁵](#), B. Vormwald [ID³⁷](#), K. Vorobev [ID⁵¹](#), M. Vos [ID¹⁶⁹](#), K. Voss [ID¹⁴⁷](#), M. Vozak [ID³⁷](#), L. Vozdecky [ID¹²³](#), N. Vranjes [ID¹⁶](#), M. Vranjes Milosavljevic [ID¹⁶](#), M. Vreeswijk [ID¹¹⁷](#), N.K. Vu [ID^{144b,144a}](#), R. Vuillermet [ID³⁷](#), O. Vujinovic [ID¹⁰²](#), I. Vukotic [ID⁴⁰](#), I.K. Vyas [ID³⁵](#), J.F. Wack [ID³³](#), S. Wada [ID¹⁶³](#), C. Wagner¹⁴⁹, J.M. Wagner [ID^{18a}](#), W. Wagner [ID¹⁷⁷](#), S. Wahdan [ID¹⁷⁷](#), H. Wahlberg [ID⁹²](#), C.H. Waits [ID¹²³](#), J. Walder [ID¹³⁷](#), R. Walker [ID¹¹¹](#), K. Walkingshaw Pass⁵⁹, W. Walkowiak [ID¹⁴⁷](#), A. Wall [ID¹³¹](#), E.J. Wallin [ID¹⁰⁰](#), T. Wamorkar [ID^{18a}](#), A. Wang [ID⁶²](#), A.Z. Wang [ID¹³⁹](#), C. Wang [ID¹⁰²](#), C. Wang [ID¹¹](#), H. Wang [ID^{18a}](#), J. Wang [ID^{64c}](#), P. Wang [ID¹⁰³](#), P. Wang [ID⁹⁸](#), R. Wang [ID⁶¹](#), R. Wang [ID⁶](#), S.M. Wang [ID¹⁵⁴](#), S. Wang [ID¹⁴](#), T. Wang [ID⁶²](#), T. Wang [ID⁶²](#), W.T. Wang [ID⁸⁰](#), W. Wang [ID¹⁴](#), X. Wang [ID¹⁶⁸](#), X. Wang [ID^{144a}](#), X. Wang [ID⁴⁸](#), Y. Wang [ID^{114a}](#), Y. Wang [ID⁶²](#), Z. Wang [ID¹⁰⁸](#), Z. Wang [ID^{144b}](#), Z. Wang [ID¹⁰⁸](#), C. Wanotayaroj [ID⁸⁴](#), A. Warburton [ID¹⁰⁶](#), A.L. Warnerbring [ID¹⁴⁷](#), N. Warrack [ID⁵⁹](#), S. Waterhouse [ID⁹⁷](#), A.T. Watson [ID²¹](#), H. Watson [ID⁵²](#), M.F. Watson [ID²¹](#), E. Watton [ID⁵⁹](#), G. Watts [ID¹⁴²](#), B.M. Waugh [ID⁹⁸](#), J.M. Webb [ID⁵⁴](#), C. Weber [ID³⁰](#), H.A. Weber [ID¹⁹](#), M.S. Weber [ID²⁰](#), S.M. Weber [ID^{63a}](#), C. Wei [ID⁶²](#), Y. Wei [ID⁵⁴](#), A.R. Weidberg [ID¹²⁹](#), E.J. Weik [ID¹²⁰](#), J. Weingarten [ID⁴⁹](#), C. Weiser [ID⁵⁴](#), C.J. Wells [ID⁴⁸](#), T. Wenaus [ID³⁰](#), B. Wendland [ID⁴⁹](#), T. Wengler [ID³⁷](#), N.S. Wenke¹¹², N. Wermes [ID²⁵](#), M. Wessels [ID^{63a}](#), A.M. Wharton [ID⁹³](#),

A.S. White [ID⁶¹](#), A. White [ID⁸](#), M.J. White [ID¹](#), D. Whiteson [ID¹⁶⁵](#), L. Wickremasinghe [ID¹²⁷](#),
 W. Wiedenmann [ID¹⁷⁶](#), M. Wielaers [ID¹³⁷](#), R. Wierda [ID¹⁵⁰](#), C. Wiglesworth [ID⁴³](#), H.G. Wilkens [ID³⁷](#),
 J.J.H. Wilkinson [ID³³](#), D.M. Williams [ID⁴²](#), H.H. Williams¹³¹, S. Williams [ID³³](#), S. Willocq [ID¹⁰⁵](#),
 B.J. Wilson [ID¹⁰³](#), D.J. Wilson [ID¹⁰³](#), P.J. Windischhofer [ID⁴⁰](#), F.I. Winkel [ID³¹](#), F. Winklmeier [ID¹²⁶](#),
 B.T. Winter [ID⁵⁴](#), M. Wittgen¹⁴⁹, M. Wobisch [ID⁹⁹](#), T. Wojtkowski⁶⁰, Z. Wolffs [ID¹¹⁷](#), J. Wollrath³⁷,
 M.W. Wolter [ID⁸⁷](#), H. Wolters [ID^{133a,133c}](#), M.C. Wong [ID¹³⁹](#), E.L. Woodward [ID⁴²](#), S.D. Worm [ID⁴⁸](#),
 B.K. Wosiek [ID⁸⁷](#), K.W. Woźniak [ID⁸⁷](#), S. Wozniewski [ID⁵⁵](#), K. Wraight [ID⁵⁹](#), C. Wu [ID¹⁶¹](#), C. Wu [ID²¹](#),
 J. Wu [ID¹⁵⁹](#), M. Wu [ID^{114b}](#), M. Wu [ID¹¹⁶](#), S.L. Wu [ID¹⁷⁶](#), S. Wu [ID¹⁴](#), X. Wu [ID⁶²](#), Y. Wu [ID⁶²](#), Z. Wu [ID⁴](#),
 J. Wuerzinger [ID¹¹²](#), T.R. Wyatt [ID¹⁰³](#), B.M. Wynne [ID⁵²](#), S. Xella [ID⁴³](#), L. Xia [ID^{114a}](#), M. Xia [ID¹⁵](#),
 M. Xie [ID⁶²](#), A. Xiong [ID¹²⁶](#), J. Xiong [ID^{18a}](#), D. Xu [ID¹⁴](#), H. Xu [ID⁶²](#), L. Xu [ID⁶²](#), R. Xu [ID¹³¹](#), T. Xu [ID¹⁰⁸](#),
 Y. Xu [ID¹⁴²](#), Z. Xu [ID⁵²](#), Z. Xu^{114a}, B. Yabsley [ID¹⁵³](#), S. Yacoob [ID^{34a}](#), Y. Yamaguchi [ID⁸⁴](#),
 E. Yamashita [ID¹⁵⁹](#), H. Yamauchi [ID¹⁶³](#), T. Yamazaki [ID^{18a}](#), Y. Yamazaki [ID⁸⁵](#), S. Yan [ID⁵⁹](#), Z. Yan [ID¹⁰⁵](#),
 H.J. Yang [ID^{144a,144b}](#), H.T. Yang [ID⁶²](#), S. Yang [ID⁶²](#), T. Yang [ID^{64c}](#), X. Yang [ID³⁷](#), X. Yang [ID¹⁴](#),
 Y. Yang [ID¹⁵⁹](#), Y. Yang⁶², W-M. Yao [ID^{18a}](#), C.L. Yardley [ID¹⁵²](#), J. Ye [ID¹⁴](#), S. Ye [ID³⁰](#), X. Ye [ID⁶²](#), Y. Yeh [ID⁹⁸](#),
 I. Yeletskikh [ID³⁹](#), B. Yeo [ID^{18b}](#), M.R. Yexley [ID⁹⁸](#), T.P. Yildirim [ID¹²⁹](#), P. Yin [ID⁴²](#), K. Yorita [ID¹⁷⁴](#),
 C.J.S. Young [ID³⁷](#), C. Young [ID¹⁴⁹](#), N.D. Young¹²⁶, Y. Yu [ID⁶²](#), J. Yuan [ID^{14,114c}](#), M. Yuan [ID¹⁰⁸](#),
 R. Yuan [ID^{144b,144a}](#), L. Yue [ID⁹⁸](#), M. Zaazoua [ID⁶²](#), B. Zabinski [ID⁸⁷](#), I. Zahir [ID^{36a}](#), A. Zaio^{57b,57a},
 Z.K. Zak [ID⁸⁷](#), T. Zakareishvili [ID¹⁶⁹](#), S. Zambito [ID⁵⁶](#), J.A. Zamora Saa [ID^{140d}](#), J. Zang [ID¹⁵⁹](#),
 R. Zanzottera [ID^{71a,71b}](#), O. Zaplatilek [ID¹³⁵](#), C. Zeitnitz [ID¹⁷⁷](#), H. Zeng [ID¹⁴](#), J.C. Zeng [ID¹⁶⁸](#),
 D.T. Zenger Jr [ID²⁷](#), O. Zenin [ID³⁸](#), T. Ženiš [ID^{29a}](#), S. Zenz [ID⁹⁶](#), D. Zerwas [ID⁶⁶](#), M. Zhai [ID^{14,114c}](#),
 D.F. Zhang [ID¹⁴⁵](#), G. Zhang [ID¹⁴](#), J. Zhang [ID^{143a}](#), J. Zhang [ID⁶](#), K. Zhang [ID^{14,114c}](#), L. Zhang [ID⁶²](#),
 L. Zhang [ID^{114a}](#), P. Zhang [ID^{14,114c}](#), R. Zhang [ID^{114a}](#), S. Zhang [ID⁹¹](#), T. Zhang [ID¹⁵⁹](#), Y. Zhang [ID¹⁴²](#),
 Y. Zhang [ID⁹⁸](#), Y. Zhang [ID⁶²](#), Y. Zhang [ID^{114a}](#), Z. Zhang [ID^{143a}](#), Z. Zhang [ID⁶⁶](#), H. Zhao [ID¹⁴²](#), T. Zhao [ID^{143a}](#),
 Y. Zhao [ID³⁵](#), Z. Zhao [ID⁶²](#), Z. Zhao [ID⁶²](#), A. Zhemchugov [ID³⁹](#), J. Zheng [ID^{114a}](#), K. Zheng [ID¹⁶⁸](#),
 X. Zheng [ID⁶²](#), Z. Zheng [ID¹⁴⁹](#), D. Zhong [ID¹⁶⁸](#), B. Zhou [ID¹⁰⁸](#), H. Zhou [ID⁷](#), N. Zhou [ID^{144a}](#), Y. Zhou [ID¹⁵](#),
 Y. Zhou [ID^{114a}](#), Y. Zhou⁷, C.G. Zhu [ID^{143a}](#), J. Zhu [ID¹⁰⁸](#), X. Zhu^{144b}, Y. Zhu [ID^{144a}](#), Y. Zhu [ID⁶²](#),
 X. Zhuang [ID¹⁴](#), K. Zhukov [ID⁶⁸](#), N.I. Zimine [ID³⁹](#), J. Zinsser [ID^{63b}](#), M. Ziolkowski [ID¹⁴⁷](#), L. Živković [ID¹⁶](#),
 A. Zoccoli [ID^{24b,24a}](#), K. Zoch [ID⁶¹](#), A. Zografos [ID³⁷](#), T.G. Zorbas [ID¹⁴⁵](#), O. Zormpa [ID⁴⁶](#), L. Zwalski [ID³⁷](#).

¹Department of Physics, University of Adelaide, Adelaide; Australia.

²Department of Physics, University of Alberta, Edmonton AB; Canada.

^{3(a)}Department of Physics, Ankara University, Ankara; ^(b)Division of Physics, TOBB University of Economics and Technology, Ankara; Türkiye.

⁴LAPP, Université Savoie Mont Blanc, CNRS/IN2P3, Annecy; France.

⁵APC, Université Paris Cité, CNRS/IN2P3, Paris; France.

⁶High Energy Physics Division, Argonne National Laboratory, Argonne IL; United States of America.

⁷Department of Physics, University of Arizona, Tucson AZ; United States of America.

⁸Department of Physics, University of Texas at Arlington, Arlington TX; United States of America.

⁹Physics Department, National and Kapodistrian University of Athens, Athens; Greece.

¹⁰Physics Department, National Technical University of Athens, Zografou; Greece.

¹¹Department of Physics, University of Texas at Austin, Austin TX; United States of America.

¹²Institute of Physics, Azerbaijan Academy of Sciences, Baku; Azerbaijan.

¹³Institut de Física d'Altes Energies (IFAE), Barcelona Institute of Science and Technology, Barcelona; Spain.

¹⁴Institute of High Energy Physics, Chinese Academy of Sciences, Beijing; China.

¹⁵Physics Department, Tsinghua University, Beijing; China.

¹⁶Institute of Physics, University of Belgrade, Belgrade; Serbia.

¹⁷Department for Physics and Technology, University of Bergen, Bergen; Norway.

^{18(a)}Physics Division, Lawrence Berkeley National Laboratory, Berkeley CA; ^(b)University of California, Berkeley CA; United States of America.

¹⁹Institut für Physik, Humboldt Universität zu Berlin, Berlin; Germany.

²⁰Albert Einstein Center for Fundamental Physics and Laboratory for High Energy Physics, University of Bern, Bern; Switzerland.

²¹School of Physics and Astronomy, University of Birmingham, Birmingham; United Kingdom.

^{22(a)}Department of Physics, Bogazici University, Istanbul; ^(b)Department of Physics Engineering, Gaziantep University, Gaziantep; ^(c)Department of Physics, Istanbul University, Istanbul; Türkiye.

^{23(a)}Facultad de Ciencias y Centro de Investigaciones, Universidad Antonio Nariño,

Bogotá; ^(b)Departamento de Física, Universidad Nacional de Colombia, Bogotá; Colombia.

^{24(a)}Dipartimento di Fisica e Astronomia A. Righi, Università di Bologna, Bologna; ^(b)INFN Sezione di Bologna; Italy.

²⁵Physikalisches Institut, Universität Bonn, Bonn; Germany.

²⁶Department of Physics, Boston University, Boston MA; United States of America.

²⁷Department of Physics, Brandeis University, Waltham MA; United States of America.

^{28(a)}Transilvania University of Brasov, Brasov; ^(b)Horia Hulubei National Institute of Physics and Nuclear Engineering, Bucharest; ^(c)Department of Physics, Alexandru Ioan Cuza University of Iasi, Iasi; ^(d)National Institute for Research and Development of Isotopic and Molecular Technologies, Physics Department, Cluj-Napoca; ^(e)National University of Science and Technology Politehnica, Bucharest; ^(f)West University in Timisoara, Timisoara; ^(g)Faculty of Physics, University of Bucharest, Bucharest; Romania.

^{29(a)}Faculty of Mathematics, Physics and Informatics, Comenius University, Bratislava; ^(b)Department of Subnuclear Physics, Institute of Experimental Physics of the Slovak Academy of Sciences, Kosice; Slovak Republic.

³⁰Physics Department, Brookhaven National Laboratory, Upton NY; United States of America.

³¹Universidad de Buenos Aires, Facultad de Ciencias Exactas y Naturales, Departamento de Física, y CONICET, Instituto de Física de Buenos Aires (IFIBA), Buenos Aires; Argentina.

³²California State University, CA; United States of America.

³³Cavendish Laboratory, University of Cambridge, Cambridge; United Kingdom.

^{34(a)}Department of Physics, University of Cape Town, Cape Town; ^(b)iThemba Labs, Western Cape; ^(c)Department of Mechanical Engineering Science, University of Johannesburg, Johannesburg; ^(d)National Institute of Physics, University of the Philippines Diliman (Philippines); ^(e)University of South Africa, Department of Physics, Pretoria; ^(f)University of Zululand, KwaDlangezwa; ^(g)School of Physics, University of the Witwatersrand, Johannesburg; South Africa.

³⁵Department of Physics, Carleton University, Ottawa ON; Canada.

^{36(a)}Faculté des Sciences Ain Chock, Université Hassan II de Casablanca; ^(b)Faculté des Sciences, Université Ibn-Tofail, Kénitra; ^(c)Faculté des Sciences Semlalia, Université Cadi Ayyad, LPHEA-Marrakech; ^(d)LPMR, Faculté des Sciences, Université Mohamed Premier, Oujda; ^(e)Faculté des sciences, Université Mohammed V, Rabat; ^(f)Institute of Applied Physics, Mohammed VI Polytechnic University, Ben Guerir; Morocco.

³⁷CERN, Geneva; Switzerland.

³⁸Affiliated with an institute formerly covered by a cooperation agreement with CERN.

³⁹Affiliated with an international laboratory covered by a cooperation agreement with CERN.

⁴⁰Enrico Fermi Institute, University of Chicago, Chicago IL; United States of America.

⁴¹LPC, Université Clermont Auvergne, CNRS/IN2P3, Clermont-Ferrand; France.

⁴²Nevis Laboratory, Columbia University, Irvington NY; United States of America.

⁴³Niels Bohr Institute, University of Copenhagen, Copenhagen; Denmark.

- ^{44(a)}Dipartimento di Fisica, Università della Calabria, Rende; ^(b)INFN Gruppo Collegato di Cosenza, Laboratori Nazionali di Frascati; Italy.
- ⁴⁵Physics Department, Southern Methodist University, Dallas TX; United States of America.
- ⁴⁶National Centre for Scientific Research "Demokritos", Agia Paraskevi; Greece.
- ^{47(a)}Department of Physics, Stockholm University; ^(b)Oskar Klein Centre, Stockholm; Sweden.
- ⁴⁸Deutsches Elektronen-Synchrotron DESY, Hamburg and Zeuthen; Germany.
- ⁴⁹Fakultät Physik , Technische Universität Dortmund, Dortmund; Germany.
- ⁵⁰Institut für Kern- und Teilchenphysik, Technische Universität Dresden, Dresden; Germany.
- ⁵¹Department of Physics, Duke University, Durham NC; United States of America.
- ⁵²SUPA - School of Physics and Astronomy, University of Edinburgh, Edinburgh; United Kingdom.
- ⁵³INFN e Laboratori Nazionali di Frascati, Frascati; Italy.
- ⁵⁴Physikalisches Institut, Albert-Ludwigs-Universität Freiburg, Freiburg; Germany.
- ⁵⁵II. Physikalisches Institut, Georg-August-Universität Göttingen, Göttingen; Germany.
- ⁵⁶Département de Physique Nucléaire et Corpusculaire, Université de Genève, Genève; Switzerland.
- ^{57(a)}Dipartimento di Fisica, Università di Genova, Genova; ^(b)INFN Sezione di Genova; Italy.
- ⁵⁸II. Physikalisches Institut, Justus-Liebig-Universität Giessen, Giessen; Germany.
- ⁵⁹SUPA - School of Physics and Astronomy, University of Glasgow, Glasgow; United Kingdom.
- ⁶⁰LPSC, Université Grenoble Alpes, CNRS/IN2P3, Grenoble INP, Grenoble; France.
- ⁶¹Laboratory for Particle Physics and Cosmology, Harvard University, Cambridge MA; United States of America.
- ⁶²Department of Modern Physics and State Key Laboratory of Particle Detection and Electronics, University of Science and Technology of China, Hefei; China.
- ^{63(a)}Kirchhoff-Institut für Physik, Ruprecht-Karls-Universität Heidelberg, Heidelberg; ^(b)Physikalisches Institut, Ruprecht-Karls-Universität Heidelberg, Heidelberg; Germany.
- ^{64(a)}Department of Physics, Chinese University of Hong Kong, Shatin, N.T., Hong Kong; ^(b)Department of Physics, University of Hong Kong, Hong Kong; ^(c)Department of Physics and Institute for Advanced Study, Hong Kong University of Science and Technology, Clear Water Bay, Kowloon, Hong Kong; China.
- ⁶⁵Department of Physics, National Tsing Hua University, Hsinchu; Taiwan.
- ⁶⁶IJCLab, Université Paris-Saclay, CNRS/IN2P3, 91405, Orsay; France.
- ⁶⁷Centro Nacional de Microelectrónica (IMB-CNM-CSIC), Barcelona; Spain.
- ⁶⁸Department of Physics, Indiana University, Bloomington IN; United States of America.
- ^{69(a)}INFN Gruppo Collegato di Udine, Sezione di Trieste, Udine; ^(b)ICTP, Trieste; ^(c)Dipartimento Politecnico di Ingegneria e Architettura, Università di Udine, Udine; Italy.
- ^{70(a)}INFN Sezione di Lecce; ^(b)Dipartimento di Matematica e Fisica, Università del Salento, Lecce; Italy.
- ^{71(a)}INFN Sezione di Milano; ^(b)Dipartimento di Fisica, Università di Milano, Milano; Italy.
- ^{72(a)}INFN Sezione di Napoli; ^(b)Dipartimento di Fisica, Università di Napoli, Napoli; Italy.
- ^{73(a)}INFN Sezione di Pavia; ^(b)Dipartimento di Fisica, Università di Pavia, Pavia; Italy.
- ^{74(a)}INFN Sezione di Pisa; ^(b)Dipartimento di Fisica E. Fermi, Università di Pisa, Pisa; Italy.
- ^{75(a)}INFN Sezione di Roma; ^(b)Dipartimento di Fisica, Sapienza Università di Roma, Roma; Italy.
- ^{76(a)}INFN Sezione di Roma Tor Vergata; ^(b)Dipartimento di Fisica, Università di Roma Tor Vergata, Roma; Italy.
- ^{77(a)}INFN Sezione di Roma Tre; ^(b)Dipartimento di Matematica e Fisica, Università Roma Tre, Roma; Italy.
- ^{78(a)}INFN-TIFPA; ^(b)Università degli Studi di Trento, Trento; Italy.
- ⁷⁹Universität Innsbruck, Department of Astro and Particle Physics, Innsbruck; Austria.
- ⁸⁰University of Iowa, Iowa City IA; United States of America.
- ⁸¹Department of Physics and Astronomy, Iowa State University, Ames IA; United States of America.

⁸²Istinye University, Sarıyer, İstanbul; Türkiye.

^{83(a)}Departamento de Engenharia Elétrica, Universidade Federal de Juiz de Fora (UFJF), Juiz de Fora; ^(b)Universidade Federal do Rio De Janeiro COPPE/EE/IF, Rio de Janeiro; ^(c)Instituto de Física, Universidade de São Paulo, São Paulo; ^(d)Rio de Janeiro State University, Rio de Janeiro; ^(e)Federal University of Bahia, Bahia; Brazil.

⁸⁴KEK, High Energy Accelerator Research Organization, Tsukuba; Japan.

⁸⁵Graduate School of Science, Kobe University, Kobe; Japan.

^{86(a)}AGH University of Krakow, Faculty of Physics and Applied Computer Science, Krakow; ^(b)Marian Smoluchowski Institute of Physics, Jagiellonian University, Krakow; Poland.

⁸⁷Institute of Nuclear Physics Polish Academy of Sciences, Krakow; Poland.

^{88(a)}Khalifa University of Science and Technology, Abu Dhabi; ^(b)University of Sharjah, Sharjah; United Arab Emirates.

⁸⁹Faculty of Science, Kyoto University, Kyoto; Japan.

⁹⁰Research Center for Advanced Particle Physics and Department of Physics, Kyushu University, Fukuoka ; Japan.

⁹¹L2IT, Université de Toulouse, CNRS/IN2P3, UPS, Toulouse; France.

⁹²Instituto de Física La Plata, Universidad Nacional de La Plata and CONICET, La Plata; Argentina.

⁹³Physics Department, Lancaster University, Lancaster; United Kingdom.

⁹⁴Oliver Lodge Laboratory, University of Liverpool, Liverpool; United Kingdom.

⁹⁵Department of Experimental Particle Physics, Jožef Stefan Institute and Department of Physics, University of Ljubljana, Ljubljana; Slovenia.

⁹⁶Department of Physics and Astronomy, Queen Mary University of London, London; United Kingdom.

⁹⁷Department of Physics, Royal Holloway University of London, Egham; United Kingdom.

⁹⁸Department of Physics and Astronomy, University College London, London; United Kingdom.

⁹⁹Louisiana Tech University, Ruston LA; United States of America.

¹⁰⁰Fysiska institutionen, Lunds universitet, Lund; Sweden.

¹⁰¹Departamento de Física Teórica C-15 and CIAFF, Universidad Autónoma de Madrid, Madrid; Spain.

¹⁰²Institut für Physik, Universität Mainz, Mainz; Germany.

¹⁰³School of Physics and Astronomy, University of Manchester, Manchester; United Kingdom.

¹⁰⁴CPPM, Aix-Marseille Université, CNRS/IN2P3, Marseille; France.

¹⁰⁵Department of Physics, University of Massachusetts, Amherst MA; United States of America.

¹⁰⁶Department of Physics, McGill University, Montreal QC; Canada.

¹⁰⁷School of Physics, University of Melbourne, Victoria; Australia.

¹⁰⁸Department of Physics, University of Michigan, Ann Arbor MI; United States of America.

¹⁰⁹Department of Physics and Astronomy, Michigan State University, East Lansing MI; United States of America.

¹¹⁰Group of Particle Physics, University of Montreal, Montreal QC; Canada.

¹¹¹Fakultät für Physik, Ludwig-Maximilians-Universität München, München; Germany.

¹¹²Max-Planck-Institut für Physik (Werner-Heisenberg-Institut), München; Germany.

¹¹³Graduate School of Science and Kobayashi-Maskawa Institute, Nagoya University, Nagoya; Japan.

^{114(a)}Department of Physics, Nanjing University, Nanjing; ^(b)School of Science, Shenzhen Campus of Sun Yat-sen University; ^(c)University of Chinese Academy of Science (UCAS), Beijing; China.

¹¹⁵Department of Physics and Astronomy, University of New Mexico, Albuquerque NM; United States of America.

¹¹⁶Institute for Mathematics, Astrophysics and Particle Physics, Radboud University/Nikhef, Nijmegen; Netherlands.

¹¹⁷Nikhef National Institute for Subatomic Physics and University of Amsterdam, Amsterdam;

Netherlands.

¹¹⁸Department of Physics, Northern Illinois University, DeKalb IL; United States of America.

^{119(a)}New York University Abu Dhabi, Abu Dhabi;^(b)United Arab Emirates University, Al Ain; United Arab Emirates.

¹²⁰Department of Physics, New York University, New York NY; United States of America.

¹²¹Ochanomizu University, Otsuka, Bunkyo-ku, Tokyo; Japan.

¹²²Ohio State University, Columbus OH; United States of America.

¹²³Homer L. Dodge Department of Physics and Astronomy, University of Oklahoma, Norman OK; United States of America.

¹²⁴Department of Physics, Oklahoma State University, Stillwater OK; United States of America.

¹²⁵Palacký University, Joint Laboratory of Optics, Olomouc; Czech Republic.

¹²⁶Institute for Fundamental Science, University of Oregon, Eugene, OR; United States of America.

¹²⁷Graduate School of Science, University of Osaka, Osaka; Japan.

¹²⁸Department of Physics, University of Oslo, Oslo; Norway.

¹²⁹Department of Physics, Oxford University, Oxford; United Kingdom.

¹³⁰LPNHE, Sorbonne Université, Université Paris Cité, CNRS/IN2P3, Paris; France.

¹³¹Department of Physics, University of Pennsylvania, Philadelphia PA; United States of America.

¹³²Department of Physics and Astronomy, University of Pittsburgh, Pittsburgh PA; United States of America.

^{133(a)}Laboratório de Instrumentação e Física Experimental de Partículas - LIP, Lisboa;^(b)Departamento de Física, Faculdade de Ciências, Universidade de Lisboa, Lisboa;^(c)Departamento de Física, Universidade de Coimbra, Coimbra;^(d)Centro de Física Nuclear da Universidade de Lisboa, Lisboa;^(e)Departamento de Física, Escola de Ciências, Universidade do Minho, Braga;^(f)Departamento de Física Teórica y del Cosmos, Universidad de Granada, Granada (Spain);^(g)Departamento de Física, Instituto Superior Técnico, Universidade de Lisboa, Lisboa; Portugal.

¹³⁴Institute of Physics of the Czech Academy of Sciences, Prague; Czech Republic.

¹³⁵Czech Technical University in Prague, Prague; Czech Republic.

¹³⁶Charles University, Faculty of Mathematics and Physics, Prague; Czech Republic.

¹³⁷Particle Physics Department, Rutherford Appleton Laboratory, Didcot; United Kingdom.

¹³⁸IRFU, CEA, Université Paris-Saclay, Gif-sur-Yvette; France.

¹³⁹Santa Cruz Institute for Particle Physics, University of California Santa Cruz, Santa Cruz CA; United States of America.

^{140(a)}Departamento de Física, Pontificia Universidad Católica de Chile, Santiago;^(b)Millennium Institute for Subatomic physics at high energy frontier (SAPHIR), Santiago;^(c)Instituto de Investigación Multidisciplinario en Ciencia y Tecnología, y Departamento de Física, Universidad de La Serena;^(d)Universidad Andres Bello, Department of Physics, Santiago;^(e)Instituto de Alta Investigación, Universidad de Tarapacá, Arica;^(f)Departamento de Física, Universidad Técnica Federico Santa María, Valparaíso; Chile.

¹⁴¹Department of Physics, Institute of Science, Tokyo; Japan.

¹⁴²Department of Physics, University of Washington, Seattle WA; United States of America.

^{143(a)}Institute of Frontier and Interdisciplinary Science and Key Laboratory of Particle Physics and Particle Irradiation (MOE), Shandong University, Qingdao;^(b)School of Physics, Zhengzhou University; China.

^{144(a)}State Key Laboratory of Dark Matter Physics, School of Physics and Astronomy, Shanghai Jiao Tong University, Key Laboratory for Particle Astrophysics and Cosmology (MOE), SKLPPC, Shanghai;^(b)State Key Laboratory of Dark Matter Physics, Tsung-Dao Lee Institute, Shanghai Jiao Tong University, Shanghai; China.

¹⁴⁵Department of Physics and Astronomy, University of Sheffield, Sheffield; United Kingdom.

- ¹⁴⁶Department of Physics, Shinshu University, Nagano; Japan.
- ¹⁴⁷Department Physik, Universität Siegen, Siegen; Germany.
- ¹⁴⁸Department of Physics, Simon Fraser University, Burnaby BC; Canada.
- ¹⁴⁹SLAC National Accelerator Laboratory, Stanford CA; United States of America.
- ¹⁵⁰Department of Physics, Royal Institute of Technology, Stockholm; Sweden.
- ¹⁵¹Departments of Physics and Astronomy, Stony Brook University, Stony Brook NY; United States of America.
- ¹⁵²Department of Physics and Astronomy, University of Sussex, Brighton; United Kingdom.
- ¹⁵³School of Physics, University of Sydney, Sydney; Australia.
- ¹⁵⁴Institute of Physics, Academia Sinica, Taipei; Taiwan.
- ¹⁵⁵^(a)E. Andronikashvili Institute of Physics, Iv. Javakhishvili Tbilisi State University, Tbilisi; ^(b)High Energy Physics Institute, Tbilisi State University, Tbilisi; ^(c)University of Georgia, Tbilisi; Georgia.
- ¹⁵⁶Department of Physics, Technion, Israel Institute of Technology, Haifa; Israel.
- ¹⁵⁷Raymond and Beverly Sackler School of Physics and Astronomy, Tel Aviv University, Tel Aviv; Israel.
- ¹⁵⁸Department of Physics, Aristotle University of Thessaloniki, Thessaloniki; Greece.
- ¹⁵⁹International Center for Elementary Particle Physics and Department of Physics, University of Tokyo, Tokyo; Japan.
- ¹⁶⁰Graduate School of Science and Technology, Tokyo Metropolitan University, Tokyo; Japan.
- ¹⁶¹Department of Physics, University of Toronto, Toronto ON; Canada.
- ¹⁶²^(a)TRIUMF, Vancouver BC; ^(b)Department of Physics and Astronomy, York University, Toronto ON; Canada.
- ¹⁶³Division of Physics and Tomonaga Center for the History of the Universe, Faculty of Pure and Applied Sciences, University of Tsukuba, Tsukuba; Japan.
- ¹⁶⁴Department of Physics and Astronomy, Tufts University, Medford MA; United States of America.
- ¹⁶⁵Department of Physics and Astronomy, University of California Irvine, Irvine CA; United States of America.
- ¹⁶⁶University of West Attica, Athens; Greece.
- ¹⁶⁷Department of Physics and Astronomy, University of Uppsala, Uppsala; Sweden.
- ¹⁶⁸Department of Physics, University of Illinois, Urbana IL; United States of America.
- ¹⁶⁹Instituto de Física Corpuscular (IFIC), Centro Mixto Universidad de Valencia - CSIC, Valencia; Spain.
- ¹⁷⁰Department of Physics, University of British Columbia, Vancouver BC; Canada.
- ¹⁷¹Department of Physics and Astronomy, University of Victoria, Victoria BC; Canada.
- ¹⁷²Fakultät für Physik und Astronomie, Julius-Maximilians-Universität Würzburg, Würzburg; Germany.
- ¹⁷³Department of Physics, University of Warwick, Coventry; United Kingdom.
- ¹⁷⁴Waseda University, Tokyo; Japan.
- ¹⁷⁵Department of Particle Physics and Astrophysics, Weizmann Institute of Science, Rehovot; Israel.
- ¹⁷⁶Department of Physics, University of Wisconsin, Madison WI; United States of America.
- ¹⁷⁷Fakultät für Mathematik und Naturwissenschaften, Fachgruppe Physik, Bergische Universität Wuppertal, Wuppertal; Germany.
- ¹⁷⁸Department of Physics, Yale University, New Haven CT; United States of America.
- ¹⁷⁹Yerevan Physics Institute, Yerevan; Armenia.
- ^a Also at Affiliated with an institute formerly covered by a cooperation agreement with CERN.
- ^b Also at An-Najah National University, Nablus; Palestine.
- ^c Also at Borough of Manhattan Community College, City University of New York, New York NY; United States of America.
- ^d Also at Center for Interdisciplinary Research and Innovation (CIRI-AUTH), Thessaloniki; Greece.
- ^e Also at Centre of Physics of the Universities of Minho and Porto (CF-UM-UP); Portugal.

- f* Also at CERN, Geneva; Switzerland.
- g* Also at CMD-AC UNEC Research Center, Azerbaijan State University of Economics (UNEC); Azerbaijan.
- h* Also at Département de Physique Nucléaire et Corpusculaire, Université de Genève, Genève; Switzerland.
- i* Also at Departament de Fisica de la Universitat Autonoma de Barcelona, Barcelona; Spain.
- j* Also at Department of Financial and Management Engineering, University of the Aegean, Chios; Greece.
- k* Also at Department of Mathematical Sciences, University of South Africa, Johannesburg; South Africa.
- l* Also at Department of Modern Physics and State Key Laboratory of Particle Detection and Electronics, University of Science and Technology of China, Hefei; China.
- m* Also at Department of Physics, Bolu Abant Izzet Baysal University, Bolu; Türkiye.
- n* Also at Department of Physics, King's College London, London; United Kingdom.
- o* Also at Department of Physics, Stanford University, Stanford CA; United States of America.
- p* Also at Department of Physics, Stellenbosch University; South Africa.
- q* Also at Department of Physics, University of Fribourg, Fribourg; Switzerland.
- r* Also at Department of Physics, University of Thessaly; Greece.
- s* Also at Department of Physics, Westmont College, Santa Barbara; United States of America.
- t* Also at Faculty of Physics, Sofia University, 'St. Kliment Ohridski', Sofia; Bulgaria.
- u* Also at Faculty of Physics, University of Bucharest ; Romania.
- v* Also at Hellenic Open University, Patras; Greece.
- w* Also at Henan University; China.
- x* Also at Imam Mohammad Ibn Saud Islamic University; Saudi Arabia.
- y* Also at Institutio Catalana de Recerca i Estudis Avancats, ICREA, Barcelona; Spain.
- z* Also at Institut für Experimentalphysik, Universität Hamburg, Hamburg; Germany.
- aa* Also at Institute for Nuclear Research and Nuclear Energy (INRNE) of the Bulgarian Academy of Sciences, Sofia; Bulgaria.
- ab* Also at Institute of Applied Physics, Mohammed VI Polytechnic University, Ben Guerir; Morocco.
- ac* Also at Institute of Particle Physics (IPP); Canada.
- ad* Also at Institute of Physics and Technology, Mongolian Academy of Sciences, Ulaanbaatar; Mongolia.
- ae* Also at Institute of Physics, Azerbaijan Academy of Sciences, Baku; Azerbaijan.
- af* Also at Institute of Theoretical Physics, Ilia State University, Tbilisi; Georgia.
- ag* Also at National Institute of Physics, University of the Philippines Diliman (Philippines); Philippines.
- ah* Also at The Collaborative Innovation Center of Quantum Matter (CICQM), Beijing; China.
- ai* Also at TRIUMF, Vancouver BC; Canada.
- aj* Also at Università di Napoli Parthenope, Napoli; Italy.
- ak* Also at University of Colorado Boulder, Department of Physics, Colorado; United States of America.
- al* Also at University of Sienna; Italy.
- am* Also at Washington College, Chestertown, MD; United States of America.
- an* Also at Yeditepe University, Physics Department, Istanbul; Türkiye.
- * Deceased